ASSESSMENT OF ROCK SLOPE STABILITY FOR A COASTAL AREA NEAR KUŞADASI, AYDIN, TURKEY

A THESIS SUBMITTED TO
THE GRADUATE SCHOOL OF NATURAL AND APPLIED SCIENCES
OF
MIDDLE EAST TECHNICAL UNIVERSITY

BY

YAVUZ KAYA

IN PARTIAL FULFILLMENT OF THE REQUIREMENTS
FOR
THE DEGREE OF MASTER OF SCIENCE
IN
GEOLOGICAL ENGINEERING

FEBRUARY 2013

Approval of the thesis:

ASSESSMENT OF ROCK SLOPE STABILITY FOR A COASTAL AREA NEAR KUŞADASI, AYDIN, TURKEY

submitted by **YAVUZ KAYA** in partial fulfillment of the requirements for the degree of **Master of Science in Geological Engineering Department, Middle East Technical University** by,

Prof. Dr. Canan ÖZGEN   _____
Dean, Graduate School   of **Natural and Applied Sciences**

Prof. Dr. Erdin BOZKURT   _____
Head of Department, **Geological Engineering**

Prof. Dr. Tamer TOPAL   _____
Supervisor, **Geological Engineering Dept., METU**

Examining Committee Members:

Prof. Dr. Nurkan KARAHANOĞLU   _____
Geological Engineering Dept., METU

Prof. Dr. Tamer TOPAL   _____
Geological Engineering Dept., METU

Prof. Dr. Erdal ÇOKÇA   _____
Civil Engineering Dept., METU

Prof. Dr. Erdin BOZKURT   _____
Geological Engineering Dept., METU

Assist. Prof. Dr. Mutluhan AKIN   _____
Mining Engineering Dept., Yüzüncü Yıl University

Date: 01.02.2013

I hereby declare that all information in this document has been obtained and presented in accordance with academic rules and ethical conduct. I also declare that, as required by these rules and conduct, I have fully cited and referenced all material and results that are not original to this work.

Name, Last Name: Yavuz KAYA

Signature   :

ABSTRACT

ASSESSMENT OF ROCK SLOPE STABILITY FOR A COASTAL AREA NEAR KUŞADASI, AYDIN, TURKEY

Kaya, Yavuz
M.Sc., Department of Geological Engineering
Supervisor: Prof. Dr. Tamer Topal
February 2013, 112 pages

The study area, which will be open to tourism in Kuşadası (Aydın), has steep and high cliffs near the Aegean coast. In the area where some slidings and rockfall problems occurred in the past the geological hazards should be investigated and nature-friendly remedial measures should be taken. The aim of this study is to perform engineering geological studies to:(i) search geological hazards, (ii) reveal the slope stability problems, (iii) recommend nature-friendly solutions in order to prevent/minimize the hazards and (iv)compare the results obtained from 2-D and 3-D rockfall analyses. To accomplish these tasks, the geological survey was performed, the information about the discontinuities was collected by means of scanline surveys, the rock samples were collected, the in-situ and laboratory tests were carried out, the slope stability and rockfall analyses were performed for different slope conditions, remedial measures were offered for the problematical areas considering the data obtained and the results of 2-D and 3-D analysis were compared. Under the light of these studies, rock removal, drainage, greening (vegetation), filling the caverns, wall building and erosion prevention were offered as remedial measures. The comparison of the 2-D and 3-D rockfall analyses shows that the end points and bounce height values are different for each method. The differences between the 2-D and 3-D model originate from the slope geometry, the algorithm used in the software and the different input parameters. According to the field observations, the 2-D model is more realistic than 3-D model.

Keywords: rockfall, 2-D analysis, 3-D analysis, stability, Kuşadası, Turkey

ÖZ

KUŞADASI YAKINLARINDAKİ BİR KIYI BÖLGESİ İÇİN KAYA ŞEV DURAYLILIĞININ DEĞERLENDİRİLMESİ, AYDIN, TÜRKİYE

Kaya, Yavuz
Yüksek Lisans, Jeoloji Mühendisliği Bölümü
Tez Yöneticisi: Prof. Dr. Tamer Topal
Şubat 2013, 112 sayfa

Kuşadası'nda (Aydın) turizme açılacak olan bir alanın kıyı kesiminde oldukça dik ve yüksek falezler bulunmaktadır. Yer yer kaymalar ve kaya düşme problemlerinin görüldüğü alanın turizm açısından kullanılabilir olabilmesi için, bu alandaki jeolojik tehlikelerin araştırılması ve mümkün olduğunca doğa dostu yaklaşımlarla önlemlerin alınması gerekmektedir. Bu çalışmanın amacı, söz konusu alan ile ilgili mühendislik jeolojisi çalışması yapmak, var olan jeolojik tehlikeleri araştırmak, şev duraylılığı ile ilgili sorunlarıortaya koymak, varolan tehlikeleri önlemek/en aza indirebilmek için doğa dostu çözümler önermek ve 2 ve 3 boyutlu kaya düşme analizlerinden elde edilen sonuçları kıyaslamaktır. Bu amaçları gerçekleştirebilmek için, öncelikle sahada jeolojik incelemeler yapılmış, hat etüdü yardımıyla süreksizlikler hakkında bilgiler edinilmiş, kayaç örnekleri alınmış, sahada ve laboratuvarda deneyler yapılmış, farklı şev durumları için şev duraylılık ve kaya düşme analizleri yapılmış, elde edilen veriler dikkate alınarak problemli alanlar için iyileştirme önerileri sunulmuş ve 2 ve 3 boyutlu kaya düşme analizi sonuçları karşılaştırılmıştır. Bu çalışmalar doğrultusunda, iyileştirme çalışmaları olarak, kaya temizleme, drenaj, yeşillendirme (bitkilendirme), oyuk doldurma, duvar yapımı ve erozyon önleme çalışması önerilmiştir. 2 ve 3 boyutlu kaya düşme analiz sonuçları karşılaştırılmış, her iki yöntem için, kayaçların düştükleri son noktaların ve sıçrama yüksekliklerinin birbirinden farklı olduğu görülmüştür. Bu farklılık, şevin geometrisinden, yazılımda kullanılan algoritmadan ve farklı girdi verilerinden kaynaklanmaktadır. Saha gözlemlerine göre, 2 boyutlu model 3 boyutlu modelden daha gerçekçidir.

Anahtar Kelimeler: kaya düşmesi, 2 boyutlu analiz, 3 boyutlu analiz, duraylılık, Kuşadası, Türkiye

To My Uncle,
Prof. Dr. Raif GÜLER

ACKNOWLEDGEMENTS

TABLE OF CONTENTS

LIST OF TABLES

TABLES

LIST OF FIGURES

FIGURES

xiv

CHAPTER 1

INTRODUCTION

1.1 Purpose and Scope

The study area will be open to tourism and the steep and high cliffs near the coast pose a great danger for the people. In the area, some slidings and rockfall problems were observed in the past. Therefore, the geological hazards should be investigated and nature-friendly remedial measures should be taken.

The study is centered on searching and analyzing the rockfall problems. Additionally, as a part of the purpose of the study, nature-friendly solutions were recommended in order to prevent/minimize the hazards, 2-D and 3-D analyses were carried out to analysis the rockfall problems and the results obtained from 2-D and 3-D analyses were compared. These tasks consist of geological survey, scanline survey, sample collection, the in-situ and laboratory tests, slope stability and rockfall analyses, offering remedial measures and comparing/discussing the 2-D and 3-Drockfall analyses results respectively.

1.2 Location, Physiography and Accessibility

Kuşadası is located within the borders of Aydın Province in Turkey and is located 71 kilometers to the northwest of Aydın's Centrum. Its distance to Izmir Centrum is approximately 95 kilometers. Kuşadası city by the Aegean Sea is one of the most important touristic centers of Turkey (Kuşadası Municipality, 2010). The study area, which has a coast in the Aegean region, is located about 5 km south-southwest of the Kuşadası county seat (Figure 1.1). The study area, which has 0.24 km^2 area, has a flat morphology in general but it steepens partially towards the coast and at the coast, it has highly steep cliffs (Figure 1.2). The sharp topographical changes were observed from the coast to the higher regions. The steep cliffs were observed especially in the western part of the region. After the first 20-25 meters from the sea level, the topography becomes gentle. The upper parts of the study area represent a flat topography. The accessibility to the study area is possible by the Kuşadası-Söke highway in all seasons.

1.3 Climate and Vegetation

A typical Mediterranean climate is dominant in the study area. It is hot and dry in summers but mild and rainy in winters. According to the meteorological data (Table 1.1), the highest temperature observed in the region was 44.6 °C in July (27.07.1987), the lowest temperature, -6.0 °C in June (15.01.1973). The annual amount of precipitation is 618.0 kg/m^2. The highest precipitation was reported in December (110.8 kg/m^2) and the lowest precipitation was in

August (2.5 kg/m^2). The seawater temperature varies between 15 °C and 24 °C in Kuşadası and its close vicinity.

The study area is a green field compared to its immediate surroundings (Figure 1.3). The area has scrub kind vegetation. Additionally, there are different tree species like black pine, stone pine, olive, eucalyptus, phoenix, palm, calabrian pine, black cypreas, pepper and locust.
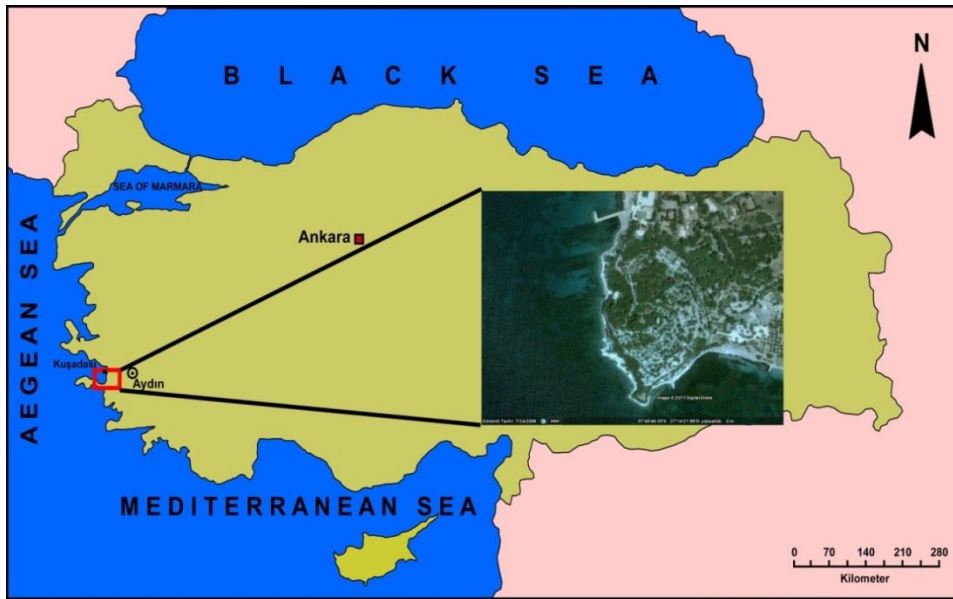
Figure 1.1 Location map of the study area.

Figure 1.2 General view of the study area and the steep cliffs near the coast.

Table 1.1 Meteorological data of Aydın between the years 1970 and 2011 (DMİ, 2012).

	MONTHS											
	Jan.	Feb.	Mar.	Apr.	May	Jun.	Jul.	Aug.	Sep.	Oct.	Nov.	Dec.
Average Temperature (°C)	8.2	9.1	11.9	15.8	20.9	26.0	28.4	27.4	23.4	18.3	12.9	9.3
The Highest Average Temperature (°C)	13.4	14.6	18.1	22.4	28.3	33.5	36.1	35.4	32.0	26.2	19.5	14.4
The Highest Temperature (°C)	23.2	25.2	32.4	33.8	39.3	44.4	44.6	43.8	43.3	37.8	30.7	25.4
The Lowest Average Temperature (°C)	4.2	4.8	6.7	10.0	14.1	18.1	20.5	20.1	16.6	12.6	8.3	5.4
The Lowest Temperature (°C)	-6.0	-5.2	-5.0	-0.8	4.6	8.4	13.4	13.7	7.6	2.0	-2.0	-3.8
The Average Sunshine Time (hour)	4.3	5.0	6.2	7.2	9.1	10.6	11.1	10.5	9.2	7.0	4.6	4.1
The Average Rainy Day Count	10.6	10.1	9.0	8.9	6.1	2.0	0.8	0.5	2.0	5.5	8.1	12.0
The Average of Total Monthly Precipitation Amount (kg/m²)	98.3	92.4	69.6	53.6	33.5	13.1	4.0	2.5	11.5	44.9	83.9	110.8

Figure 1.3 Appearance of dense vegetation in the study area (looking east).

1.4 Methods of Study

The study was conducted in five main stages. At the first stage, a detailed literature survey was performed, the previous works were searched, topographical and geological data were collected, and the topographical studies at the cliffs to complete the missing contour profiles were directed.

In the second stage, geological studies and detailed scanline surveys all around the coast were performed. At this process, Schmidt rebound measurements were carried out with Schmidt Hammer from different levels of the rocks outcropping in the field. Many samples were taken for the laboratory tests. Geological hazards like slide and rockfall were investigated. Because of the different literature values of the coefficient of restitution which is one of the most important parameters used in rockfall analyses, in-situ rockfall tests were carried out by falling a total of 66 rock blocks along 2 different routes (profile 13 and profile 39).

In the third stage, for the purpose of use in the 2-D and 3-D analyses, unit weight, effective porosity, water absorption and point load strength tests were performed on the samples collected from the field.

In the fourth stage, slope stability and rockfall (2-D and 3-D) analyses for 43 profiles were carried out. Rockfall analyses for the 43 profiles were repeated by using the computer programs RocFall 4.0 (Rocscience, 2004c) and ROTOMAP32 (Scioldo, 1991). The accuracy of the model was verified by comparing the results derived from the programs and the location of the rock blocks fallen in the site before. 2-D and 3-D rockfall modeling were carried out considering the all data obtained from the tests and analyses, using the computer programs RocFall 4.0 (Rocscience, 2004c) and ROTOMAP32 (Scioldo, 1991) respectively. Finally, a detailed comparison was made to discuss and evaluate the modeling results.

In the fifth stage, nature-friendly remedial measure suggestions were made to solve the geological problems with the nature-friendly methods by considering the results of rockfall analyses.

1.5 Previous Studies

The previous works about the study area are related to the regional geology.

Ercan et al. (1986) carried out a geological study for Söke-Selçuk-Kuşadası region. They established a detailed stratigraphy of rock units exposed in the region.

Yılmazer et al. (1994) carried out a geological study between Kuşadası and Davutlar. They studied the western part of Büyük Menderes Graben, Söke-Kuşadası-Davutlar region. They observed that a fault extending to the Kirazlı and the faults passing from the south of Türkoğlu Hill. The general tectonism in the region has a tendency to E-W, NE-SW and NW-SE according to the authors.

Ünay and Göktaş (1999) used the name "Kuşadası formation" to define a rock assemblage of sandstone, mudstone, calcareous siltstone, marlstone, clayey limestone, and calcareous claystone.

Gürer et al. (2001) studied Neogene basin around Söke-Kuşadası (western Anatolia) and its bearing on tectonic development of the Aegean region. They presented detailed information about the Kuşadası and Söke formations. They mentioned that The Kuşadası-Söke region is located to the north of the Büyük Menderes River valley, where there is a large Neogene outcrop. They observed that the basement consists of the metamorphic rocks of the Menderes Massif. The Neogene cover sediments lie above the basement. They investigated that the Kuşadası formation which is in the middle unit consists chiefly of clayey limestone, alternating with micritic limestone and marl. There are subordinate siltstones and sandstones within the unit, which crop out extensively around Kuşadası and the surrounding areas. The Kuşadası formation is medium to thinly-bedded and rather uniform. It is about 300 to 400 m thick. The lower beds of the Kuşadası formation are transitional to the underlying Fevzipaşa formation.

Çakmakoğlu (2007) studied pre-Neogene tectonostratigraphy of around Dilek Peninsula-Söke-Selçuk. He prepared a 1/25.000 scale detailed geological map between 1992 – 1996 to define the rock units of Menderes Massif around Dilek Peninsula, Söke, Ortaklar, Kuşadası

and Selçuk. The revision, correlation and compilation studies also carried out in these studies. He defined the study area as Neogene sediments. The age of the Neogene sediments are given in Middle Miocene and Late-Early Miocene.

Ring et al. (2007) carried out a detailed study about Cycladic blueschist unit in the eastern Aegean, Greece, and Turkey. In their study, they defined the study area as Neogene sediments.

Sümer et al. (2013) carried out a geological study about the tectonic evolution of the Söke Basin. They gave detailed information about the Kuşadası formation. They observed that the best and most expanded sections of the Kuşadası formation are found along the main road between the Söke and Kuşadası formations. The Kuşadası Formation is composed of a clayey to micritic limestone-mudstone-marl-dominated sequence and also contains sandstone, carbonaceous siltstone and calcareous claystone (Figure 1.4). It commences with sandstones conformably above the Davutlar conglomerate; fine-grained conglomerates and mudstone intercalations are common at the lower levels. The fine- to coarse-grained (locally pebbly) sandstones are grey and massive to thick bedded. The mudstones are grey to light green, massive to thin bedded (and laminated) and alternate with thin clayey limestone beds. The marls are yellowish and thin to thick bedded, and alternate with thin to thick bedded, beige micritic limestones and mudstone beds. The thickness of the unit is reported as more than 115 (Sümer et al., 2013). The age of the formation, based on fossil content (freshwater ostracods and gastropods) and radiometric age of the Hisartepe volcanics, is suggested as Middle–Late Miocene age (Sümer et al., 2013).

Quaternary	Alluvium		alluvial fan and alluvial plain deposits with deltaic sediments of Büyük Menderes system
Late Pliocene-Pleistocene	Yamaçköy Formation		blocky conglomerate
	Büyük Menderes Group / Fevzipasa Formation	Savulca member	alternation of conglomerate, gravelly sandstone
		Kartaltepe member	mudstone with limestone intercalations and ash layers
			fining upward conglomerate
Late Miocene	Hisartepe volcanics		trachyandesite, andesite, basaltic andesite lava flows and, rhyodacite and dacite domes
	Kusadasi Formation		clayey limestone, sandstone, carbonaceous siltstone, marl and mudstone
	Dededag/Davutlar Formation		marble-dominated blocky conglomerate, sandstone and mudstone
Early - Middle Miocene	Soke Formation	Maden limestone	white micritic limestone, clayey limestone and thin mudstone
			lignite beds
		Seytan member	sandstone, siltstone, mudstone, bituminous shale and lignite beds
			lignite beds
			cobble-pebble conglomerate and sandstone
		Kemalpasa conglomerate	
Triassic-Cretaceous	Ayricadag Formation		marble, cherty marble, dolomite
Palaeozoic	Meryemana formation		marble, thin-bedded dolomite, calcschist
			phyllite, quartz-muscovite schist, quartzite, meta quartz arenite

Figure 1.4 Generalized stratigraphic section of the Büyük Menderes Graben in the area between Söke to the east and Atburgazı to the west (slightly modified from Sümer et al., 2013).

7

CHAPTER 2

BACKGROUND INFORMATION ON ROCKFALL

Because of the discontinuous nature of rock, the rock slope stability has a great importance in terms of stability and safety in geotechnical engineering. This holds for both the design and construction stages of the projects. The most widely used classification of the slope movements was compiled by Varnes (1978). There are six basic considered types of slope movements: Falls, topples, slides, lateral spreads, flows and complex movements. Currently, a number of methods are being used for the assessment of slope stability and excavatability (Hoek and Bray, 1981; Goodman, 1989; Pettifer and Fookes, 1994). Kinematical, limit equilibrium and numerical analyses are generally preferred for the evaluation of the stability of the rock slopes. Failure in rocks may be in the form of planar, wedge, topple, rotational and rockfall. Because these movement types with the exception of rockfall are very well documented in the literature and generally known by the researchers, the background information on rockfall is included in this thesis.

2.1 Introduction

Rockfall can be described as the rapid movement down a slope of one or a few boulders. (Varnes, 1978) (Figure 2.1). The rockfall may be formed because of jointing, weathering, freeze–thaw, water effect, earthquake, or tree roots (Chen et al., 1994; Wasowski and Gaudio, 2000; Marzorati et al., 2002; Dorren, 2003; Topal et al., 2007; Krautblatter and Moser, 2009; Wick et al., 2010). Rockfall threatens humans and can cause significant damage to structures (Topal et al., 2012). For landuse planning in rockfall prone-areas, causes of rockfall events and remedial measures should be considered (Raetzo et al., 2002; Agliardi and Crosta, 2003; Corominas et al., 2005; Jaboyedoff et al., 2005; Straub and Schubert, 2008; Fell et al., 2008; Agliardi et al., 2009). The dynamic processes of rockfall event may be free-fall, bouncing or rolling, depending on the geometrical features and mechanical properties (friction, roughness, rolling resistance, restitution characteristics, etc.) of the slope and rock blocks (Ritchie, 1963; Agliardi and Crosta, 2003; Alejano et al., 2010). As the profile changes, two or more of the rockfall modes may also be observed, depending on the different dynamic processes. Additionally, initial velocity, weight and shape as well as the fragmentation of the blocks and the properties of the slope-forming material may control rockfall event (Giani, 1992; Azzoni et al., 1995; Dorren, 2003).

2.2 Research on Rockfalls

The first research about rockfall was carried in 1963 by Arthur M. Ritchie. He noted that there is a clear need for a means of predicting the stability of material on the surface of a rock cut (Ritchie, 1963). After this work, many papers have been published about rockfall during the past 30 years and considerable progress has been made in explaining the rockfall

behavior. These works are about stopping boulders reaching roads and railway lines. Effective methods like digging catch ditches, installing catch fences, or covering the whole slope with a net are developed and analyzed to restrict boulders. Even though the basic rockfall phenomenon is understood in recent times, rockfalls pose problems because of their random behaviors (Rayudu, D.N.P., 1997) (Figure 2.2).
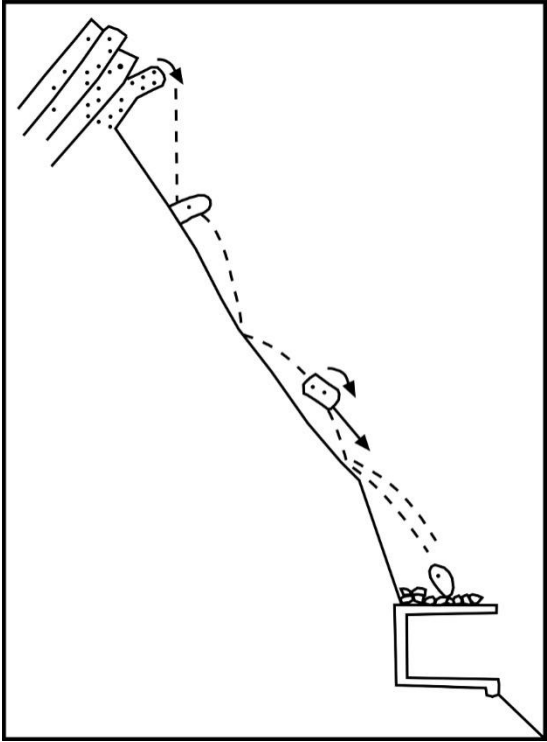
Figure 2.1 Different particle positions during a rockfall (Descoeudres et al., 1999).

Figure 2.2 Highway closure caused by rockfall in very strong, blocky granite from a height of about 300 m (Dorren, 2002).

2.3 Rockfall Mechanics

2.3.1 Causes of Rockfall

Rockfall occurs usually a cliff face (Figure 2.3). Detachment of rocks from bedrock slopes starts the movement. The weathering in the bedrock slopes may cause fracturing, opening of joints and therefore to promotion of rockfall (Dorren, 2003). Physical and chemical weathering, and the bedrock type affect the degree of rockfall promotion (Schumm and Chorley, 1964; Day, 1997). Except from the weathering, trigger mechanisms also cause rockfall. The slope geometry and the rocks having potentially falling risk are the most important factors determining whether or not a rock could fall (Dorren, 2003). The frost–thaw activity is a well-known promoter and causes of rockfall (Grove, 1972; Porter and Orombelli, 1980, 1981; Coutard and Francou, 1989; McCarrol et al., 1998; Matsuoka and Sakai, 1999). The morphological and geological character of the cliff and rock surface temperature fluctuations control the rockfall. Zellmer (1987), Bull et al. (1994) and Vidrih et al. (2001) searched the relationship between seismic activity and rockfall. They come to a conclusion that seismic activity triggered the rockfall. Additionally, animals like chamois can cause rockfalls by climbing steep cliff faces (Dorren, 2003). According to these observations, the causes of rockfalls can be gathered under topographical, geological and climatological factors.

Figure 2.3 Fallen rocks in the study area.

2.3.2 Motion Types of Falling Rocks

The types of motion depend on the mean slope gradient (Figure 2.4). These motion types are falling, bouncing and rolling.

a) Freefall of Rocks: This type of movement occurs on steep slopes. According to Ritchie (1963) freefall occurs when the slope gradient exceeds 76°. In different field conditions this value varies. For this reason Figure 2.4 shows that about 70° the motion of the rock gradually transforms from bouncing to falling. During freefall of rocks translation of the center of rock and rotation of the block around its center movements can occur. (Azzoni et al., 1995). Air friction and collision with other falling rocks affect the velocity of a falling rock. According to Bozzolo and Pamini (1986), there is no important effect of air friction on the movement of the rock.
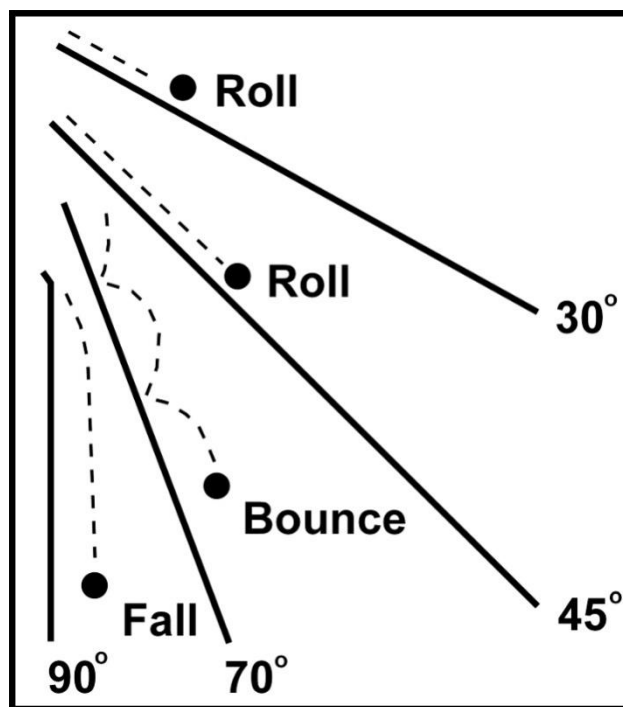
Figure 2.4 General modes of motion of rocks during their descent on gradients (Ritchie, 1963).

b) Movement at or near the Slope Surface: The decreasing of the mean slope gradient causes colliding on the slope surface. This is defined as bouncing (Dorren, 2003). The incompetent rocks may be broken during the first bounce (Bozzolo and Pamini, 1986). At this first impact, the rocks lose their energy (Broilli, 1974; Evans and Hungr, 1993). When the mean slope gradient is less than approximately 45°, bouncing movement transforms into rolling. The rock is in contact with the slope surface while rolling (Hungr and Evans, 1988).

The rotation of the rock is very fast during the transition between bouncing and rolling. Another motion type is sliding. It generally occurs in the initial and final stages of a rockfall. When the mean slope gradient increases, a sliding rock starts falling, bouncing or rolling. If the mean slope gradient does not change while sliding, the rock usually stops because of energy loss due to friction (Bozzolo and Pamini, 1986).

2.4 Comparison of Rockfall Models

To calculate runout zones of rockfall events, many different models can be used. All these models can be classified in three main groups: (1) empirical models, (2) process based models and (3) GIS-based models.

2.4.1 Empirical Models

This kind of rockfall models are generally based on relationships between topographical factors and the length of the runout zone. These models are defined as statistical models (Keylock and Domaas, 1999). Tianchi (1983) stated two relationships from 76 major rockfalls. The first one is an inverse logarithmic correlation between the volume of the rockfall and the ratio of the maximum vertical drop to the maximum horizontal distance travelled. The second relationship is a positive logarithmic correlation between the volume of the rockfall and the area covered by the fallen mass. On the basis of the two correlations, Tianchi (1983) developed a model for a preliminary estimate of the extent of a threatening rockfall, if the volume can be estimated. Toppe (1987) and Evans and Hungr (1993) suggest the Fahrböschung principle (Heim, 1932) to predict runout zones of rockfall events. The Fahrböschung is the angle between a horizontal plane and a line from the top of a rockfall source scar to the stopping point for any given rockfall (Figure 2.5). It is important that the line follows the falltrack of the boulder.

2.4.2 Process-based Models

In these models, the modes of motion of falling rocks are defined over slope surfaces. Kirkby and Statham (1975) and Statham (1976) developed a process-based rockfall model. They assume that rocks only slide over a talus slope surface. Keylock and Domaas (1999) enhanced the "simple dynamics rockfall model". This is a process-based model based on the model of Kirkby and Statham (1975). In this model, the data presented by Domaas (1994) are used. Keylock and Domaas (1999) concluded that the model did not appear to hold a significant advantage over the empirical models tested in their study. In addition to the models of Kirkby and Statham (1975) and Keylock and Domaas (1999), there is a large group of process-based models that are rather similar (Wu, 1985; Bozzolo and Pamini, 1986; Hungr and Evans, 1988; Bozzolo et al., 1988; Pfeiffer and Bowen, 1989; Kobayashi et al., 1990; Evans and Hungr, 1993; Budetta and Santo, 1994; Chen et al., 1994; Azzoni et al., 1995, Chau et al., 1998). All these models have three common factors. First, these models are two-dimensional slope-scale models. For this reason, the simulation of lateral movement is not possible. Secondly, the rockfall track was defined as a composite of connected straight lines with a

slope angle equal to the measured mean slope gradient on the represented segment of the rockfall track as visualized in Figure 2.6. Finally, motions were simulated as a succession of flying phases and contact phases. The flying phase was simulated with a parabola equation based on the initial velocity in x and y directions and the acceleration due to gravity. The collision point of the rock on the slope surface was calculated with the intersection of the parabolic flying function and the straight slope segments.
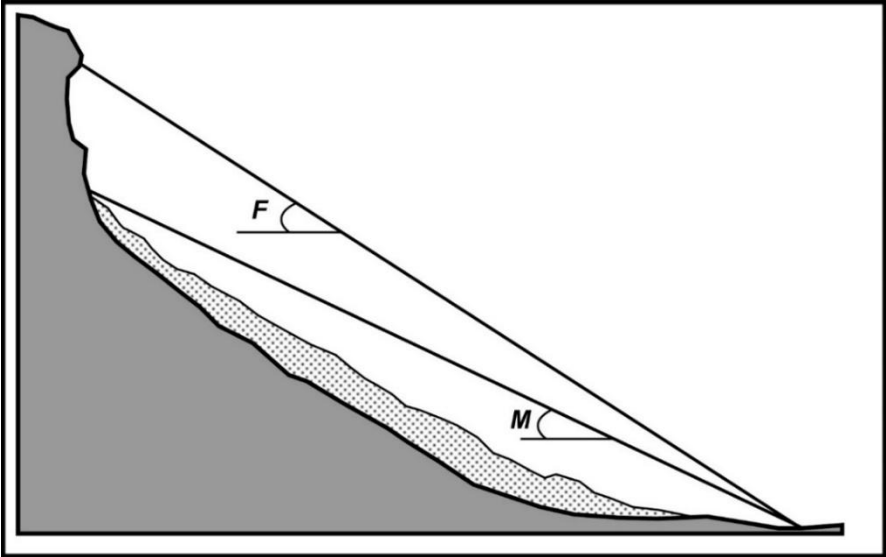
Figure 2.5 The Fahrböschung (F) and the minimum shadow angle (M) of a talus slope (Dorren, 2003).
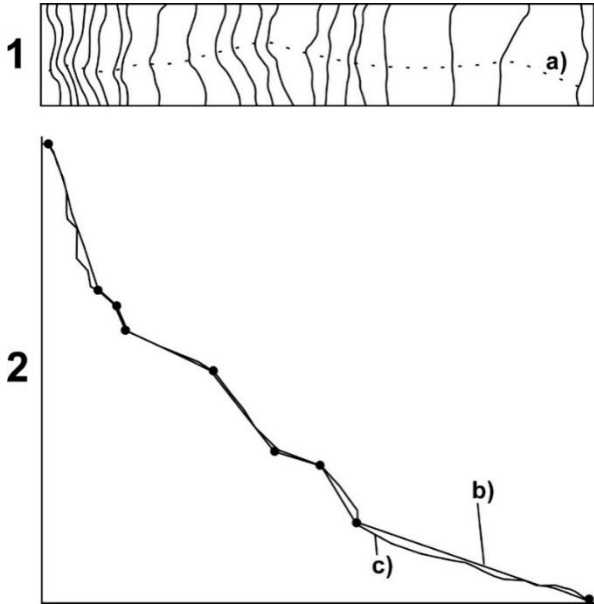
Figure 2.6 The upper figure (1) shows the actual rockfall path (a) projected on a contour line map. The lower figure (2) shows the slope segments (b) used in two-dimensional rockfall models representing the actual slope of the rockfall path (c) (Dorren, 2003).

14

Azzoni et al. (1995) developed a model based on the coefficient for the efficiency of collision. The model was projected and calibrated with the experience and data obtained from several field experiments in Italy. The model considered the falling rock as an ellipsoid (Figure 2.7) and simulated bouncing, sliding and rolling based on the algorithms described by Bozzolo and Pamini (1986). Energies before and after the bounce was calculated from the angular velocity. Kobayashi et al. (1990) developed a model that simulated the contact phases with different characterizations for bouncing and rolling. Bouncing was also based on the coefficient for the efficiency of collision. Their main conclusion was that boulder shape is important in governing the modes of motion, but variations in topography control the mode of motion. All the above-described process-based slope-scale models did not simulate multiple falling rocks and the complex interactions between them.
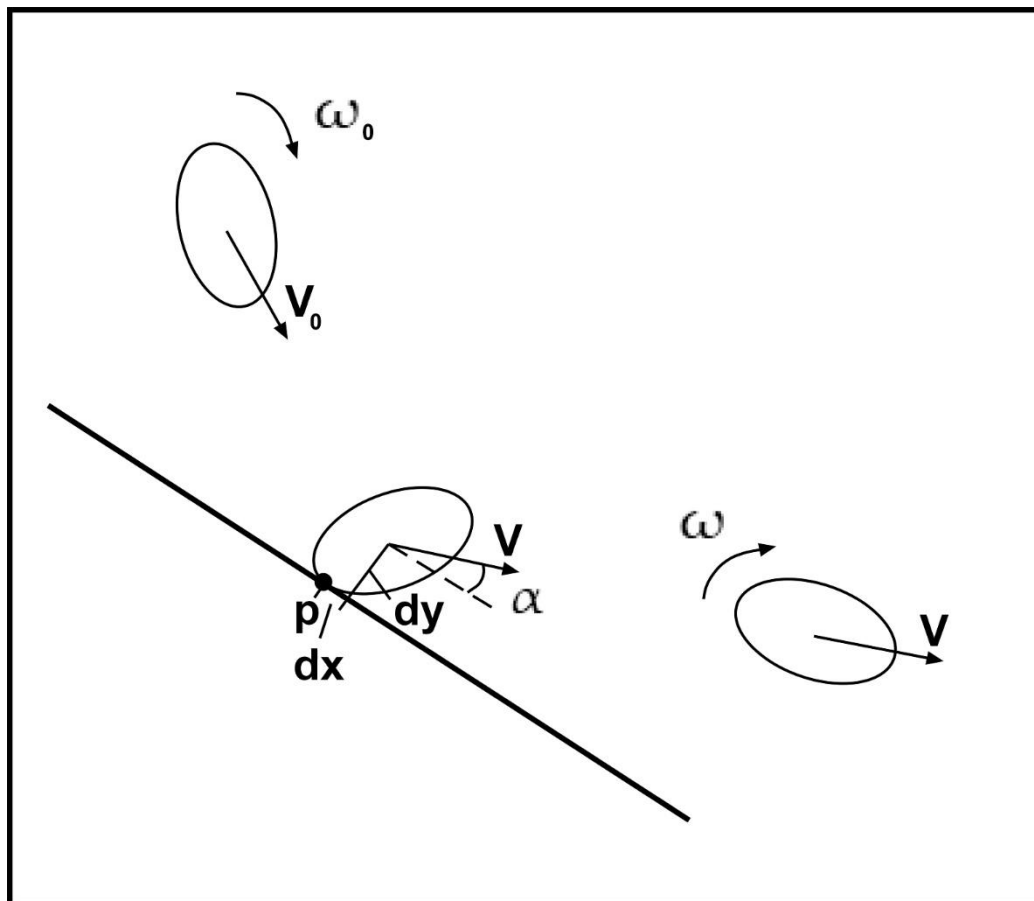
Figure 2.7 An ellipsoidal rock with initial angular velocity (ω_0) and initial velocity (V_0) continues its fall with angular velocity (ω) and velocity (V) after impact. The angle a is determined by the ratio of the tangential distance (dx) to the normal distance (dy) between the center of the rock and impact point (p) (after Bozzolo and Pamini, 1986; Azzoni et al., 1995).

2.4.3 GIS-based Models

These kind of models are either running within a GIS environment or they are raster-based models for which input data is provided by GIS analysis. These models consist of three main procedures. The first one is identifying the rockfall source areas in the region of interest, the second one is determining the falltrack and the third one is calculating the length of the runout zone (Hegg and Kienholz, 1995). Meissl (1998) developed two GIS-based rockfall models using an empirical model for calculating the runout zone. The first model was Schattenwinkel. This model was based on the minimum shadow angle principle (Evans and Hungr, 1993). The second model of Meissl (1998) was called Geometrische Gefälle. This model was based on the angle of the shortest line between the top of the rockfall source scar and the stopping point. Apart from these principles both models were identical, since both models used an identical module for calculating the falltrack and the source areas.

2.5 The Parameters Used in Rockfall Analyses

2.5.1 Bounce Height

This output mostly depends on the coefficient of restitution value, the weight of rock and initial velocity. The bounce height values obtained from the field and models are used to define the height of protective barriers, embankments (Figure 2.8), walls and ditches.

Figure 2.8 Appearance of a rockfall protection embankment (Maccaferri Ltd., 2013).

2.5.2 Total Kinetic Energy

Total kinetic energy of a rock depends on the velocity and the weight of the rock. This parameter is used to design the protective fences and barriers. The impact on the protection system varies according to the kinetic energy of the rock. This variety depends on the kinetic energy of the rock.

2.5.3 End Point

The end point of the rolling rocks depends on the slope geometry, initial velocity and slope roughness. This kind of data is useful to define the proper placement of the protection systems.

2.5.4 Coefficient of Restitution

This retarding capacity of the surface material is expressed mathematically by a term called the coefficient of restitution. The value of this coefficient depends upon the nature of the materials that form the impact surface. Clean surfaces of hard rock have high coefficients of restitution while soil, gravel and completely decomposed rocks have low coefficients of restitution. This is why gravel layers are placed on catch benches in order to prevent further bouncing of falling rocks (Rocscience, 2004).

The coefficient of restitution for a material is defined as the ratio of outgoing velocity to the incoming velocity.

$$R = \mid V_{outgoing} / V_{incoming} \mid$$

A perfectly elastic material will have a coefficient of restitution of 1. An object striking this material will rebound with the same speed. A perfectly inelastic material will have a coefficient of restitution of 0. This means that an object striking this material will rebound with zero velocity, i.e. it will come to a halt. All real materials have coefficients of restitution between 0 and 1 (Rocscience, 2004).

The tangential coefficient of restitution (R_t) and normal coefficient of restitution (R_n) are the two coefficient of restitution components of a material. The tangential coefficient defines the ratio of the outgoing velocity (tangential to the surface) to the incoming velocity (tangential to the surface). The normal coefficient defines the ratio of the outgoing velocity (normal to the surface) to the incoming velocity (normal to the surface). The tangential coefficient of restitution is generally equal to or larger than the normal coefficient of restitution. Coefficients of restitution are often determined from back calculation of known rock paths and rock endpoints. If you have observations of past rockfall events (knowing the starting point, the end point, and the path of the rock) you can use these to help calibrate your model. Once you have these "known" rock paths and endpoints, you can pick a value from the coefficient of restitution table (pick the value that best describes your site – so you have a decent starting point), and then adjust the coefficients of restitution in the model until the rock paths in the model are similar to the observed rock paths (Rocscience, 2004). As a

general rule, harder materials will have higher coefficients of restitution than softer materials, and if the normal coefficient of restitution increases so will the tangential coefficient of restitution.

Unfortunately, there is little data available, and it is difficult to draw anything but broad conclusions from the data. For example, there are a lot of data points where the same value of R_n (e.g. ~ 0.4) is paired with a wide range of R_t (e.g. 0.56 to 0.85) (Rocscience, 2004).

2.6 Possible Measures to Reduce Rockfall Hazards

It is neither possible nor practical to detect all potential rockfall hazards by any techniques currently in use in rock engineering (Rocscience, 2012). In some cases, for example, when dealing with boulders on the top of slopes, the rockfall hazards are obvious. However, the most dangerous types of rock failure occur when a block is suddenly released from an apparently sound face by relatively small deformations in the surrounding rock mass. If it is accepted that it is not possible to detect or to prevent all rockfalls, then methods for restraining those rockfalls, which do occur, must be considered. These methods are illustrated in Figure 2.9.
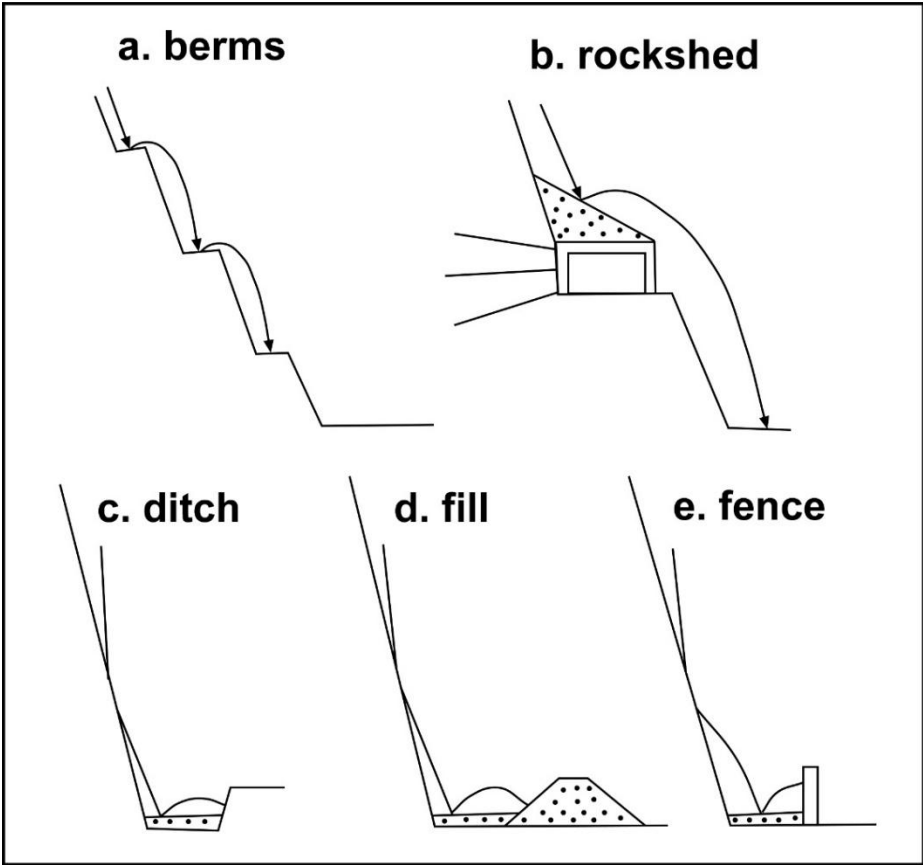
Figure 2.9 Possible measures to reduce the damage due to rockfalls (Spang, 1987).

Berms (Figure 2.10) are very effective means of catching rockfalls, and are frequently used on permanent slopes. However, berms can only be excavated from the top downwards and they are of limited use in minimizing the risk of rockfalls during construction (Rocscience, 2012).

Figure 2.10 A typical berm structure designed for a cut slope (Merck, J., 2010).

Rocksheds or avalanche shelters are widely used on steep slopes above narrow railways or roadways (Figure 2.11). It is generally advisable to place a fill of gravel or soil on top of the rockshed in order to act as both a retarder and a deflector for rockfalls (Rocscience, 2012).

Figure 2.11 A rockshed structure constructed for a railway (Trainweb, 2000).

Probably the most effective permanent rockfall protective system for most highways is the construction of a catch ditch at the toe of the slope. The base of this ditch should be covered by a layer of gravel to absorb the energy of falling rocks, and a sturdy barrier fence should be placed between the ditch and the roadway.

Figure 2.12 A ditch structure form a highway (TranBC, 2010).

Installed below potentially loose and unstable rock faces catch fences (Figure 2.13 are designed to catch falling rocks and boulders, stopping them falling onto infrastructure or developments.

Figure 2.13 Impact moment of a rock to a fence (Geobrugg, 2013).

CHAPTER 3

GEOLOGY AND ENGINEERING GEOLOGICAL PROPERTIES OF THE ROCKS EXPOSED IN THE STUDY AREA

3.1 Geology

The study area is in the west of the Büyük Menderes Graben. The Menderes Massif metamorphics comprise the basement of the study area (Yılmazer et al., 1994).

Various geological units crop out in the study area and its close vicinity (Figure 3.1). They are schist (Upper Paleozoic), marble (Middle Triassic-Cretaceous), meta-flysch (Upper Cretaceous) and terrestrial carbonates (Middle-Upper Miocene) from the older to the younger. The terrestrial carbonates are the unit observed in the study area. This unit is gray, light brown, thin to thick bedded, moderately weathered, alternation of weak sandstone-claystone-marl.

The study area is located on a tectonically active region (Yılmazer et al., 1994). The most prominent structure of the study area is the PSF (Priene-Sazlı Fault). Faults observed in the NW block of the PSF footwall can be classified into two groups. The first includes a south-dipping low-angle normal fault (Oyukdağı detachment fault) that separates metamorphic rocks in the footwall from ophiolitic rocks in the hangingwall. The second group is the youngest structures and is characterized by high-angle fault surfaces (Karagedik, Yavansu, Mağriboğlu, Pilav, Caferli, Ağaçlı and Yamaçköy faults) that can be categorized by their strikes, dip/dip directions, and slip vectors (Figure 3.2) (Sümer et al., 2013).
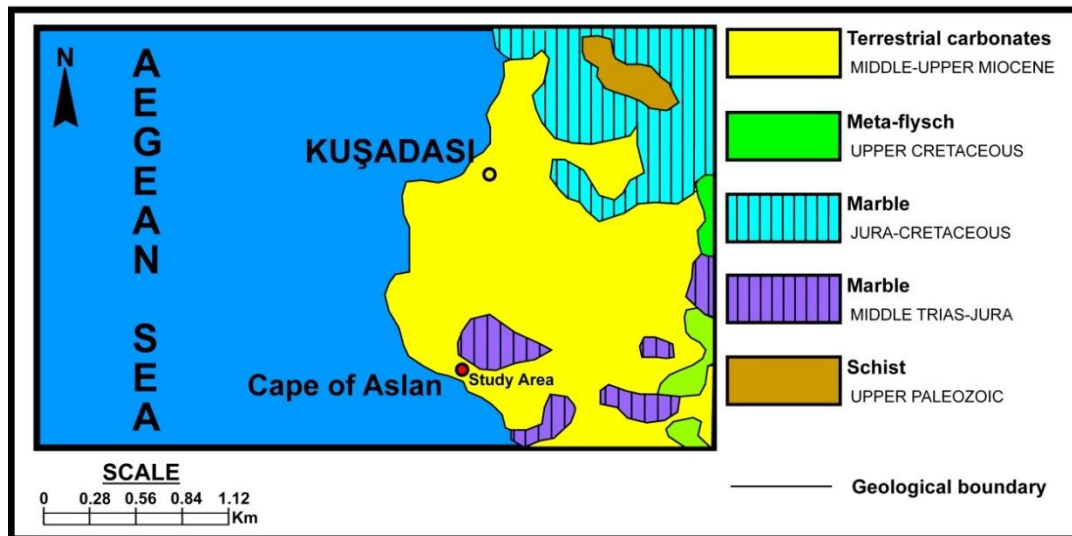
Figure 3.1 The geological map of the study area and its close vicinity (simplified from MTA (2002)).

Figure 3.2 The faults around the study area (modified from Sümer et al., 2013).

The study area is located in the 1st degree earthquake zone (Figure 3.3) according to the Earthquake Zoning Map of Turkey (GDDA (abrogated), 1996). The peak horizontal ground acceleration value is greater than or equal 0.4g in the study area (GDDA (abrogated), 1996). The main faults, fault zones and grabens around the study area can be seen in the Figure 3.4.
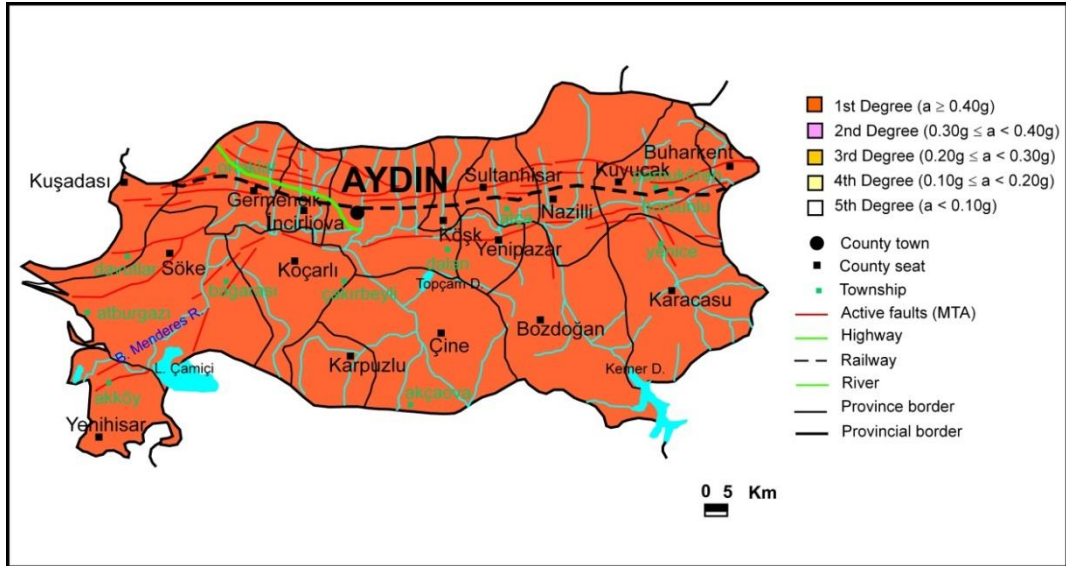
Figure 3.3 Earthquake zoning map of the study area and its close vicinity (GDDA, 1996).

Figure 3.4 The main faults around the study area (modified from MTA, 2012).

3.2 Engineering Geological Properties of the Rocks Exposed in the Study Area

In this section, the engineering geological properties of the rocks observed in the study area will be given by means of the field and laboratory studies.

In the field studies, the terrestrial units were investigated in terms of engineering geological properties, the data about the discontinuities were collected according to the Priest (1993) by the help of the scan-profile survey carried out along 10 profiles (Figure 3.5), Schmidt rebound hardness measurements were taken, sample collection was carried out for the laboratory studies and rockfall tests were made in 2 different locations (Figure 3.5).

In the laboratory studies, unit weight, effective porosity, water absorption and point load strength tests were performed on ten samples taken from the field according to ISRM (1981) and (1985).

3.2.1 Field Studies

The terrestrial units in the study area are generally gray, light brown, thin to thick bedded, moderately weathered. They consist of alternation of sandstone-claystone-marl. The pervasive discontinuity is the bedding plane. Additionally, there are joints developed in 2 different directions. The major discontinuity sets obtained from the Dips 5.1(Rocscience, 2004a) software are presented in Figure 3.6. The changes observed in the major discontinuity sets are related to the deformation of the layers and joints arising from the folding.
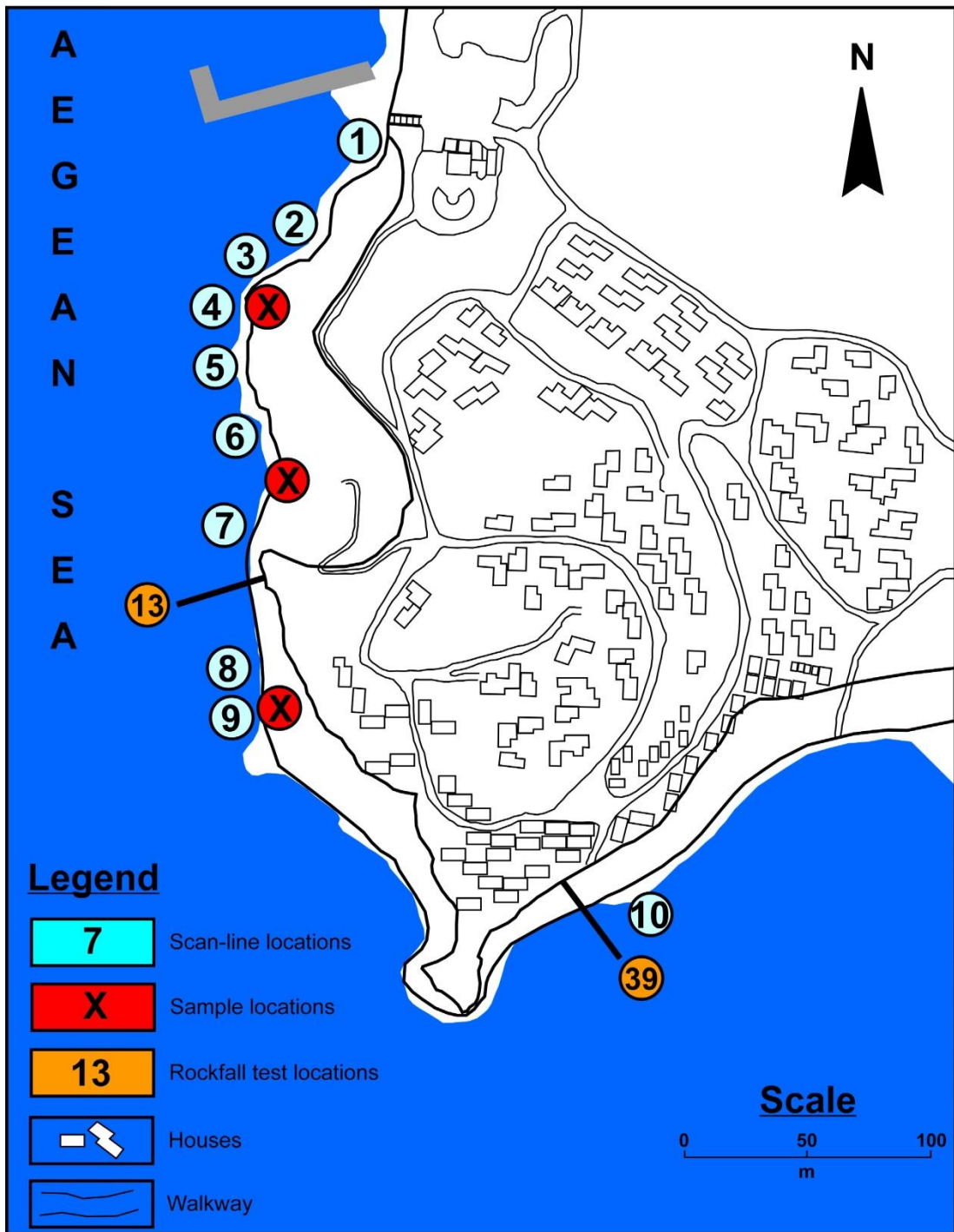
Figure 3.5 The scan-profile, sample and rockfall test locations.
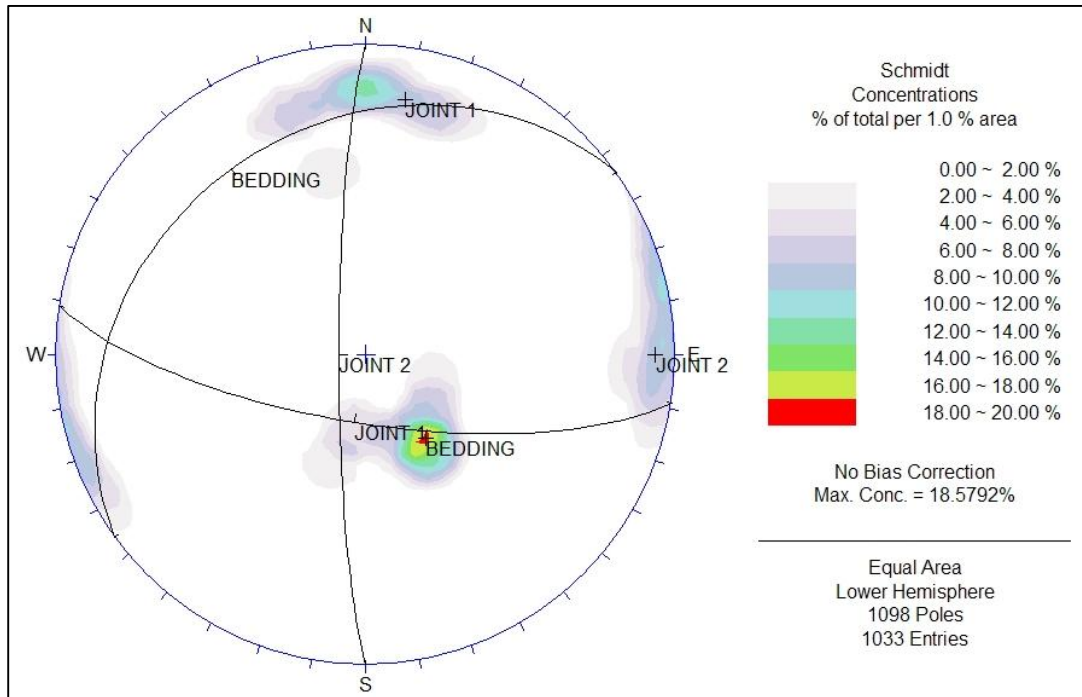
Figure 3.6 Stereographic projection (lower hemisphere) of major discontinuity sets in the study area.

In the first location, light brown, thin-bedded, moderately weathered, weak sandstone is exposed (Figure 3.7). In this area, a slide occurred parallel to the bedding plane. The new topography is therefore shaped parallel to the bedding plane and a small part of the discontinuity plane had been remained because of the vegetation in the upper elevations. The strike and dip values for the bedding plane, first joint and second joint are N56-80°E/22-33°NW, N01-11°E/70-72°NW and N63-86°W/47-77°SW, respectively. These major discontinuity sets are given in Figure 3.8. According to the kinematic analysis (Figure 3.9), any kind of failure is not expected at this location. The thickness of the layer changes between 1and 50 cm. The layers are continuous and the surface of them is rough. The joints have 35 – 180 cm spacing, tight to 1 mm aperture, and about 50 cm – 1 m persistence. The average Schmidt hardness value for hard sandstone is38. However, the Schmidt hardness measurements could not be taken from the softer levels because of the lack of rebounding. The groundwater was not encountered in the area.

Figure 3.7 Outcrops of thin-short bedded sandstone at the first location (looking west).
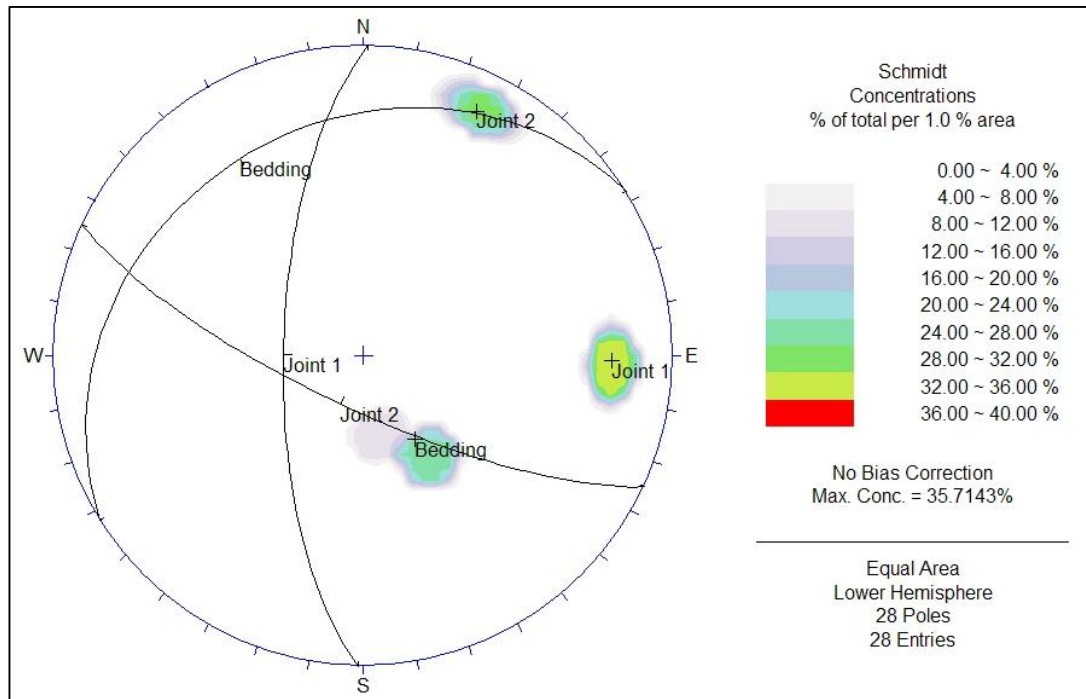
Figure 3.8 Stereographic projection (lower hemisphere) of the major discontinuity sets in the first location.
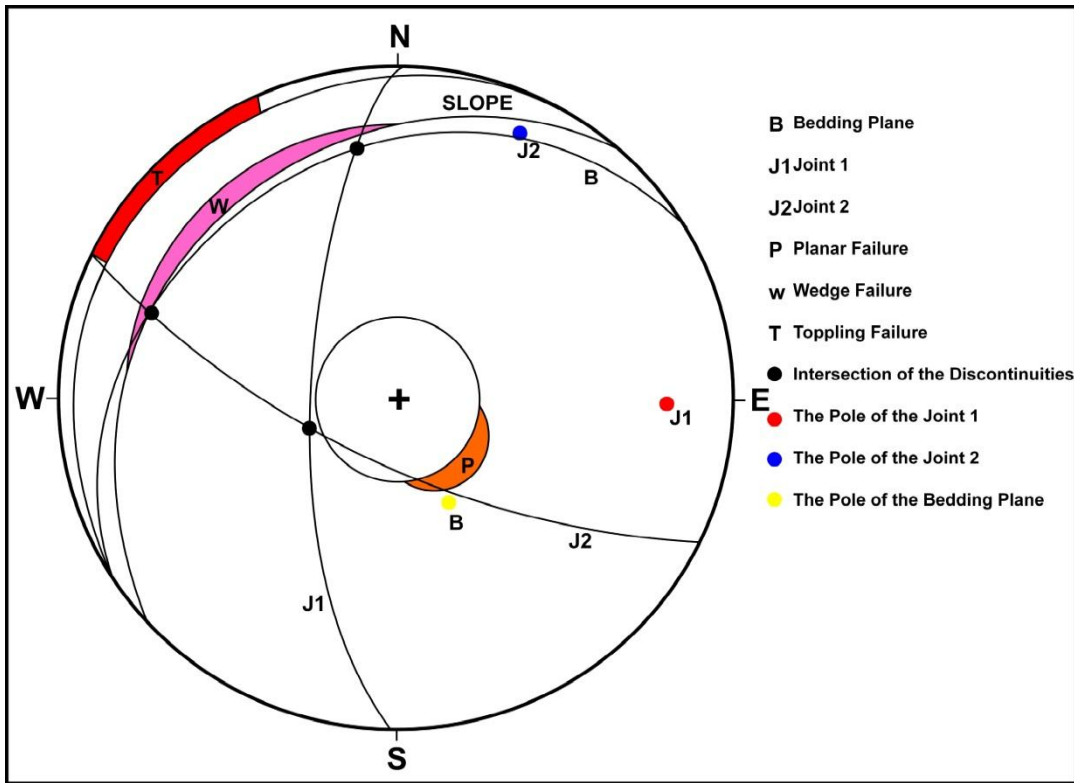
Figure 3.9 Kinematic analysis results for the location 1.

In the second location, light gray, thin-bedded (1 – 5 cm), very weak sandy siltstone is observed. The unit is like a soil rather than rock due to excessive weathering. The total thickness of this weak zone is approximately 18 m. At the upper part of this zone, sliding type (plane failure) movements and erosion could be seen (Figure 3.10). Strike/dip and Schmidt measurements could not be taken because of the soil texture. The groundwater is not encountered in the area.

In the third location, gray, thin to thick bedded, moderately weathered, alternation of weak sandstone-claystone-marl unit is observed (Figure 3.11). Similar to the first location, a sliding occurred parallel to the bedding plane. The new topography is now parallel to the bedding plane and a small part remained because of the vegetation in the upper elevations. The strike and dip values for the bedding plane, first and second joints are N75°E/34°NW, N75°E/80-85°NW and N01-12°E/85°NW, respectively. These major discontinuity sets are given in Figure 3.12. According to the kinematic analysis results (Figure 3.13), any kind of failure is not expected at this location. The thickness of the layers ranges between 2 and 30 cm. The layers are continuous and their surfaces are rough. The joints have 1 – 3 m spacing, tight to 1 mm aperture, and about 50 cm – 1 m persistence. The oxidation marks on the joint surfaces are occasional. The groundwater is not encountered in the area. The average Schmidt hardness value of the unit is 42.

28
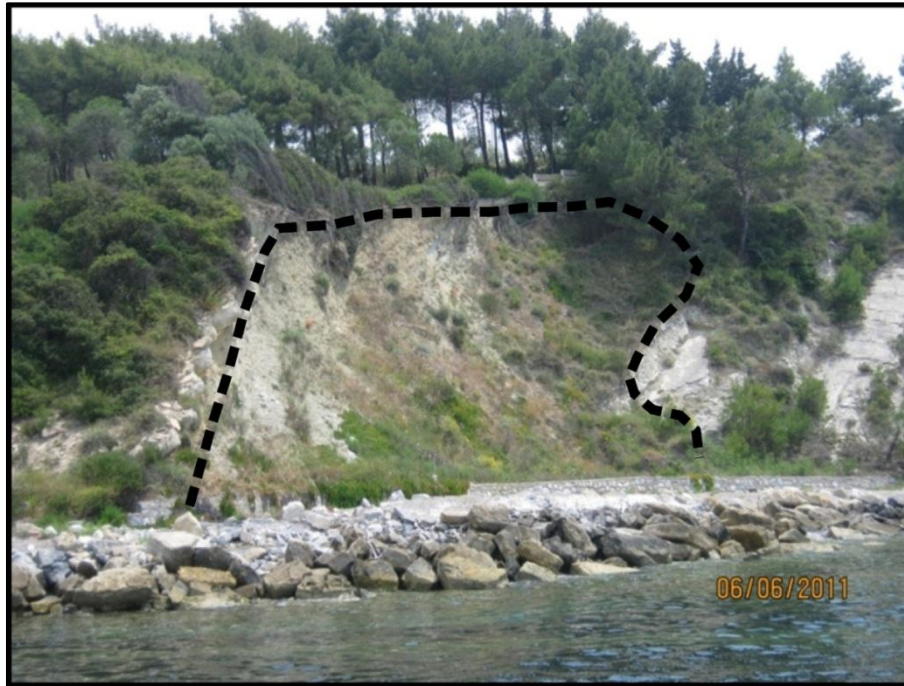
Figure 3.10 Very weak sandy siltstone unit (the plants hanging on the upper part of the slope because of the sliding and erosion can be seen) (looking northwest).
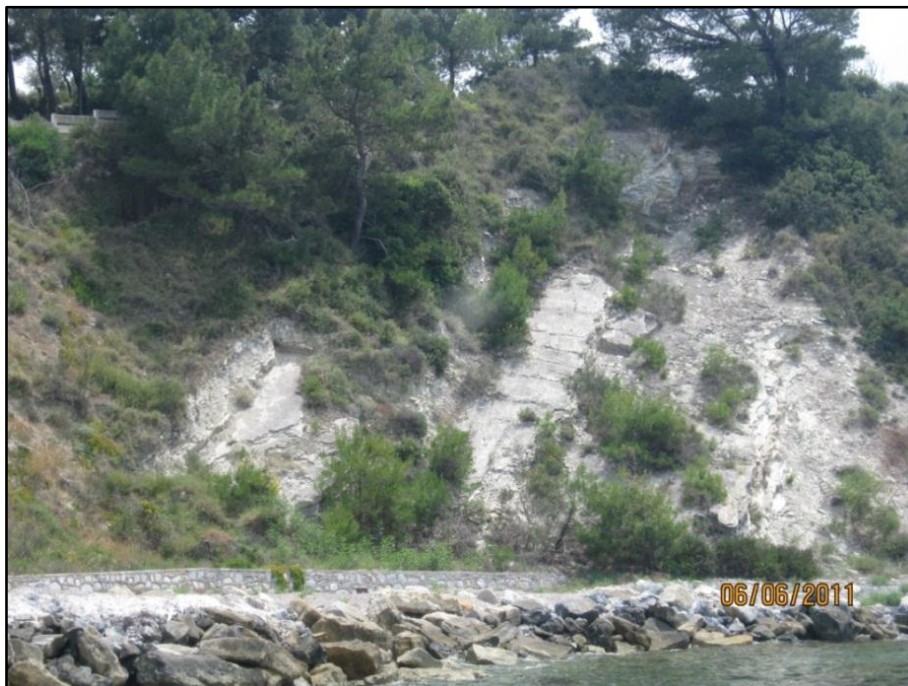
Figure 3.11 The alternation of thin bedded sandstone-claystone-marl in the third location (looking northwest).
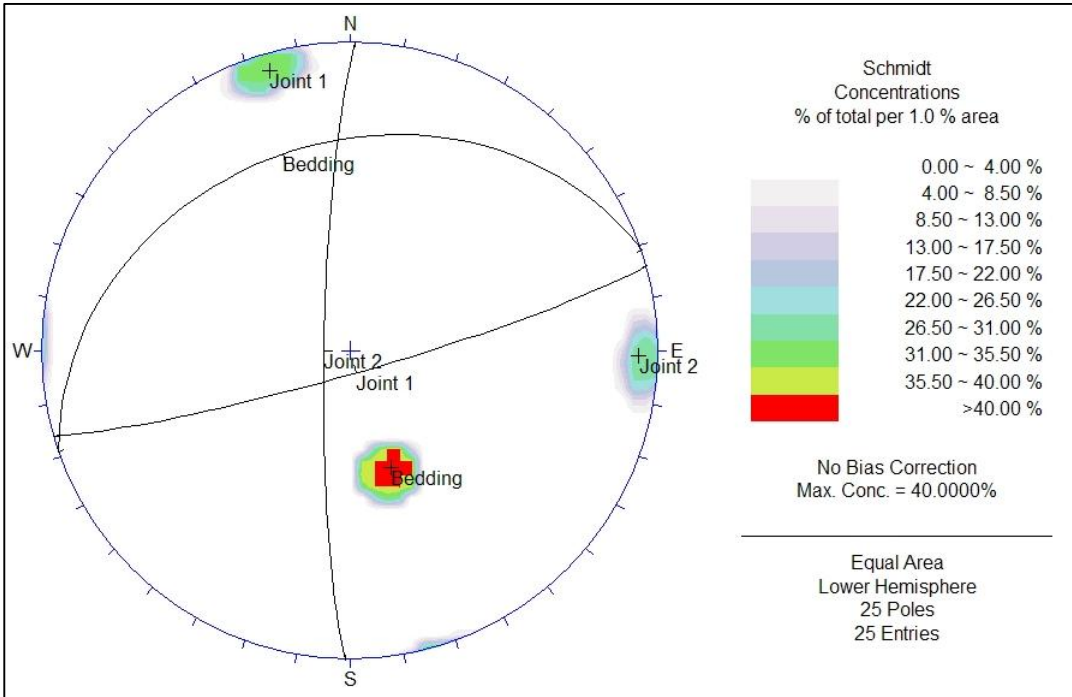
Figure 3.12 Stereographic projection (lower hemisphere) of the major discontinuity sets in the third location.
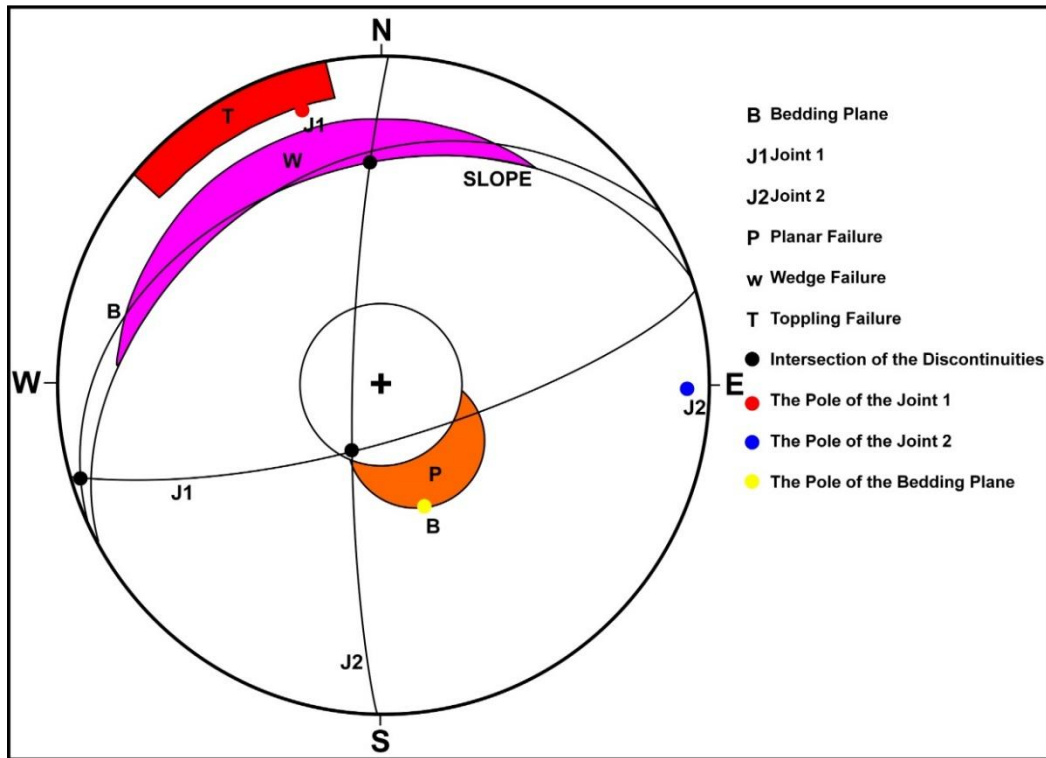
Figure 3.13 Kinematic analysis results for the location 3.

In the fourth location, gray, thin to thick bedded, slightly-moderately weathered, alternation of weak sandstone-claystone-marl unit is exposed (Figure 3.14). The strike and dip values for the bedding plane, first and second joints are N70°W/30°SW, N80°E/50°SE and N10°W/85°SW, respectively. The major discontinuity sets measured in the location are given in Figure 3.15.According to the kinematic analysis (Figure 3.16), wedge failure is expected at this location due to the bedding plane and joint 2. Because the dimension of the blocks causing to the wedge failure is too small, the failure behaves as a rockfall. The thickness of the layers ranges between 5 – 80 cm. The layers are continuous and their surfaces are rough. The joints have 40 – 70 cm spacing, tight to 1 mm aperture and about 1 m – 2 m persistence. The oxidation on the joint surfaces is occasional. The groundwater is not encountered in the area. The Schmidt hardness value varies between 36 and 39.

Figure 3.14 The alternation of thin-bedded sandstone-claystone-marl in the fourth location (looking west).
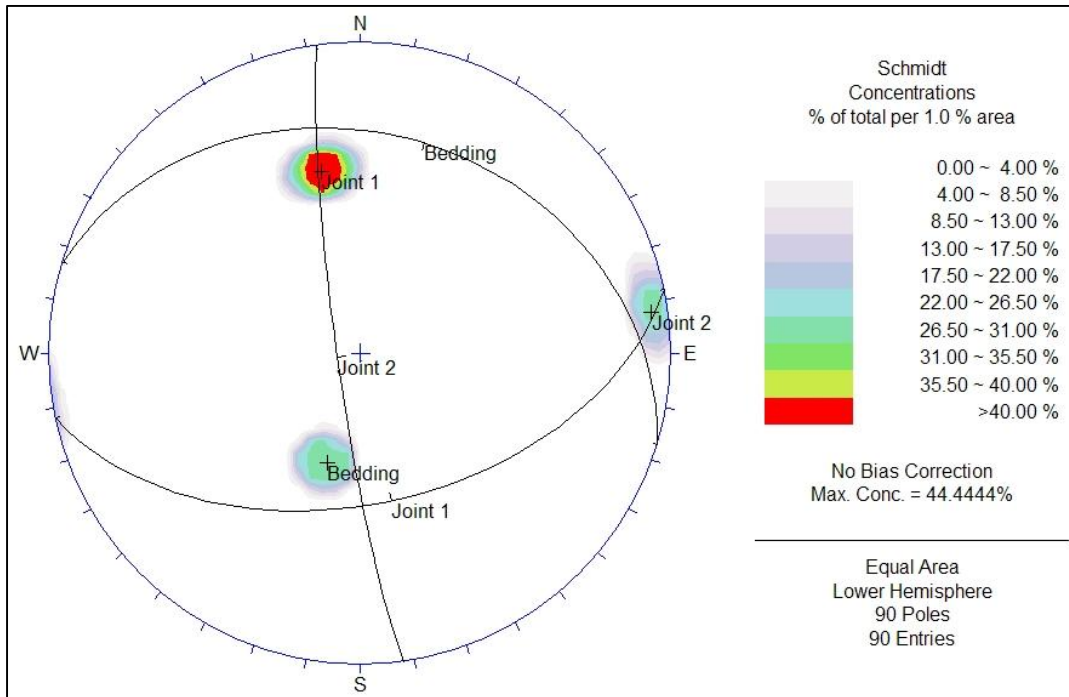
Figure 3.15 Stereographic projection (lower hemisphere) of the major discontinuity sets in the fourth location.
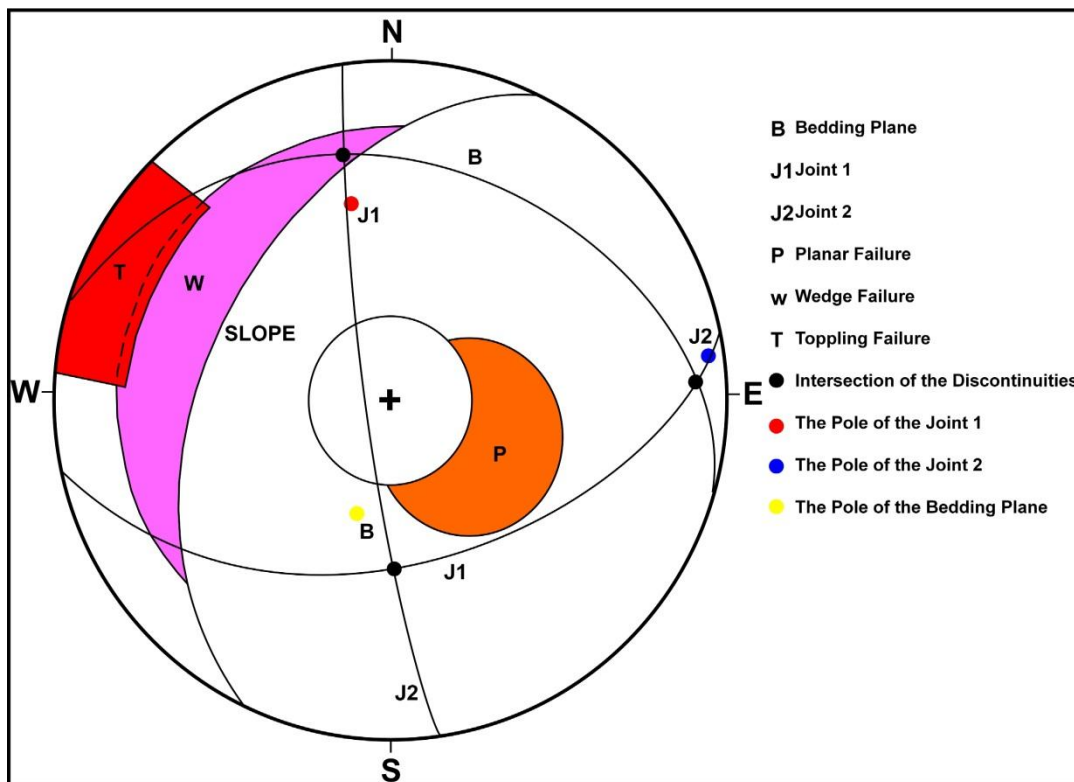
Figure 3.16 Kinematic analysis results for the location 4.

In the fifth location, gray, thin to thick bedded, slightly to moderately weathered, alternation of weak sandstone-claystone-marl unit is exposed (Figure 3.17). Any sliding problem is not expected because the cut is in dip direction but small-scale rockfalls exist. Because of the erosion of weak material, undercutting of the unit may occur. The strike and dip values for the bedding plane, first and second joints are N76°E/30°NW, N75°W/69°SW and N08°E/85°NW, respectively. The major discontinuity sets are given in Figure 3.18.According to the kinematic analysis (Figure 3.19), wedge failure between the bedding plane and joint 1 is expected at this location. Because the dimension of the blocks causing to the wedge failure is too small, the failure behaves like a rockfall. The thickness of the bedding ranges between 1 and 30 cm. The layers are continuous and their surfaces are rough. The joints have 15 – 50 cm spacing, tight to 2 mm aperture and about 20 cm – 3 m persistence. The oxidation marks on the joint surfaces are occasional. The groundwater is not encountered in the area. The average Schmidt hardness value is 42.
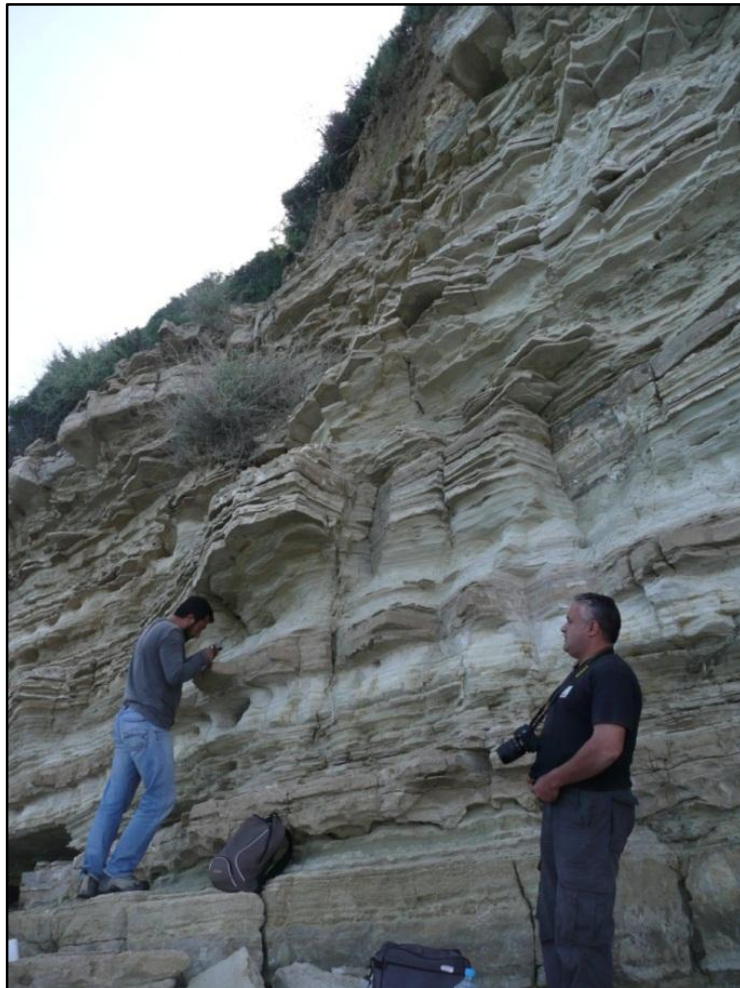
Figure 3.17 The alternation of thin-bedded sandstone-claystone-marl in the fifth location.
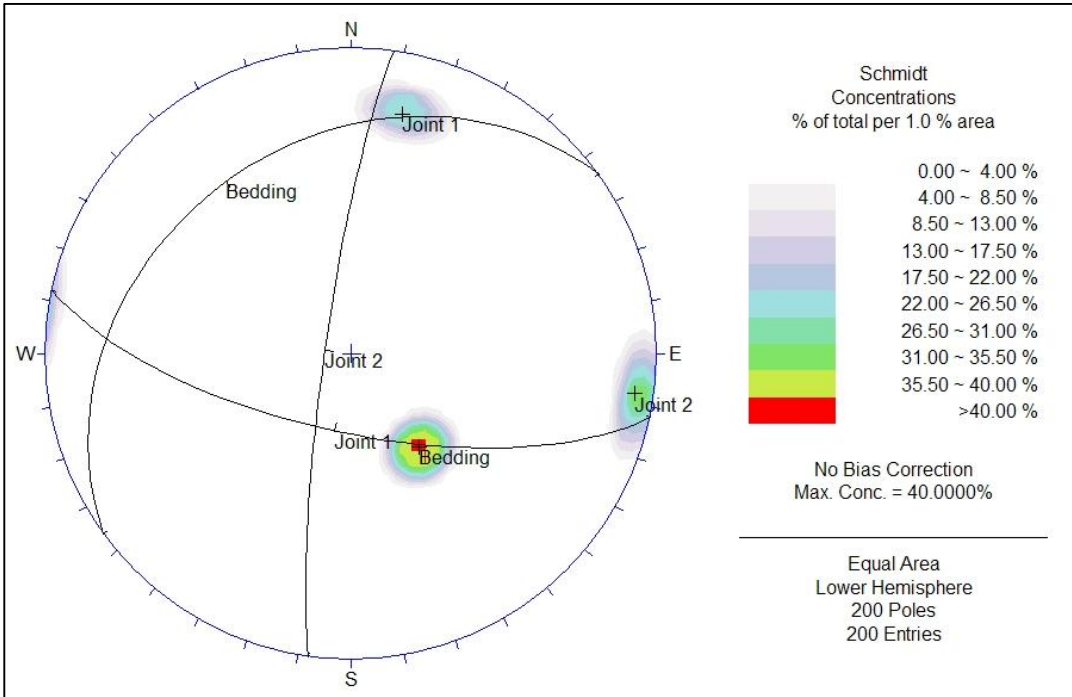
Figure 3.18 Stereographic projection (lower hemisphere) of the major discontinuity sets in the fifth location.
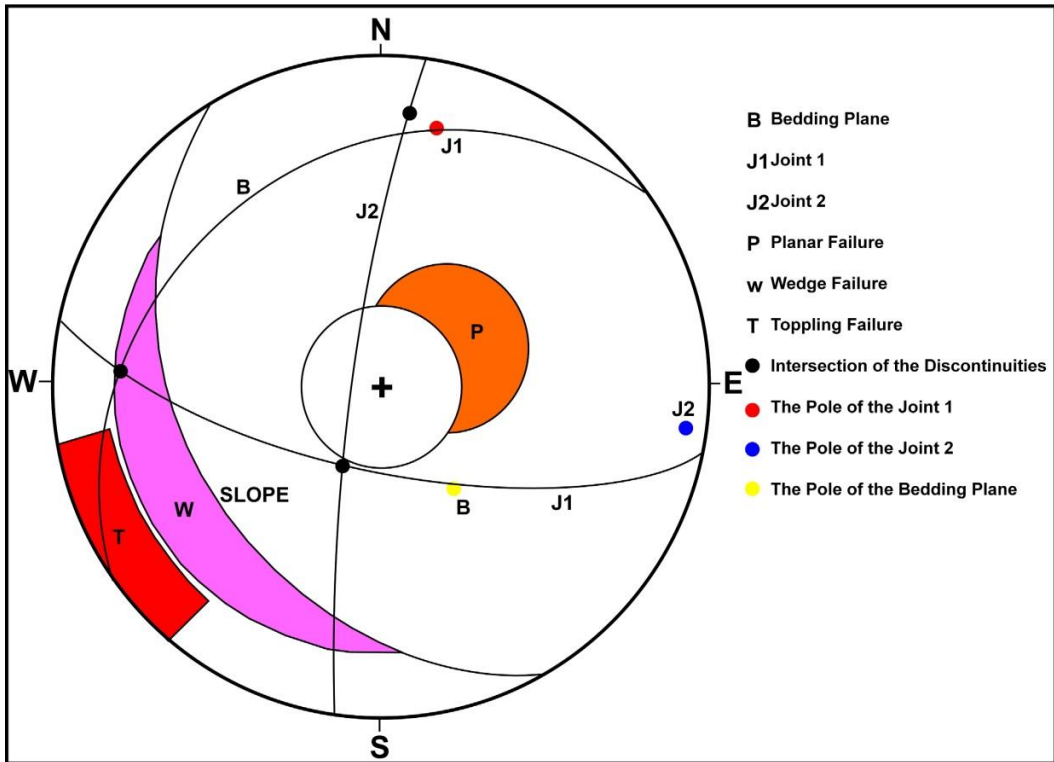
Figure 3.19 Kinematic analysis results for the location 5.

The sixth location has the same properties with the previous location. In this area, gray, thin to thick bedded, slightly to moderately weathered, alternation of weak sandstone-claystone-marl unit is observed (Figure 3.20). Any sliding problem is not expected because the cut is in dip direction but small-scale rockfalls may occur. Because of the erosion of the weak material, undercutting of the formation may occur. The strike and dip values for the bedding plane, first and second joints are N65°E/24°NW, N70°W/72°SW and N01°E/77°NW, respectively. These major discontinuity sets are given in Figure 3.21. According to the kinematic analysis (Figure 3.22), any kind of failure is not expected at this location. The thickness of the layer ranges between 1 and 30 cm. The layers are continuous and the surface of them is rough. The joints have 10 – 20 cm spacing, tight to 1 mm aperture and about 20 cm – 3 m persistence. The oxidation marks on the joint surfaces are occasional. The groundwater is not encountered in the area. The average Schmidt hardness value is44.
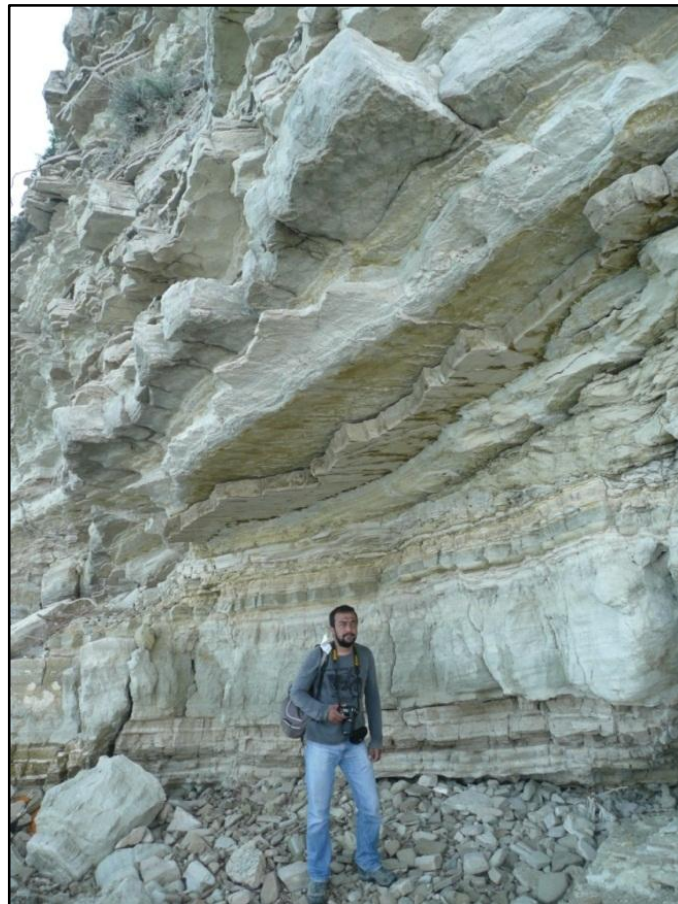
Figure 3.20 The appearance of the alternation of thin-bedded sandstone-claystone-marl in the sixth location (looking northwest).
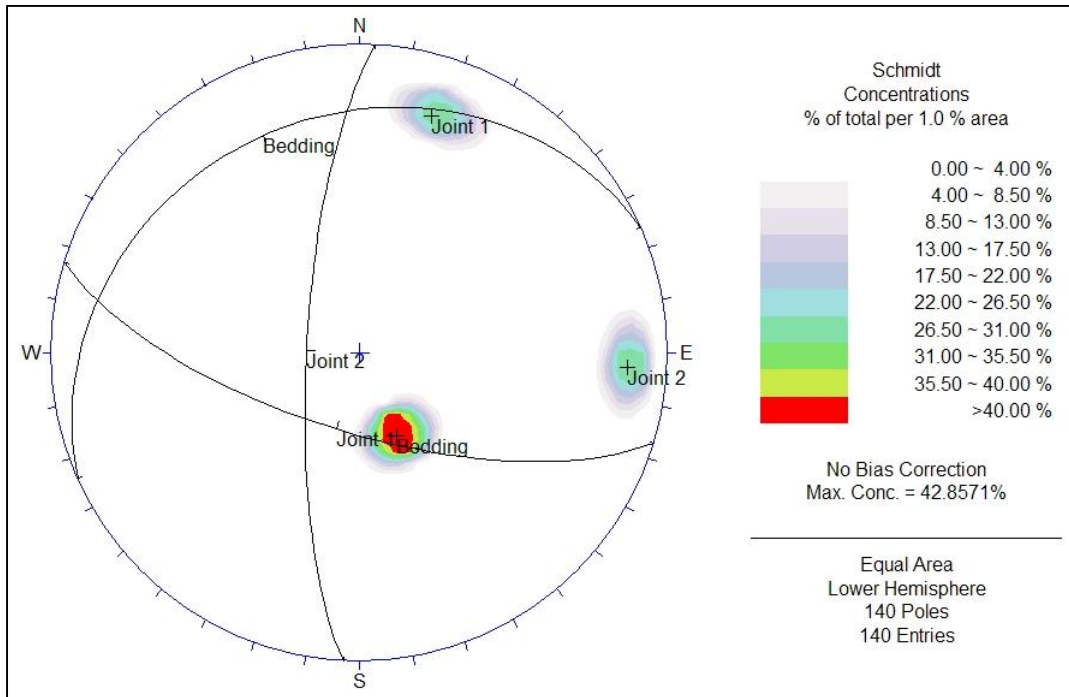
Figure 3.21 Stereographic projection (lower hemisphere) of the major discontinuity sets in the sixth location.
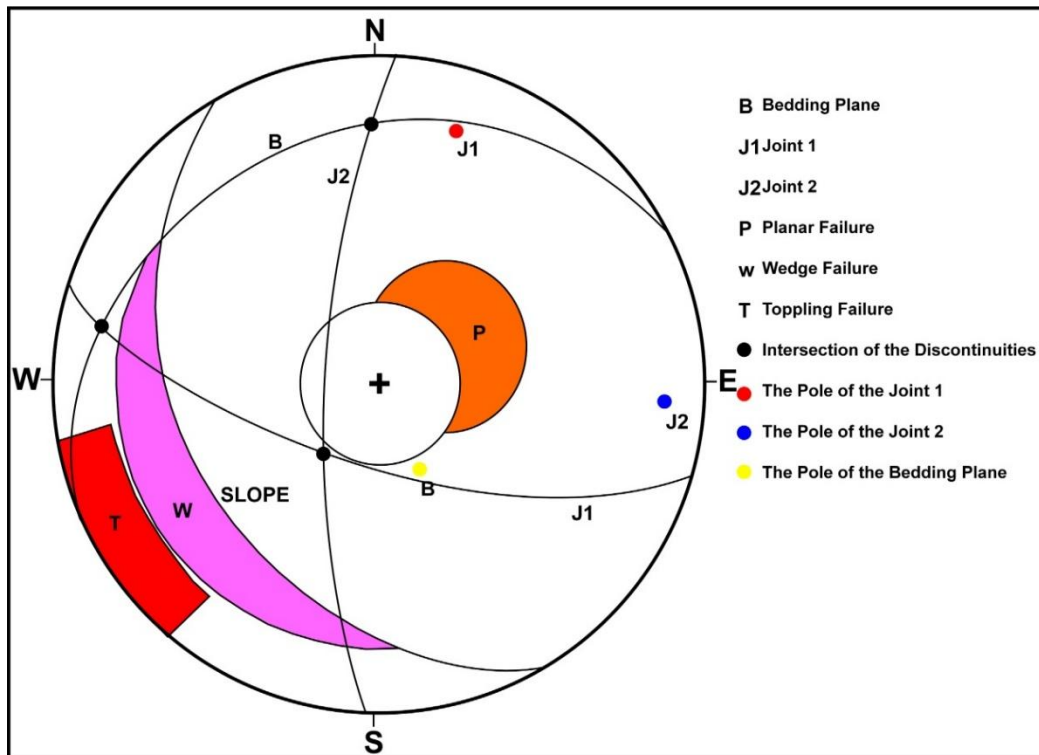

Figure 3.22 Kinematic analysis results for the location 6.

The seventh location has the same properties with the fifth location. In this area, gray, thin to thick bedded, slightly to moderately weathered, alternation of weak sandstone-claystone-marl unit is observed (Figure 3.23). Any sliding problem is not expected because the cut is in dip direction but small-scale rockfalls may occur. The cavities are formed by undercutting of the sea and a zone prone to fall is formed at the upper part of this zone. The strike and dip values for the bedding plane, first and second joints are N80°W/20°NE, N85°W/85°SW and N10°W/85°SW, respectively. These major discontinuity sets are given in Figure 3.24. According to the kinematic analysis (Figure 3.25), any kind of failure is not expected at this location. The thickness of the layers ranges between 1 and 50 cm. The layers are continuous and their surfaces are rough. The joints have 10 – 40 cm spacing, tight to 1 mm aperture and about 20 cm – 2 m persistence. The oxidation marks and calcite infilling on the joint surfaces are occasional. The groundwater is not encountered in the area. The average Schmidt hardness value is 39.

Figure 3.23 The appearance of the alternation of thin-bedded sandstone-claystone-marl in the seventh location (looking northwest).
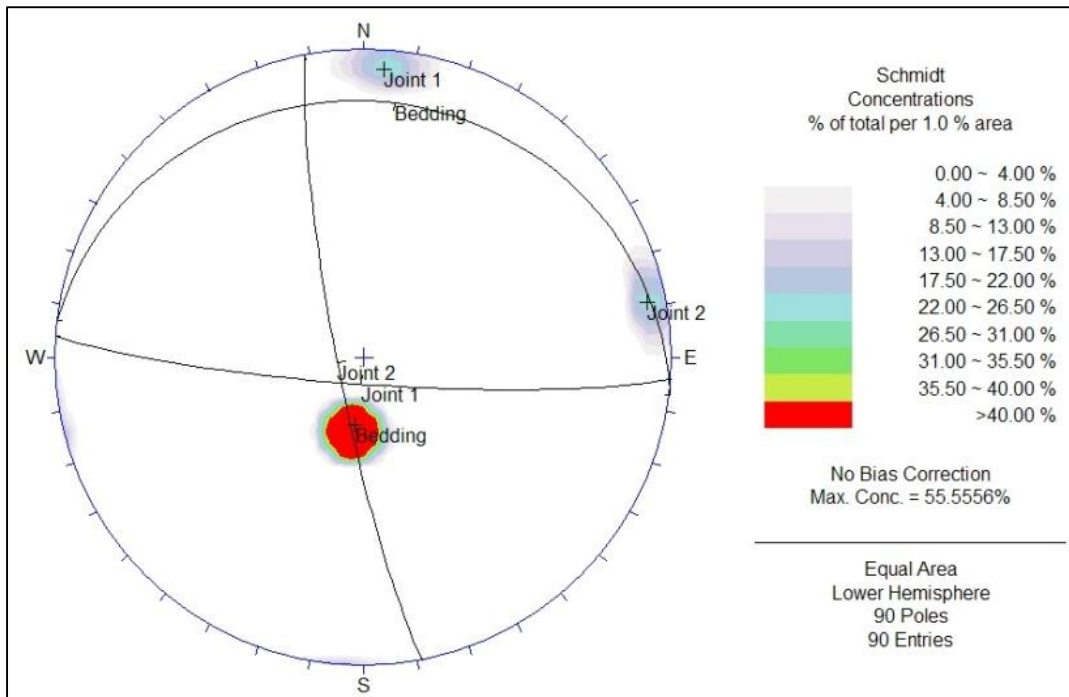
Figure 3.24 Stereographic projection (lower hemisphere) of the major discontinuity sets in the seventh location.
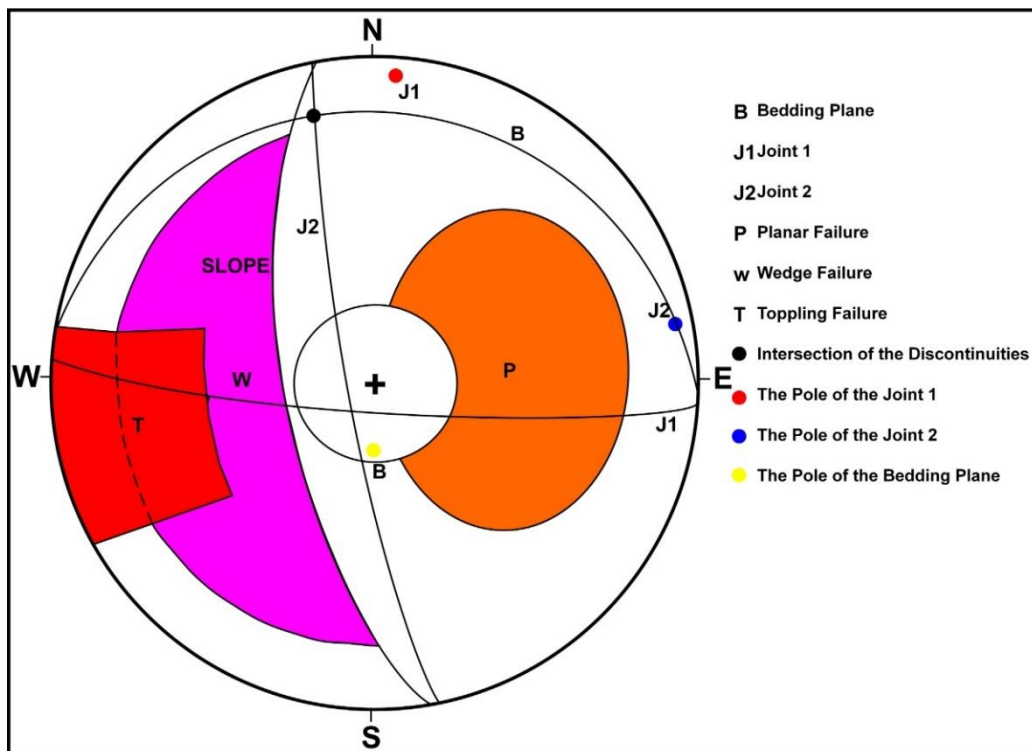
Figure 3.25 Kinematic analysis results for the location 7.

The eighth location has the same properties with the fifth location. In this area, gray, thin to thick bedded, slightly-moderately weathered, alternation of weak sandstone-claystone-marl unit is exposed (Figure 3.26). Any sliding problem is not expected because the cut is in dip direction but small-scale rockfalls may occur. The cavities are formed by undercutting of the sea and a zone prone to collapse is formed at the upper part of this zone. The strike and dip values for the bedding plane, first and second joints are N58°E/30°NW, N18°W/88°SW and N88°E/74°SE, respectively. These major discontinuity sets are given in Figure 3.27. According to the kinematic analysis (Figure 3.28), any kind of failure is not expected at this location. The thickness of the layers ranges between 1 and 50 cm. The layers are continuous and the surface of them is rough. The joints have 10 – 30 cm spacing, tight to 1 mm aperture and about 20 cm – 2 m persistence. The oxidation marks and calcite infilling on the joint surfaces are occasional. The groundwater is not encountered in the area. The average Schmidt hardness value is 44.

Figure 3.26 The alternation of thin-bedded, cavernous sandstone- claystone-marl in the eighth location (looking west).
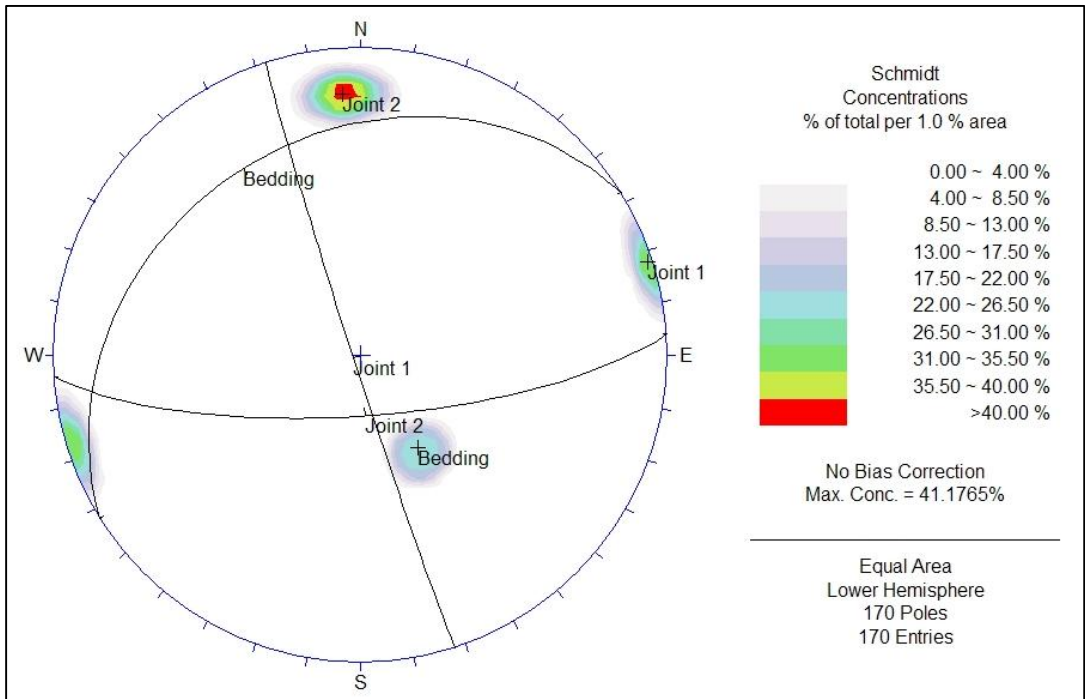
Figure 3.27 Stereographic projection (lower hemisphere) of the major discontinuity sets in the eighth location.
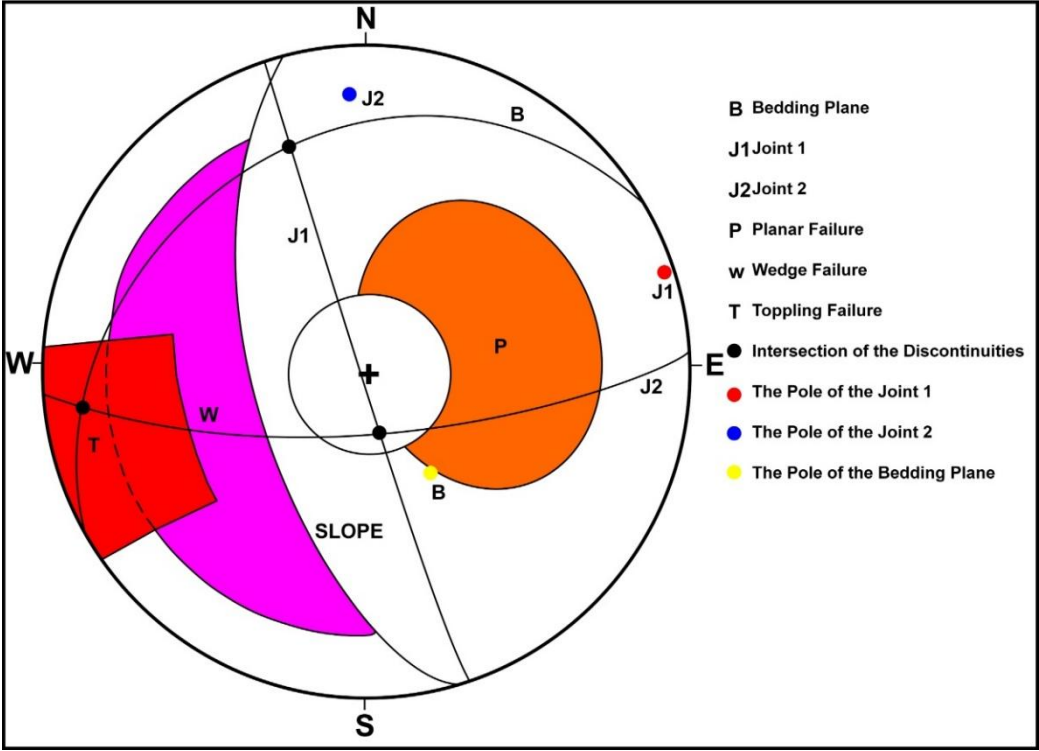

Figure 3.28 Kinematic analysis results for the location 8.

The ninth location has the same properties with the fifth location. In this area, gray, thin to thick bedded, slightly to moderately weathered, alternation of weak sandstone-claystone-marl unit is exposed (Figure 3.29). Any sliding problem is not expected because the cut is in dip direction but small-scale rockfalls may occur. Quite big cavities (5 – 6 m depth) are formed by undercutting of the sea. The strike and dip values for the bedding plane, first and second joints are N43°E/23°NW, N85°W/75°SW and N03°W/88°NE, respectively. These major discontinuity sets are given in Figure 3.30.According to the kinematic analysis (Figure 3.31), any kind of failure is not expected at this location. The thickness of the layers ranges between 1 and 40 cm. The layers are continuous and the surface of them is smooth. The joints have 10 – 30 cm spacing, tight to 1 mm aperture and about 20 cm – 1 m persistence. The oxidation marks on the joint surfaces are occasional. The groundwater is not encountered in the area. The average Schmidt hardness value of the unit is 40.

Figure 3.29 The alternation of thin-bedded, cavernous sandstone-claystone-marl in the ninth location (looking west).
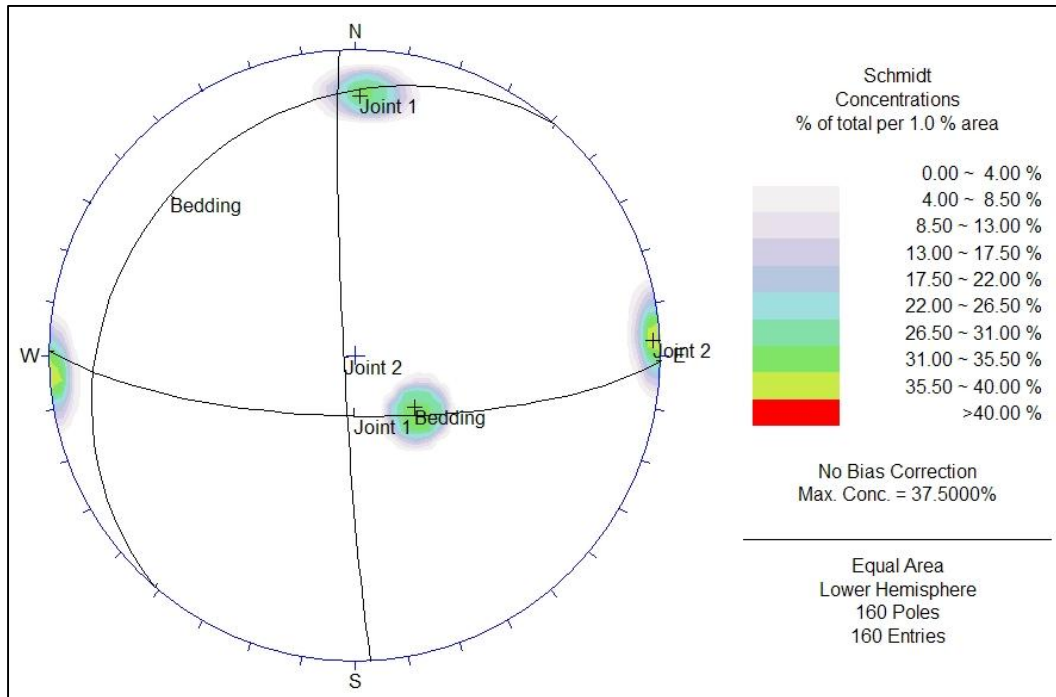
Figure 3.30 Stereographic projection (lower hemisphere) of the major discontinuity sets in the ninth location.
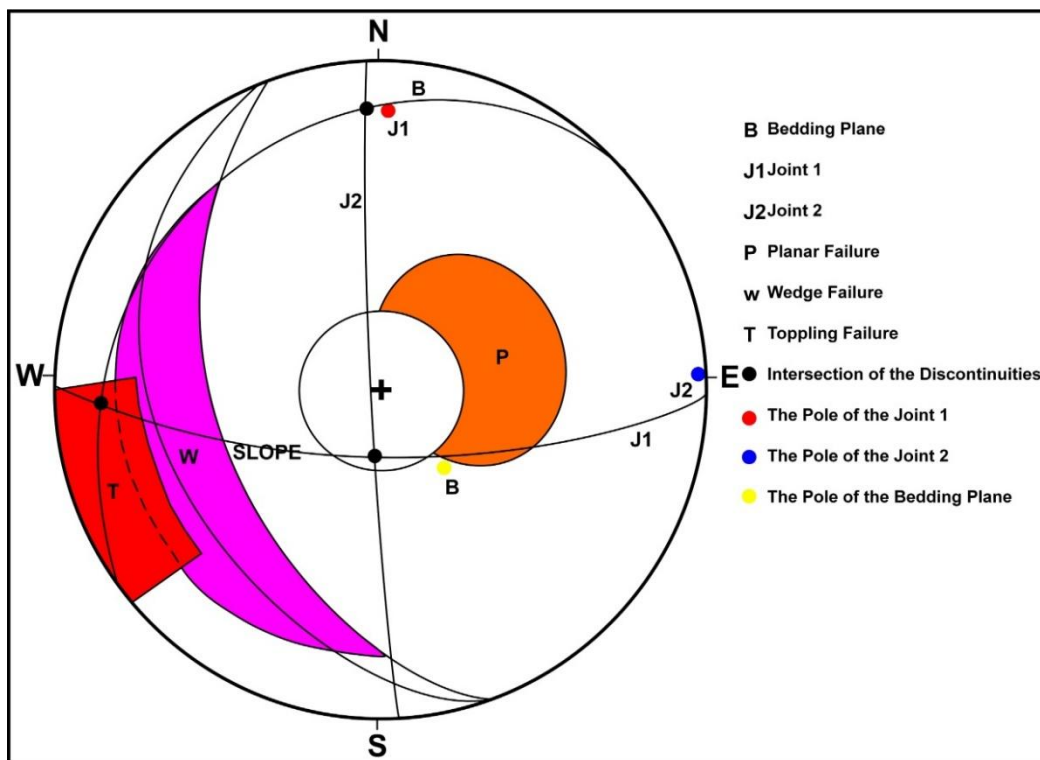
Figure 3.31 Kinematic analysis results for the location 9.

The tenth location is located in the south of the study area. In this area, gray, thin to thick bedded, slightly to moderately weathered, alternation of weak sandstone-claystone-marl unit is exposed. Soil cover is much more than the other studied locations (Figure 3.32). The small rock particles may fall from the cliff which is parallel to the strike of the slope. In this section, it is possible to see small size undercutting. The strike and dip values for the bedding plane, first and second joints are N20°E/19°NW, N72°E/70°SE and N28°W/87°NE, respectively. These major discontinuity sets are given in Figure 3.33. According to the kinematic analysis (Figure 3.34), any kind of failure is not expected at this location. The thickness of the layers ranges between 1 and 20 cm. The layers are continuous and the surface of them is rough. The joints have 10 – 30 cm spacing, tight to 1 mm aperture and about 20 cm – 50 cm (sometimes up to 1 m) persistence. The oxidation marks on the joint surfaces are occasional. The groundwater is not encountered in the area. The average Schmidt hardness value is 17.


Figure 3.32 The alternation of thin-bedded sandstone-claystone-marl in the tenth location (looking east).
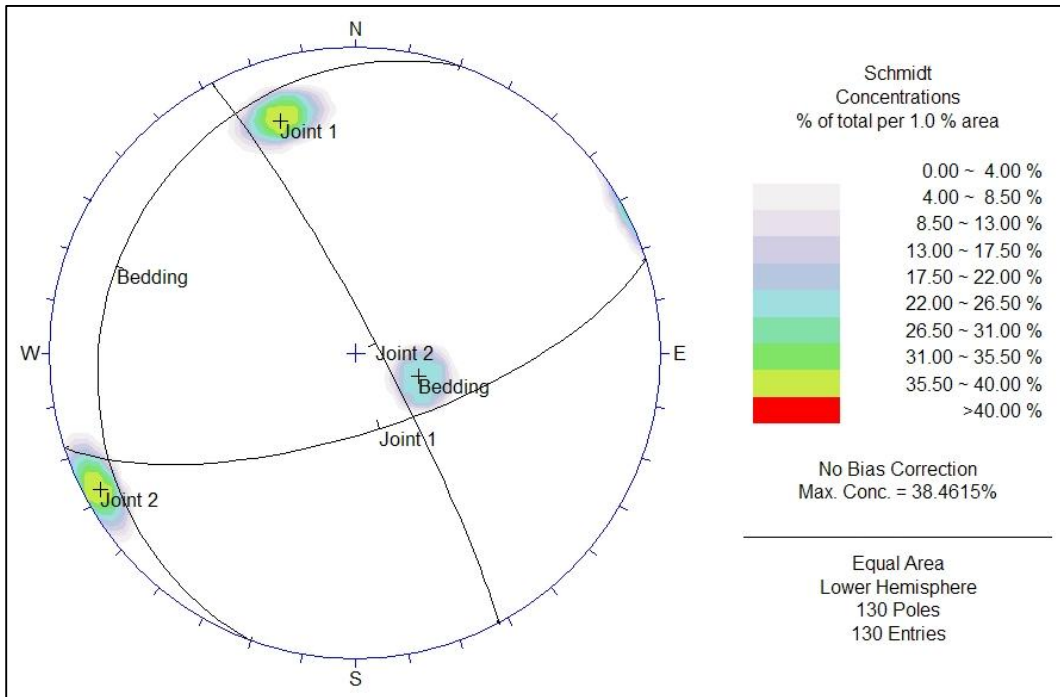
Figure 3.33 Stereographic projection (lower hemisphere) of the major discontinuity sets in the tenth location.
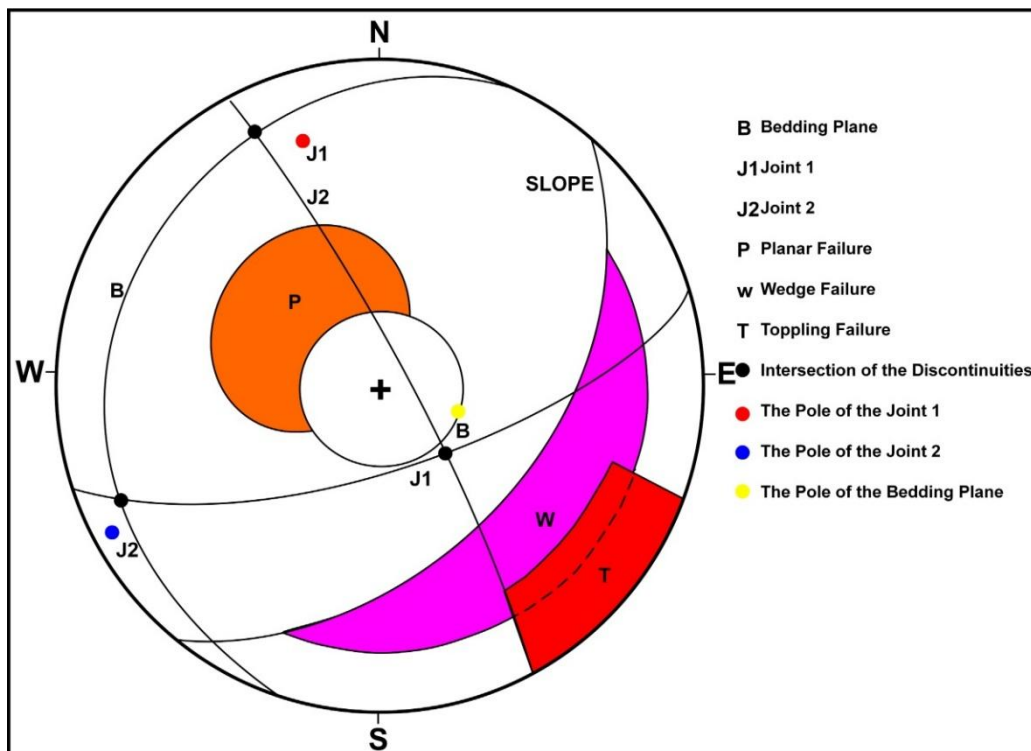
Figure 3.34 Kinematic analysis results for the location 10.

Beside the scan-profile survey, the coefficient of restitution, which is one of the most important parameters affecting the rockfall analyses, was defined by the help of the rockfall analyses. In the field, 66 block samples were fallen along the two different sections. The detailed information about these analyses will be given in Chapter IV on "Slope Stability and Rockfall Analyses".

3.2.2 Laboratory Studies

In the laboratory studies, unit weight, effective porosity, water absorption and point load strength tests were performed on ten samples taken from the field according to ISRM (1981) and (1985). According to the tests performed on intact siltstone-marl (Table 3.1), 23.60 kN/m^3 and 24.48 kN/m^3 are the dry and saturated unit weights, respectively. Effective porosity and water absorption values are 9.01% and 3.89%, respectively. According to the point load strength test results, Is$_{(50)}$ value is 6.06 MPa. Because the claystone is very weak, the sampling could not be performed. The terrestrial units have moderate unit weight and porosity with respect to Anon (1979).

Table 3.1 Laboratory results of the samples taken from the field.

TESTS PERFORMED	NUMBER OF SAMPLES	AVERAGE VALUE
Unit weight-dry (kN/m^3)	10	23.60
Unit weight-saturated (kN/m^3)	10	24.48
Point load strength (MPa)	10	6.06
Effective porosity (%)	10	9.01
Water absorption by weight (%)	10	3.89

CHAPTER 4

SLOPE STABILITY AND ROCKFALL ANALYSES

Planar failures occurred in the past were observed in the northern region of the study area. Because the dip of the slope and dip of the layer are the same, planar failure is not expected except in a very small area (Figure 4.1). The wedge failure is expected in the fourth and fifth locations. Because the dimension of the blocks causing to the wedge failure is too small, the failures behave as a rockfall. The toppling failure is not expected.

Figure 4.1 A small scale planar failure view from the field (looking west).

Because the cliffs at the coast are steep and high, detailed circular rock mass failure and rockfall analyses were carried out along 43 cross-sections (Figure 4.2). Details of these analyses will be given in the following sections.
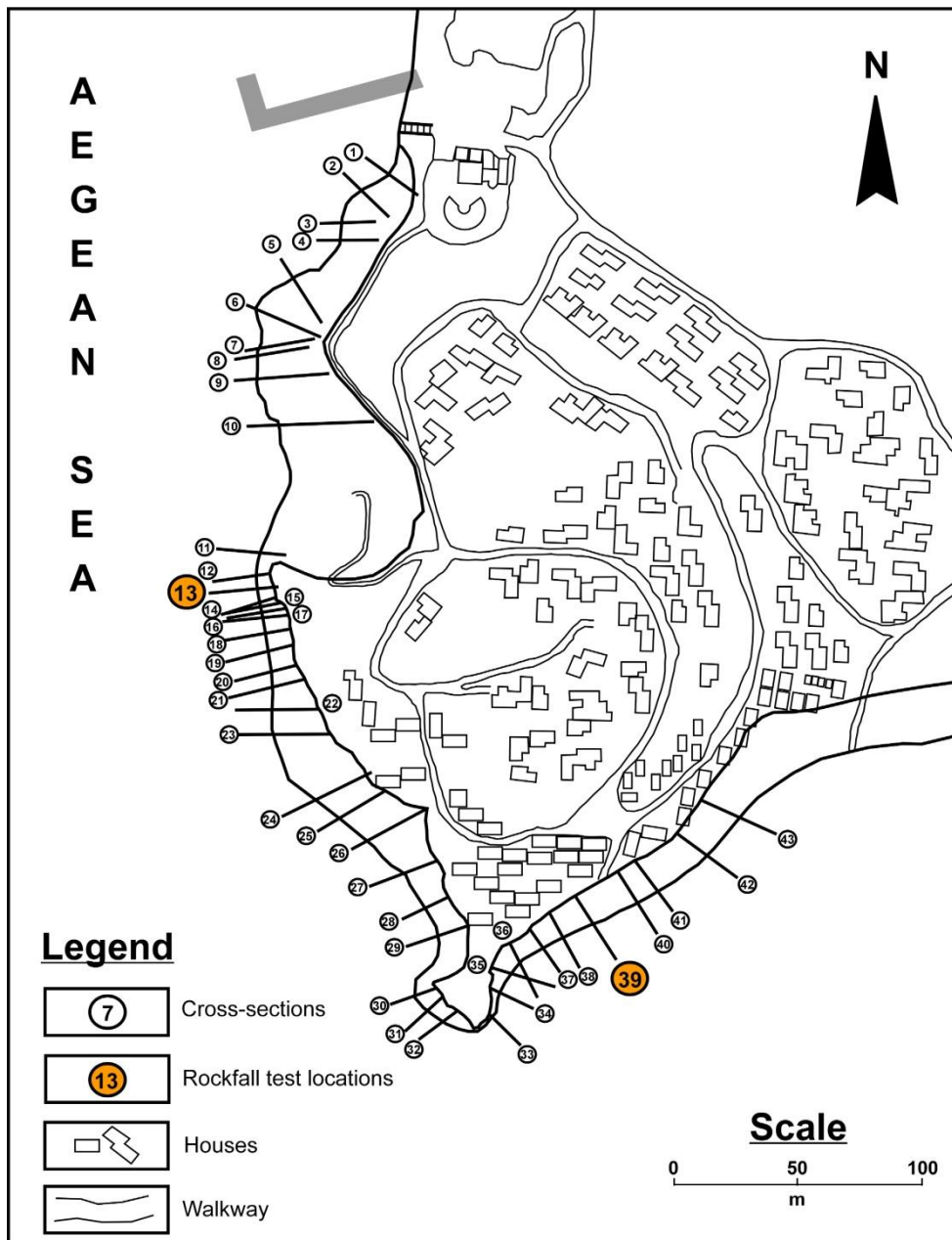
Figure 4.2 Locations of the cross-sections for the rock mass failure and rockfall analyses.

4.1 Rock Mass Stability Analyses

Limit equilibrium analyses were performed to investigate the mass stability of the cliffs along 43 cross-sections. The required shear strength parameters for the limit equilibrium analyses were obtained by using RocLab 1.0 (Rocscience, 2007). Geological Strength Index (GSI) was defined as shown in Figure 4.3. Because of blocky structure and very poor surface conditions, the GSI value was defined as 33. The uniaxial compressive strength (σ) = 35 MPa, Geological Strength Index (GSI) = 33, the intact rock parameter (mi) = 5 and Disturbance

Factor (D) = 0.7 were used as input values in the RocLab software. The uniaxial compressive strength value was obtained by correlating the average Schmidt hardness and unit weight values. The shear strength parameters (c, ϕ) were determined by considering the height of every cross-section (Figure 4.4).
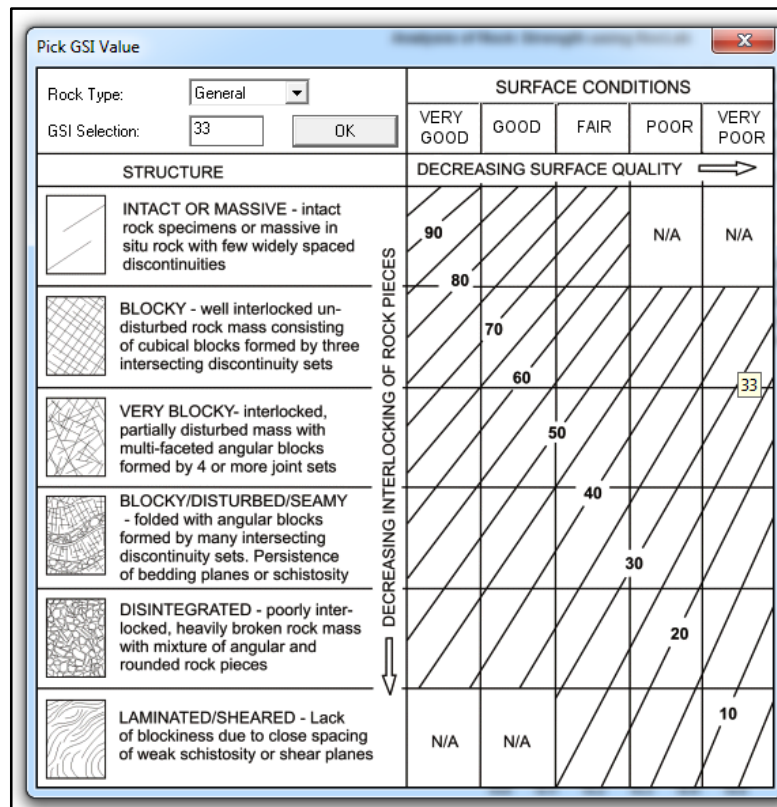
Figure 4.3 The graph used for determining the GSI value (Rocscience, 2007).
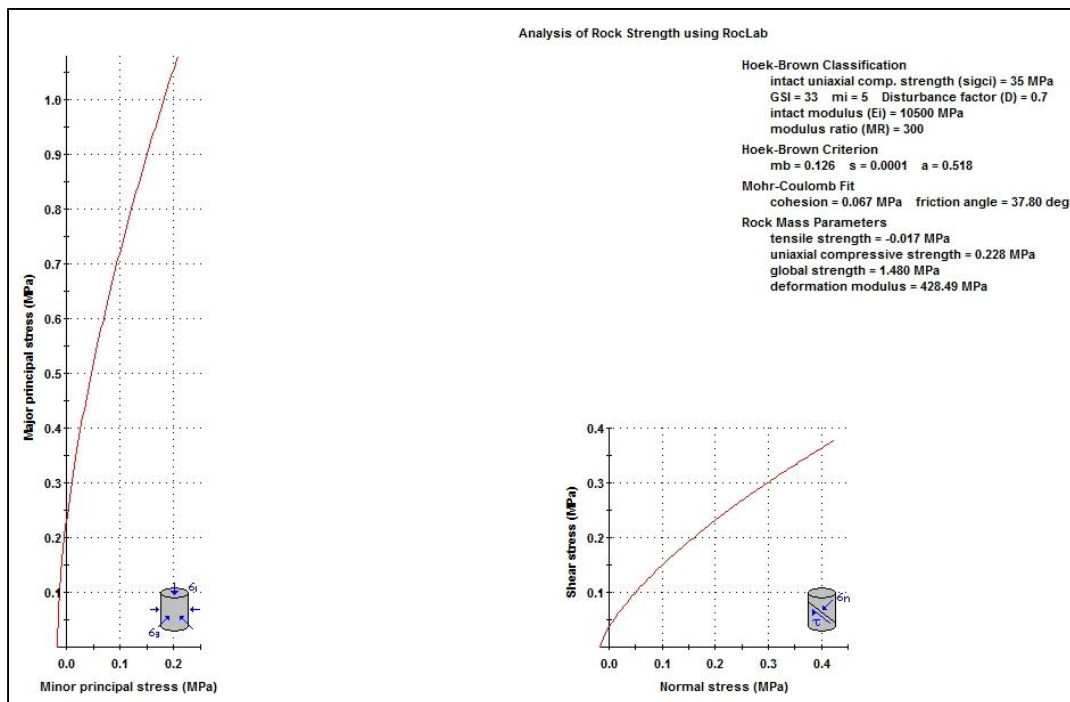
Figure 4.4 The shear strength values for a typical slope (Rocscience, 2007).

The obtained shear strength values were used in Slide 5.1 software (Rocscience, 2004b). Limit equilibrium analyses were performed separately for three different conditions at every slope cross-section (original slope, 5 m inclined slope and 5 m inclined one-benched slope). The rock mass was divided into 30 slices and analyzed with Simplified Bishop Method. Maximum horizontal ground acceleration value of 0.15g is considered for the analyses. Because the groundwater is not encountered in the area, the analyses were performed in dry conditions. The saturated unit weight value was used to represent the rainy conditions. The typical examples of limit equilibrium analysis for the 39th profile of the original, 5 meter inclined and 5 meter inclined one-benched slope are given in Figures 4.5, 4.6 and 4.7, respectively. The factors of safety values for all slope types are much higher than 1.5 for all three slope conditions (Table 4.1). That is why circular mass failures are not expected in the cliffs of the study area.
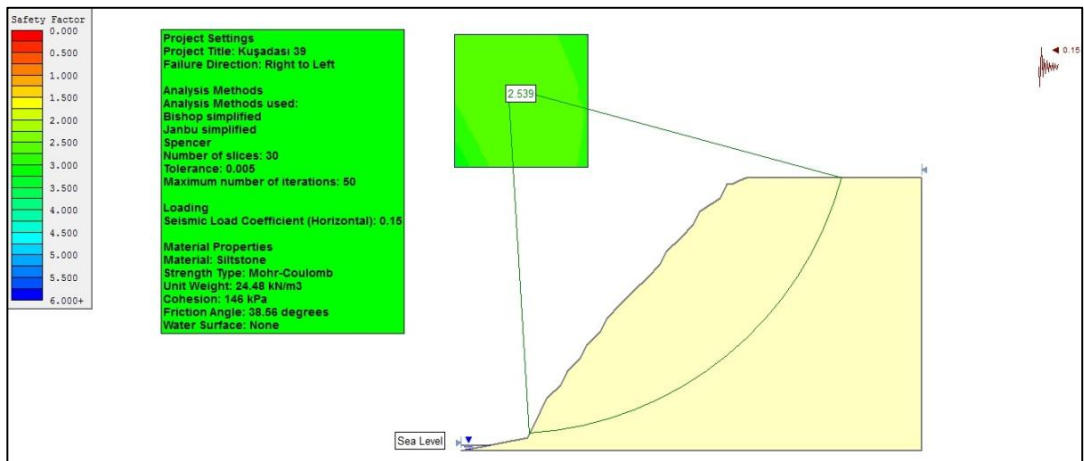
Figure 4.5 The result of limit equilibrium analysis for the 39th profile of the original slope.
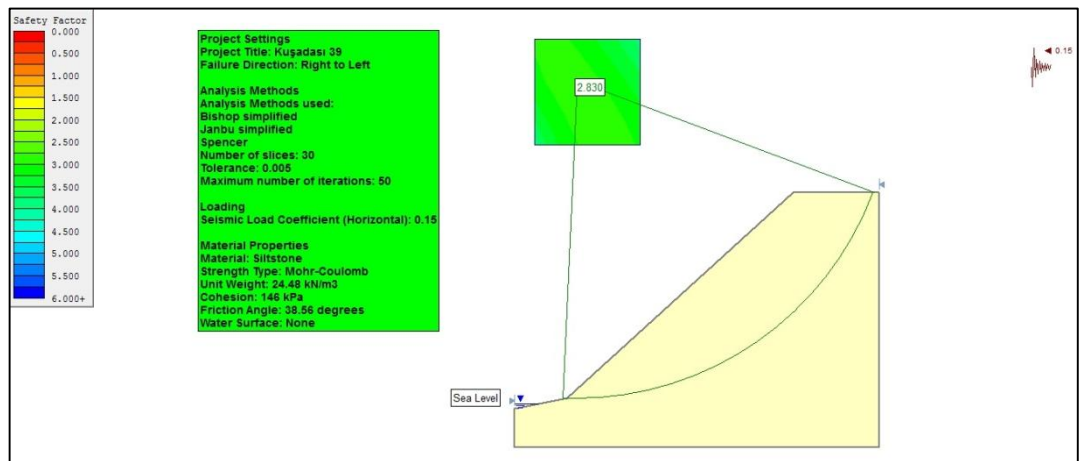
Figure 4.6 The result of limit equilibrium analysis for the 39th profile of the 5 meter inclined slope.
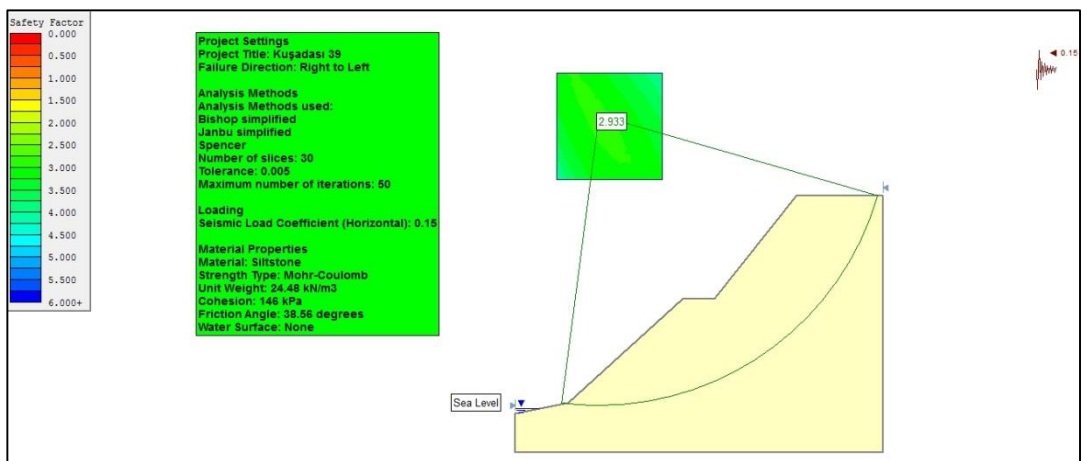
Figure 4.7 The result of limit equilibrium analysis for the 39th profile of the 5 meter inclined one-benched slope.

Table 4.1 The factor of safety values of the 43 profiles for three different slope conditions.

PROFILE NUMBER	FACTOR OF SAFETY		
	ORIGINAL SLOPE	5 M INCLINED SLOPE	BENCHED SLOPE
Profile 1	3.63	3.94	4.01
Profile 2	3.65	3.67	3.74
Profile 3	3.85	4.38	4.46
Profile 4	2.37	2.70	2.74
Profile 5	3.12	3.30	3.34
Profile 6	3.13	3.50	3.60
Profile 7	2.80	3.12	3.18
Profile 8.1	2.83	3.11	3.15
Profile 9.1	3.13	3.34	3.39
Profile 10	2.88	3.09	3.13
Profile 11	2.75	3.44	3.66
Profile 12	2.43	3.00	3.11
Profile 13	2.43	2.93	3.03
Profile 14	2.52	2.85	2.94
Profile 15	2.54	2.90	2.99
Profile 16	2.36	2.74	2.82
Profile 17	2.47	2.86	2.93
Profile 18	2.35	2.65	2.72
Profile 19	2.10	2.39	2.46
Profile 20	2.03	2.24	2.30
Profile 21	2.09	2.31	2.37
Profile 22	2.67	2.83	2.88
Profile 23	2.68	2.84	2.87
Profile 24	2.62	2.84	2.92
Profile 25	2.61	2.86	2.96
Profile 26	2.72	2.88	2.95
Profile 27	2.97	3.21	3.25
Profile 28	2.85	3.47	3.54
Profile 29	3.41	3.75	3.82
Profile 30	4.20	4.47	4.55
Profile 31	3.92	4.38	4.46
Profile 32	4.03	4.60	4.71
Profile 33	2.71	4.44	5.76
Profile 34	3.45	4.23	4.54
Profile 35	3.82	4.35	4.55
Profile 36	2.89	3.58	3.67
Profile 37	1.88	2.19	2.26
Profile 38	2.80	3.14	3.20
Profile 39	2.54	2.83	2.93
Profile 40	1.66	1.87	1.91
Profile 41	2.69	2.94	3.05
Profile 42	2.61	2.93	3.03
Profile 43	2.67	2.94	3.01

4.2 Rockfall Analyses

2-D and 3-D rockfall analyses were performed respectively. Through the use of the data obtained from these analyses, a comprehensive discussion was performed to compare the results.

4.2.1 2-D Analysis

To perform the 2-D rockfall analyses, the dimensions of the blocks must be defined in the field. The dimension of these blocks prone to fall was defined by analyzing the dimension and positions of the fallen blocks and by the scan-profile survey data performed in ten locations. In this context, the representative blocks were selected. A total of 66 rock blocks were fallen along the profile 13 (Figures 4.8 and 4.9) and the profile 39 (Figures 4.10 and 4.11) by dividing the number of rock blocks into two equal parts to define the normal and tangential coefficient of restitutions (R_n and R_t). The RocFall 4.0 software (Rocscience, 2004c) was used for the 2-D rockfall analyses. As a result of the back analysis of the blocks reached up to coast, the $R_n = 0.28 \pm 0.06$ and the $R_t = 0.72 \pm 0.13$ for the profile 13 (Figure 4.12). For the profile 39, the $R_n = 0.30 \pm 0.13$ and the $R_t = 0.64 \pm 0.24$ (Figure 4.13).

Figure 4.8 The rockfall test photographs of the profile 13.

Figure 4.9 The fallen blocks after the rockfall test performed in the profile 13.

Figure 4.10 The fallen blocks in the profile 39.

Figure 4.11 Photograph of the slope at the profile 39.
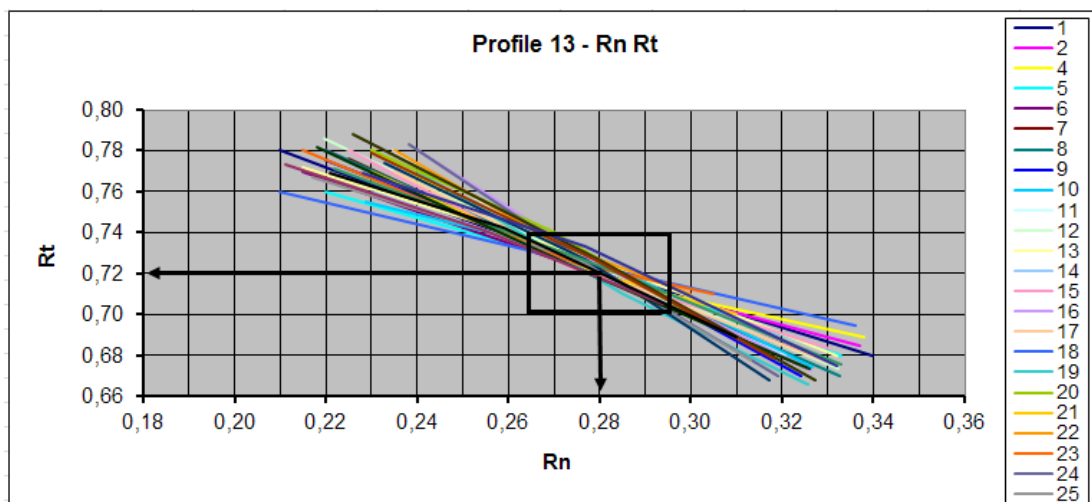
Figure 4.12 The back analysis result for the profile 13.
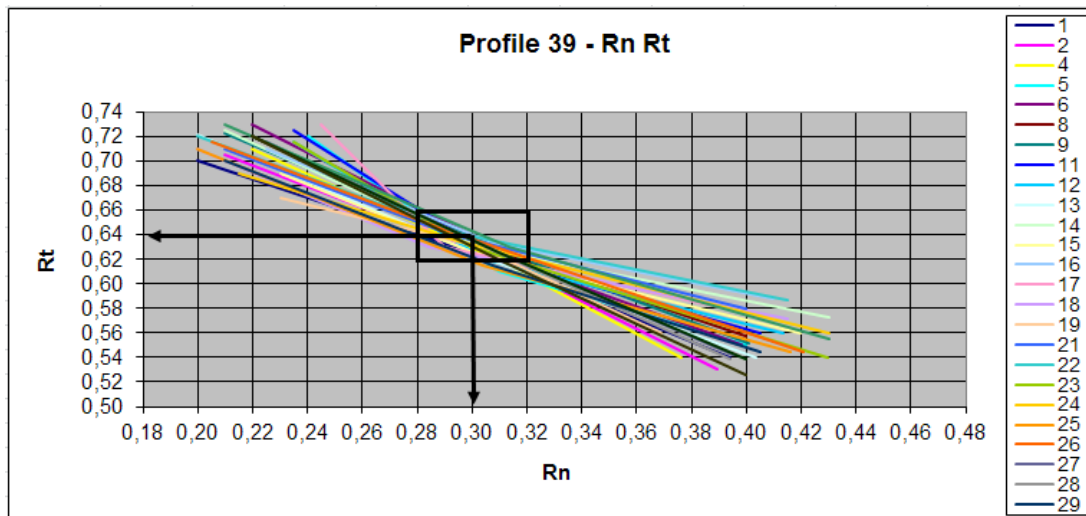
Figure 4.13 The back analysis result for the profile 39.

The 2-D rockfall analyses were carried out along 43 profiles to define the rockfall end point. The R_n and R_t values obtained from the profile 13 were used for the cross-sections between 1 - 17 and the R_n and R_t values obtained from the profile 39 were used for the cross-sections between 18 – 43. The other parameters used in the analyses are given in Table 4.2. The 2-D rockfall analyses were performed separately along 43 profiles for the original slope, 5 m inclined slope and benched slope. The 2-D rockfall analyses for the original, 5 meter inclined, 5 meter inclined one-benched slope are given in Figure 4.14, 4.15 and 4.16, respectively.

Table 4.2 The parameters used in the 2-D rockfall analyses.

PARAMETERS	VALUE
Total number of fallen blocks	1000
Friction angle (degrees)	20
Slope roughness	0
Block weight (kg)	88
Initial velocity (m/s)	1.5
Minimum velocity cut-off (m/s)	0.1
Number of throws	1000
Sampling interval	100

When the rocks were fallen from the original slope (Figure 4.17a) some blocks can reach up to the sea. This also applies to the other slopes (Figure 4.17b,c,d). The end point, bounce height, velocity and kinetic energy values for the four slope conditions are given in Tables

56

4.4, 4.5, 4.6 and 4.7, respectively. The change in the velocity and kinetic energy values are given in Figures 4.18 and 4.19, respectively. When the rockfall end points were considered in all slope conditions (Figure 4.20), it is understood that the rockfall blocks act in falling mode and stop in shorter distance in original slope conditions. On the other hand, rolling and bouncing movements are dominant in the other slope conditions and the end points are further. This condition may poses a danger for the people near the coast. In conclusion, the stability of existing slope must be preferred with its original condition.
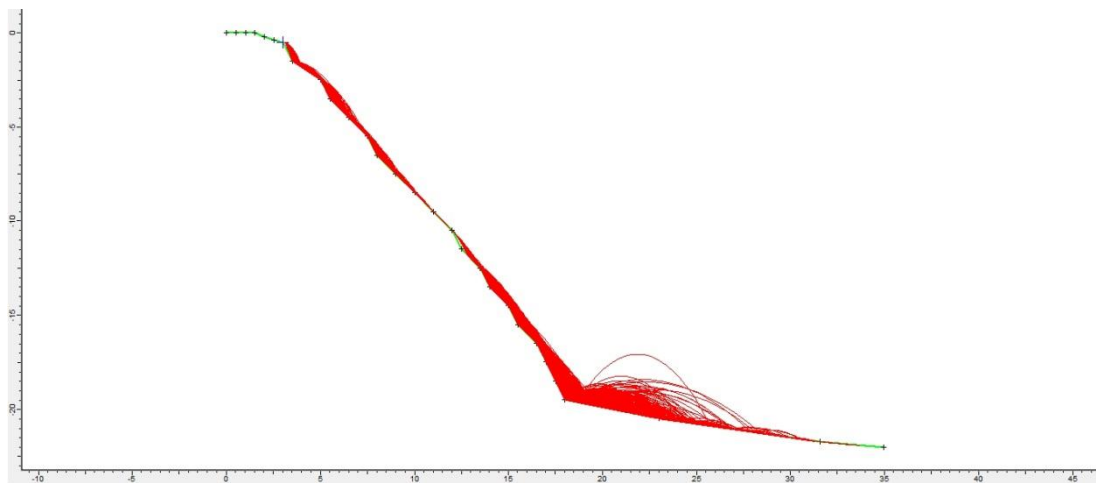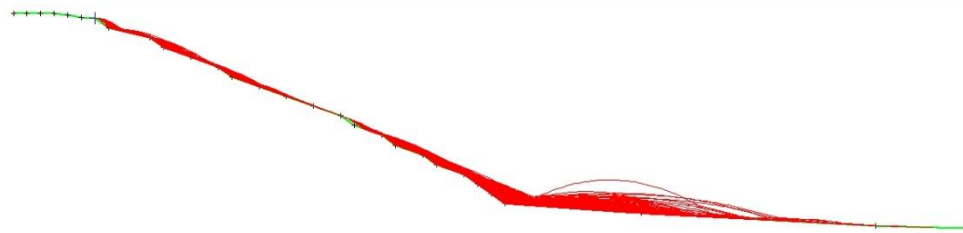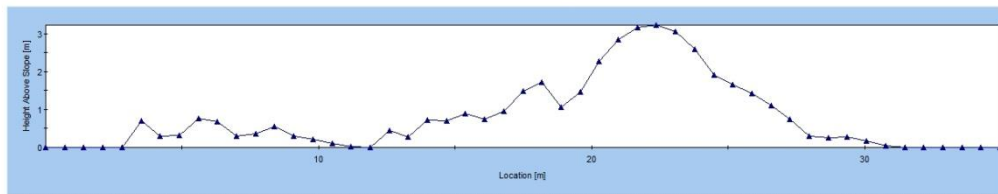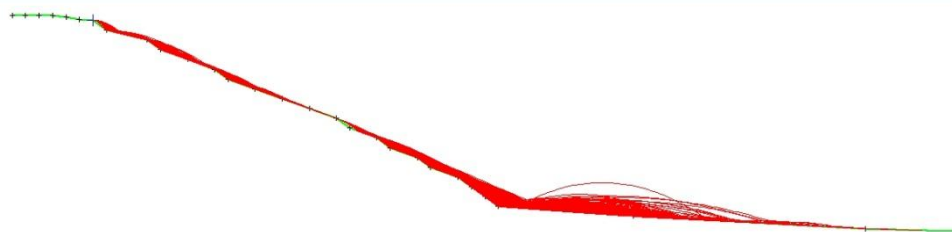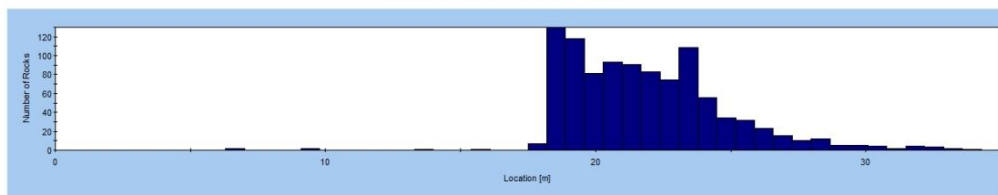
Figure 4.14 2-D rockfall analysis for the original slope performed in the profile 39.
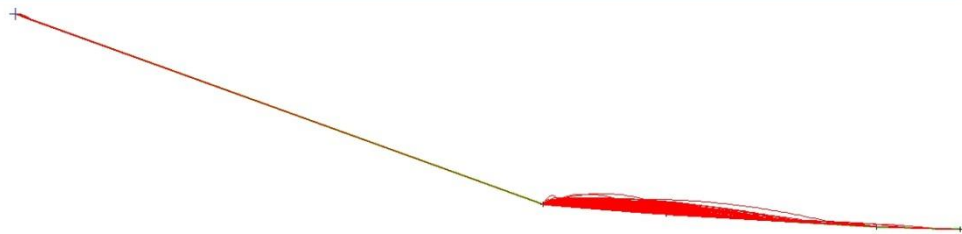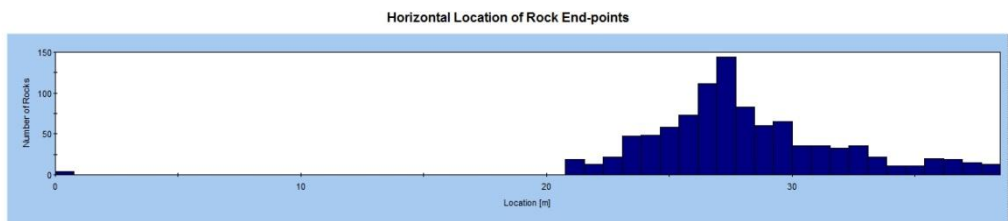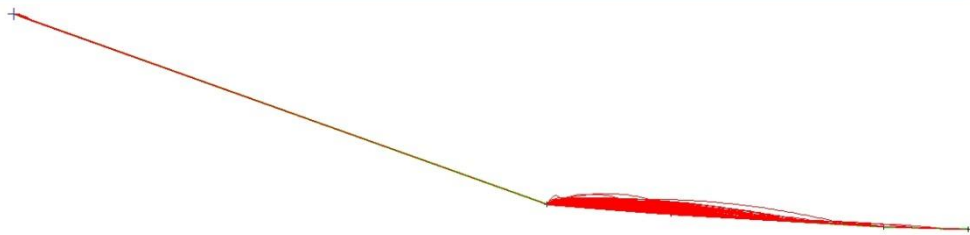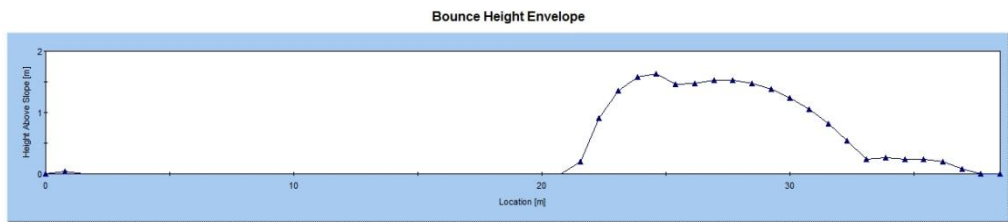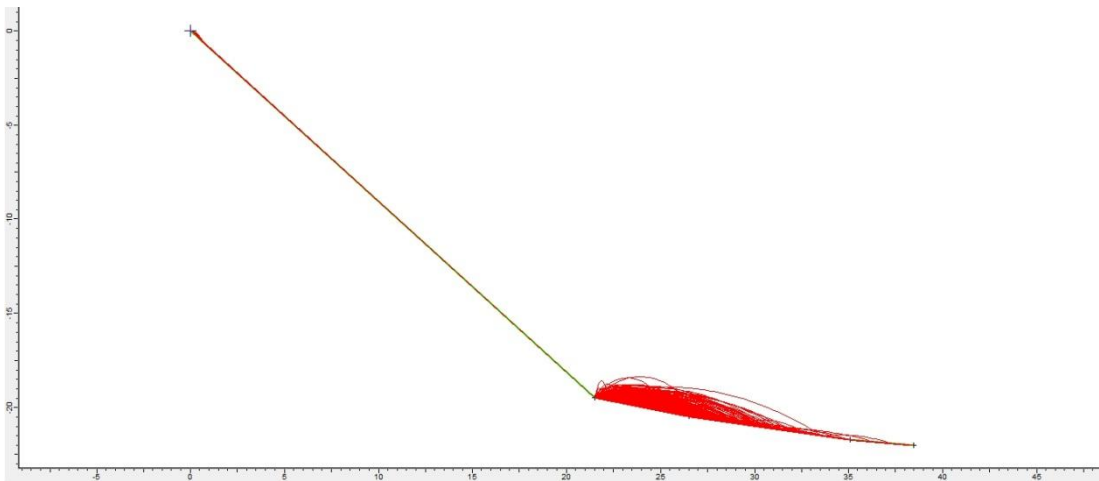
Figure 4.15 2-D rockfall analysis for the 5 meter inclined slope performed in the profile 39.
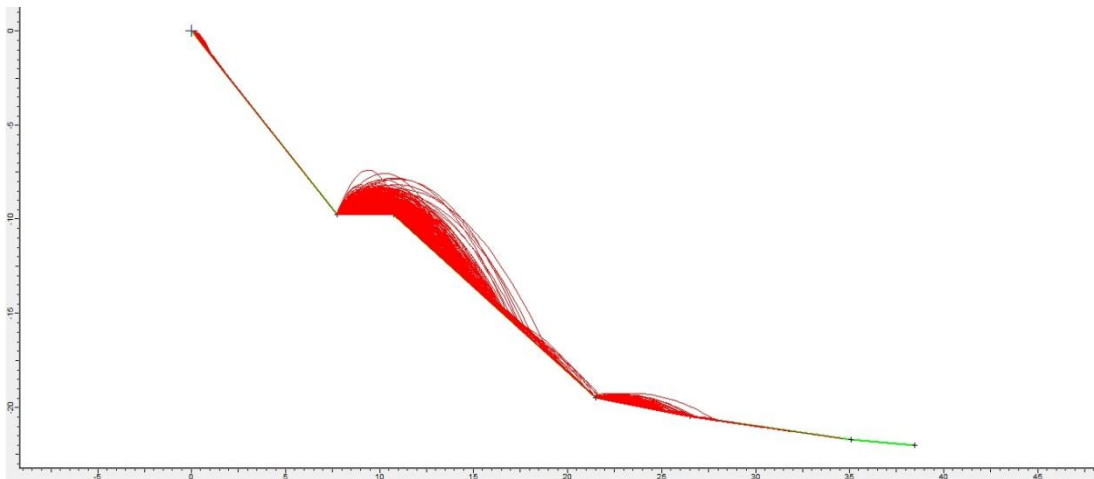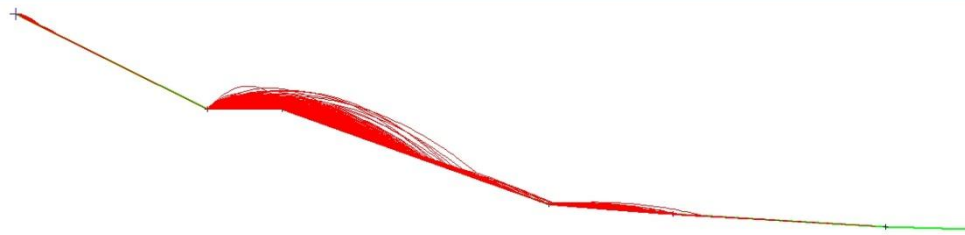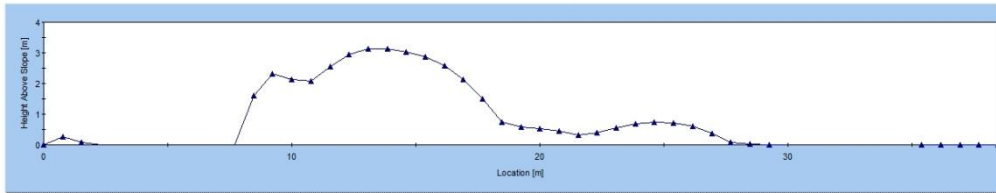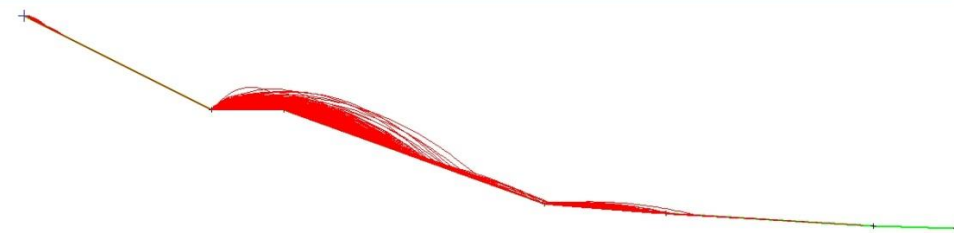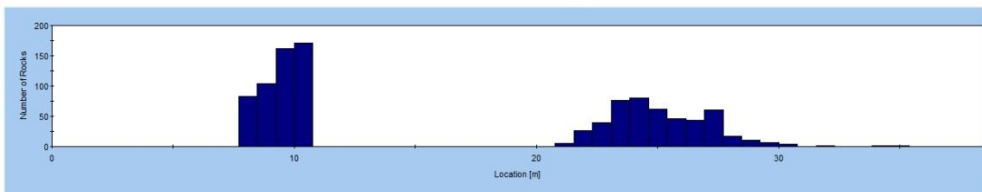
Figure 4.16 2-D rockfall analysis for the 5 meter inclined one-benched slope performed in the profile 39.

60

The maximum bouncing height is 5.75 m in the profile 33 (Table 4.3), and occurs at the middle of the slope, where the falling movement results in fading. For this reason, the wall which will be built considering the case mentioned above would be lower height.

Table 4.3 The maximum bouncing heights along the profiles.

PROFILE	BOUNCING POINT (m)	MAX. BOUNCING HEIGHT (m)
1	20.64	0.03
2	26.19	0.07
3	19.61	0.51
4	20.25	0.45
5	32.12	0.22
6	34.85	0.08
7	29.97	0.21
8	28.49	0.12
9	33.74	0.09
10	32.49	0.17
11	18.40	0.77
12	16.91	2.37
13	19.88	3.23
14	15.93	2.06
15	18.74	3.27
16	17.42	3.23
17	21.05	0.84
18	20.48	0.72
19	22.25	3.48
20	19.24	3.99
21	26.04	4.79
22	26.71	0.83
23	29.75	0.59
24	35.60	0.94
25	28.09	0.60
26	34.82	0.22
27	27.48	0.46
28	18.52	0.67
29	17.85	1.02
30	15.49	0.05
31	16.53	0.31
32	15.23	0.73
33	15.42	5.75
34	14.03	1.07
35	22.32	0.81
36	16.91	0.63
37	20.22	2.05
38	22.40	1.35
39	30.42	1.77
40	26.35	0.80
41	23.24	0.99
42	24.93	1.60
43	26.26	2.50
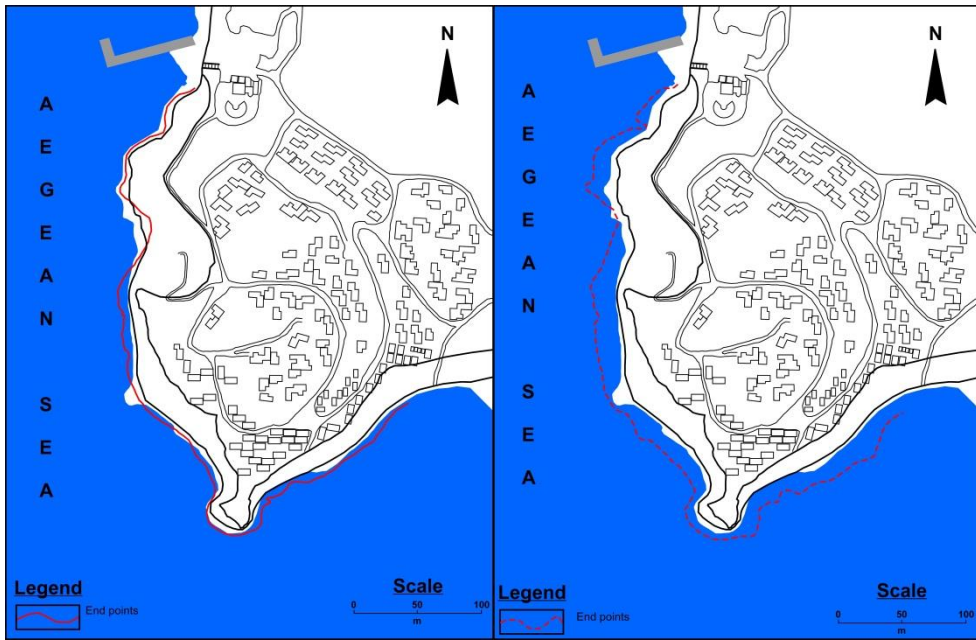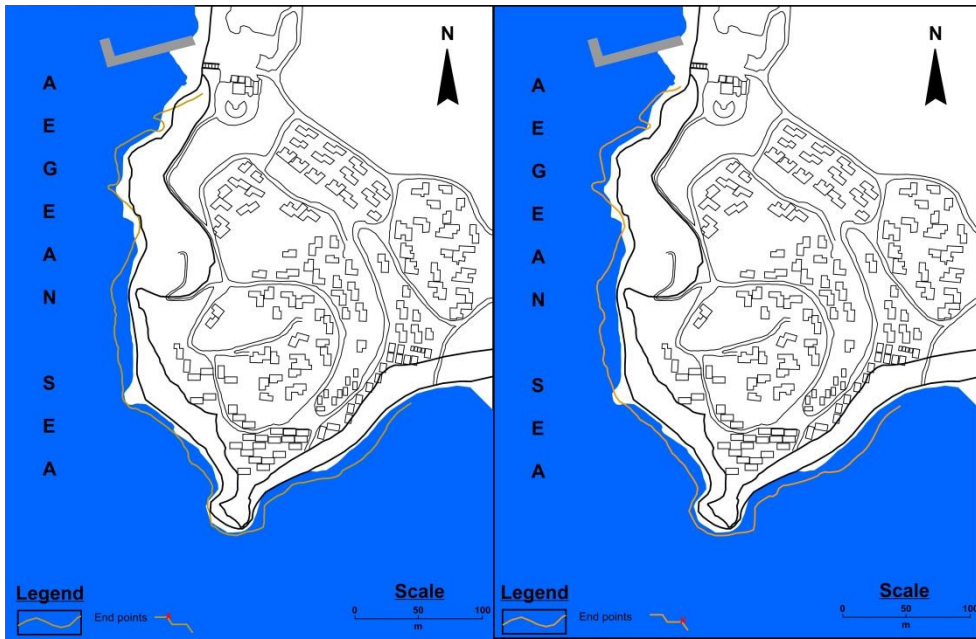
Figure 4.17 End points of the falling rocks according to the rockfall analyses: (a) Original slope, (b) 5 m inclined slope, (c) benched slope – falling from upper bench, (d) benched slope – falling from lower bench.
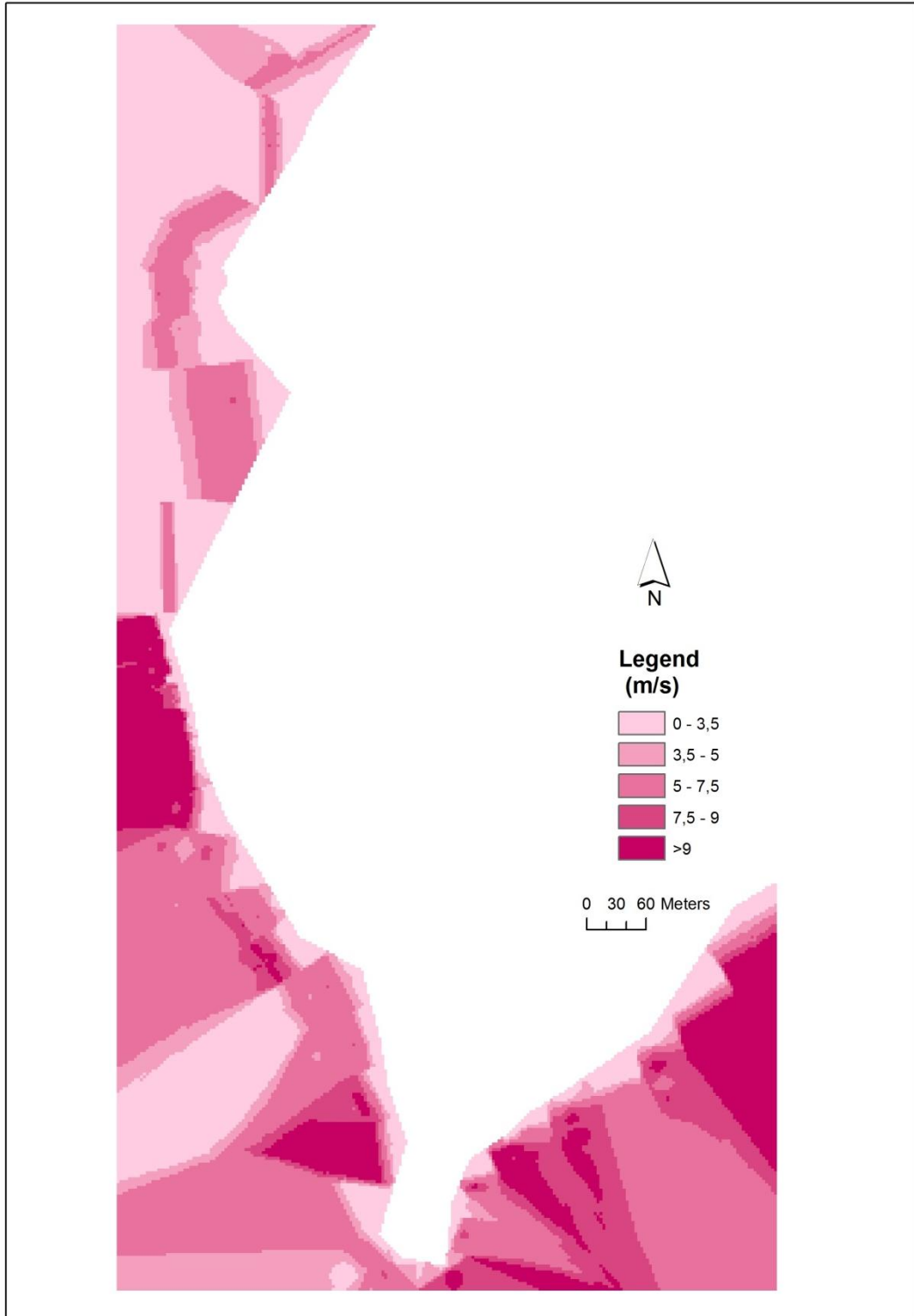
Figure 4.18 The velocity distribution map for 2D analysis.
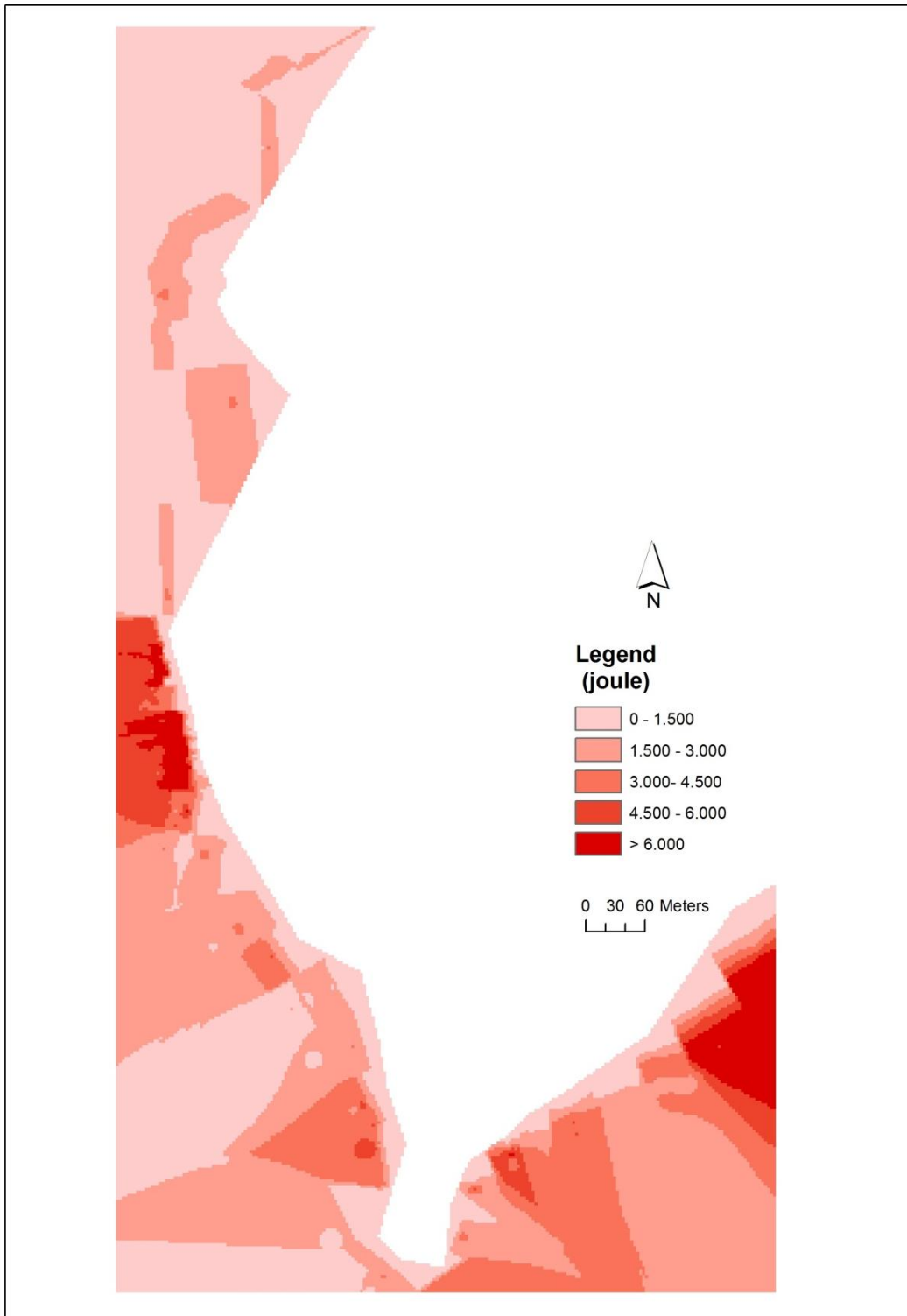
Figure 4.19 The kinetic energy distribution map for 2D analysis.

Table 4.4 The end point, bounce height, velocity and kinetic energy values for the original slope.

PROFILE	END POINT (m)	BOUNCE HEIGHT (m)	VELOCITY (m/s)	KINETIC ENERGY (j)
1	20.64	0.03	1959.61	5.77
2	26.19	0.07	1280.42	6.03
3	19.61	0.51	3292.99	7.64
4	20.25	0.45	4210.70	9.04
5	32.12	0.22	2474.35	6.85
6	34.85	0.08	2444.34	6.97
7	29.97	0.21	3578.18	7.81
8	28.49	0.12	3001.97	7.21
9	33.74	0.09	2509.75	6.93
10	32.49	0.17	3770.43	8.35
11	18.40	0.77	4520.05	8.73
12	16.91	2.37	8714.14	14.05
13	19.88	3.23	10061.20	15.10
14	15.93	2.06	9060.56	13.01
15	18.74	3.27	9598.00	14.22
16	17.42	3.23	9019.04	14.25
17	21.05	0.84	5096.19	9.81
18	20.48	0.72	5642.96	11.53
19	22.25	3.48	13009.70	17.78
20	19.24	3.99	11989.00	16.15
21	26.04	4.79	11643.50	16.53
22	26.71	0.83	7710.25	13.84
23	29.75	0.59	4116.04	9.48
24	35.60	0.94	4546.96	10.08
25	28.09	0.60	5274.15	10.71
26	34.82	0.22	3001.84	8.10
27	27.48	0.46	3218.60	8.73
28	18.52	0.67	6765.08	11.79
29	17.85	1.02	6253.79	11.88
30	15.49	0.05	2159.48	6.60
31	16.53	0.31	2642.81	7.36
32	15.23	0.73	3779.22	9.35
33	15.42	5.75	6834.64	13.60
34	14.03	1.07	5975.94	11.45
35	22.32	0.81	4135.68	10.10
36	16.91	0.63	5646.04	10.65
37	20.22	2.05	8317.54	13.84
38	22.40	1.35	7237.07	12.77
39	30.42	1.77	8088.54	13.91
40	26.35	0.80	3596.92	8.81
41	23.24	0.99	4711.39	10.52
42	24.93	1.60	7785.08	13.00
43	26.26	2.50	10743.10	15.48

Table 4.5 The end point, bounce height, velocity and kinetic energy values for the 5 meter inclined slope.

PROFILE	END POINT (m)	BOUNCE HEIGHT (m)	VELOCITY (m/s)	KINETIC ENERGY (j)
1	24.33	0.04	6.06	1673.36
2	31.46	0.001	6.58	1981.32
3	28.76	0.04	6.53	1946.42
4	27.36	0.14	8.99	3647.65
5	40.89	0.23	11.18	5615.20
6	46.65	0.06	10.02	4507.43
7	43.14	0.30	12.50	7005.03
8	45.20	0.17	12.00	6443.70
9	43.86	0.12	12.12	6579.50
10	43.34	0.26	13.14	7691.90
11	29.47	0.47	12.44	6944.01
12	23.74	1.80	14.14	9038.57
13	26.67	1.17	14.57	9640.55
14	27.70	1.21	14.86	10014.60
15	27.76	1.11	14.71	9762.24
16	32.46	1.66	15.62	10965.37
17	32.83	1.10	15.49	10788.61
18	32.42	1.55	15.73	9368.06
19	32.76	2.85	17.64	11864.29
20	34.26	2.41	18.24	12583.49
21	36.95	2.54	18.15	12383.20
22	42.40	2.26	16.28	9920.83
23	45.09	1.05	14.02	7366.28
24	44.78	0.72	15.06	8687.79
25	44.48	1.03	14.88	8326.61
26	48.10	1.05	14.20	7549.73
27	38.66	0.81	12.08	5473.01
28	29.94	1.01	11.48	4980.72
29	26.97	1.80	9.78	3612.07
30	23.52	0.12	6.30	1533.39
31	22.28	0.28	8.61	2819.79
32	19.41	0.38	8.38	2694.54
33	22.99	0.78	10.74	4361.26
34	23.01	0.46	9.30	3272.99
35	27.28	0.53	10.37	4075.19
36	28.41	0.98	12.23	5670.58
37	31.55	1.93	13.23	6629.88
38	29.03	1.65	13.69	7071.67
39	37.31	1.87	14.97	8852.02
40	37.54	1.67	14.68	8093.03
41	36.04	1.36	14.45	7820.84
42	40.78	1.13	14.54	7959.61
43	33.96	1.04	14.23	7608.42

Table 4.6 The end point, bounce height, velocity and kinetic energy values for the benched slope - falling from upper bench.

PROFILE	END POINT (m)	BOUNCE HEIGHT (m)	VELOCITY (m/s)	KINETIC ENERGY (j)
1	10.68	0.11	6.40	1906.71
2	12.95	0.12	6.52	1947.23
3	27.14	0.13	6.58	1958.13
4	22.56	0.22	7.62	2669.03
5	38.07	0.56	9.08	4183.62
6	45.57	0.7	8.43	3355.43
7	36.64	1.00	10.41	5655.17
8	41.33	0.82	9.55	4661.93
9	42.01	0.77	10.03	5165.92
10	41.47	1.23	11.36	7180.39
11	24.51	1.00	9.72	4641.96
12	19.57	0.95	10.05	5173.35
13	21.40	1.74	10.60	5756.93
14	21.02	1.48	11.08	6058.23
15	23.30	1.62	11.30	6027.35
16	26.49	2.24	13.21	8209.11
17	27.88	1.55	11.74	6464.84
18	25.45	4.52	15.97	9892.43
19	26.55	4.98	16.23	10048.79
20	25.61	7.06	17.44	11598.39
21	27.99	6.88	17.88	12189.66
22	34.19	4.58	16.26	10442.41
23	40.03	1.82	11.71	5977.73
24	38.04	3.08	14.04	8046.23
25	33.99	2.92	14.50	9294.06
26	42.72	2.34	13.48	7484.20
27	37.03	1.12	9.94	4720.46
28	23.71	1.33	9.82	3992.56
29	22.43	0.56	8.40	2725.42
30	9.90	0.25	6.42	1604.97
31	17.78	0.86	7.66	2350.67
32	15.33	0.75	7.28	2156.73
33	19.75	1.16	9.27	3512.57
34	20.85	0.62	8.07	2755.89
35	22.40	0.94	8.82	3270.54
36	21.54	1.51	9.82	3842.15
37	22.69	2.09	11.98	5701.11
38	23.02	2.87	12.78	6465.71
39	27.31	3.46	13.90	7891.49
40	32.76	4.29	15.22	9134.48
41	30.73	3.60	14.34	8725.13
42	33.61	2.91	13.63	7947.73
43	30.91	2.73	13.75	8505.34

Table 4.7 The end point, bounce height, velocity and kinetic energy values for the benched slope - falling from lower bench.

PROFILE	END POINT (m)	BOUNCE HEIGHT (m)	VELOCITY (m/s)	KINETIC ENERGY (j)
1	23.63	0.03	4.38	897.19
2	29.24	0.01	4.75	1056.68
3	27.95	0.005	4.67	1019.79
4	23.52	0.09	6.43	1913.68
5	39.01	0.09	7.96	2903.71
6	45.57	0.02	7.12	2307.47
7	37.57	0.15	8.75	3468.63
8	40.44	0.09	8.58	3335.13
9	42.94	0.06	8.65	3404.44
10	41.47	0.12	9.33	3942.18
11	25.75	0.23	8.79	3519.89
12	21.09	0.49	9.91	4547.62
13	21.98	0.65	10.18	4705.22
14	22.36	0.61	10.31	4894.51
15	24.57	0.57	10.34	4885.78
16	25.75	0.60	10.96	5442.73
17	28.59	0.53	10.78	5337.18
18	24.75	0.79	10.98	4654.80
19	28.62	1.99	12.22	5818.08
20	26.33	1.30	12.83	6392.25
21	29.48	1.69	12.73	6229.54
22	35.10	0.98	11.46	5008.11
23	41.04	0.75	9.80	3922.07
24	40.92	0.35	10.69	4408.60
25	33.99	0.43	10.69	4385.44
26	43.73	0.58	10.25	3983.73
27	35.41	0.44	8.60	2811.60
28	28.14	0.55	8.01	2449.16
29	25.27	0.23	6.90	1822.10
30	22.46	0.07	4.61	847.09
31	20.93	0.12	6.16	1482.92
32	16.59	0.12	5.98	1404.92
33	21.25	0.37	7.68	2276.80
34	22.32	0.16	6.70	1754.15
35	22.94	0.30	7.37	2106.39
36	21.54	0.38	8.64	2929.55
37	24.91	0.81	9.35	3371.06
38	25.02	0.75	9.65	3592.63
39	31.16	0.99	10.43	4158.82
40	31.28	0.89	10.54	4282.99
41	33.76	0.69	10.19	3967.94
42	35.40	0.60	10.24	4008.45
43	30.15	0.37	10.00	3832.05
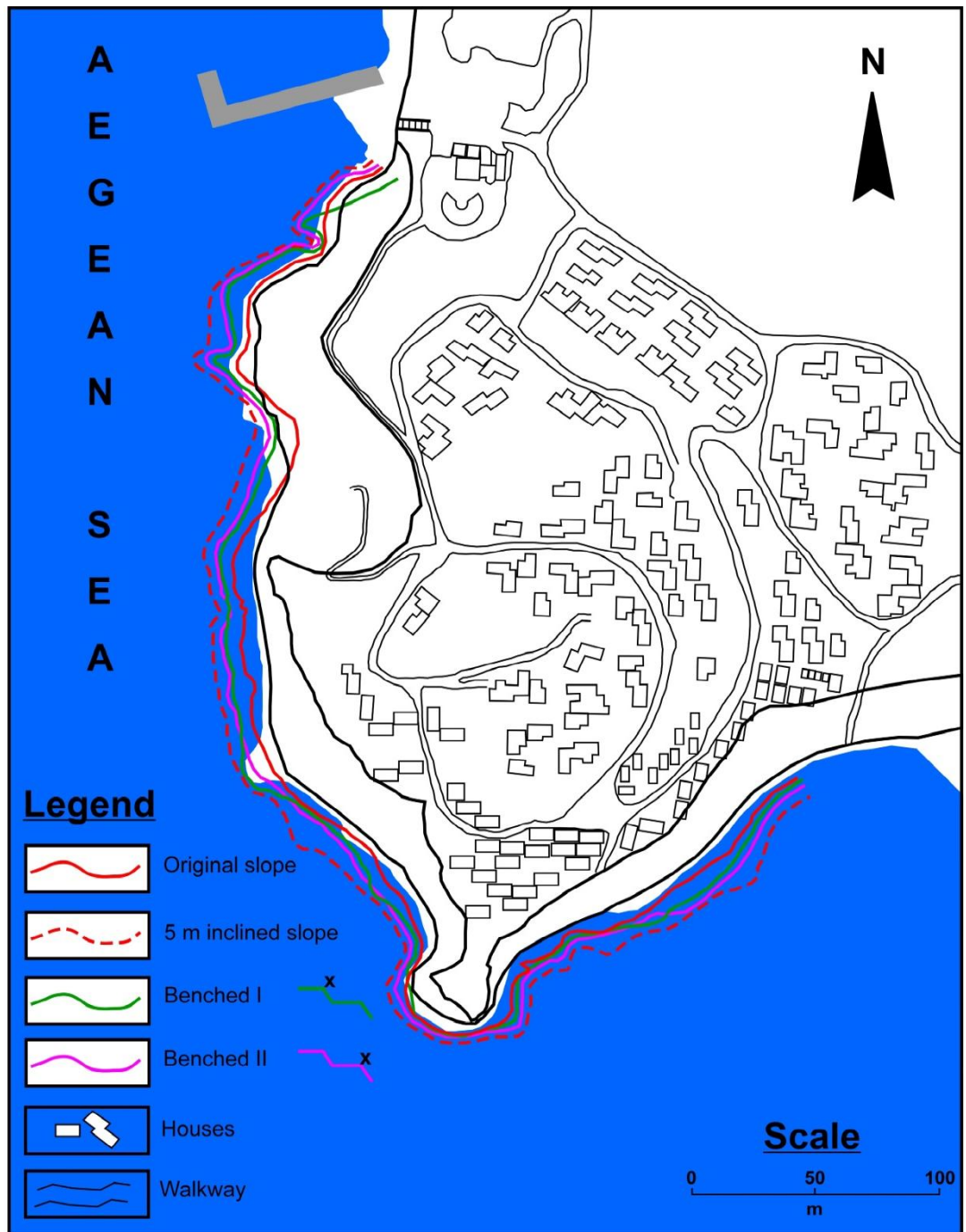
Figure 4.20 Map showing rockfall end points obtained from 2-D analysis for all conditions.

4.2.2 3-D Analysis

In this study, 3-D analyses were performed using the ROTOMAP (Scioldo, 1991) software. It is a three-dimensional software that is used for rockfall analysis and design of protective systems. A statistical approach consists of the software background. Simulating a large number of rockfalls can be hold on and, from the distribution of the average and maximum kinetic energies, it identifies the proper places of the protective systems (GeoSoft, 2005).

Because the real behavior of boulders depends on apparently insignificant geometric and mechanical details when rolling down a slope, the rockfall problem is quite complex. There is no linear interaction between the slope geometry and the rock trajectories. The relation between the initial conditions and fall trajectory is not directly proportional. Small changes in the initial conditions cause big (and thus inconspicuous) differences in the final conditions. This does not mean that there is no solution of the problem; the calibration of the model is not possible with only a few simulations, therefore the forecasting of the path and stop point of a single real boulder is not possible. In this case, a statistical approach is a reasonable solution. In this way the stop points could not be considered individually (GeoSoft, 2005).

The first phase is geometrical reconstruction of the slope. After the definition of the topographic surface, the geological and geomorphological data collection is necessary.

Firstly, grid generation was performed to create a base for the model. The whole model was run on the basis of this grid. The rockfall parameters used in the model are selected based on the field conditions (Table 4.8).

Table 4.8 The rockfall parameters used in the 3-D model.

PARAMETERS	VALUE
Flying limit angle (°)	9
Colliding limit angle (°)	9
Bouncing limit angle (°)	9
Number of starting points	20
Number of initial velocities	10
Minimum initial velocity (m/s)	0.5
Maximum initial velocity (m/s)	1.5
Number of initial directions	5
Maximum angular deviation (°)	40
Boulder mass (t)	0.083
Normal coefficient of restitution (R_n)	0.28 and 0.30
Tangential coefficient of restitution (R_t)	0.72 and 0.64
Friction coefficient of boulders	0.5

4.2.2.1 The Rockfal Parameters Used in the 3-D Model

Flying limit angle (°): It is used to define flying moment of the boulders after the bounce. For starting a boulder to fly, the angle of the trajectory must be greater than the limit angle.

Colliding limit angle (°): This limit angle is used to define flying moment of the boulders over the slope. For starting a boulder to fly, increasing in the dip of slope must be greater than the limit angle.

Bouncing limit angle (°): It is used to define impact moment of the boulders with the ground and bounce. For starting a boulder to bounce, decreasing in the dip of the slope must be greater than the limit angle.

Number of starting points: This parameter represents the starting points aligned along the starting points. The boulders start from these points according to the unstable slope geometry.

Number of initial velocities: This parameter represents the number of initial velocities for every point. The boulders start from these points according to the unstable slope geometry.

Number of initial directions: This parameter represents the initial directions. These directions are chosen in a given range around the dip direction. The simulations should be carried out enormously. This causes good statistical results. In the simulation, different velocities, directions and starting points should be used. To calculate the total number of falling rocks, the following equation is used: "Number of initial directions * Number of initial velocities * Number of starting points"

Minimum and maximum initial velocities (m/s): These parameters represent the initial velocities of the boulders.

Maximum angular deviation (°): It defines the range of the interval around the dip direction, in which the starting directions are chosen.

Boulders mass (t): This value is multiplied by the $v^2/2$ value and related with the barriers capacity. It is used to evaluate the design of protection system.

Starting angle (°): It must be between 0°and90°. When it is 0°, the parameter is overpassed and the boulders start in a direction parallel to the ground.

Free fall height (m): It is used when the starting angle is bigger than 0°. This parameter allows to simulate a block which start from a point placed over the ground level at the given height (GeoSoft, 2005).

In the geomechanical parameters menu, the area was divided into 3 parts according to the R_n, R_t and friction coefficient values (Figure 4.21). The blue part represents the sea. The R_n, R_t and friction angle (F.A) values were selected for this part 0.1, 0.9 and 0.9 respectively. The red and green parts represent the profiles 1-17 and 18-43 respectively. For the red part, R_n = 0.28, R_t = 0.72 and friction angle = 0.5 and for the green part, R_n = 0.30, R_t = 0.64 and friction angle = 0.5. The R_n and R_t values for the red and green parts were obtained from the back analysis.
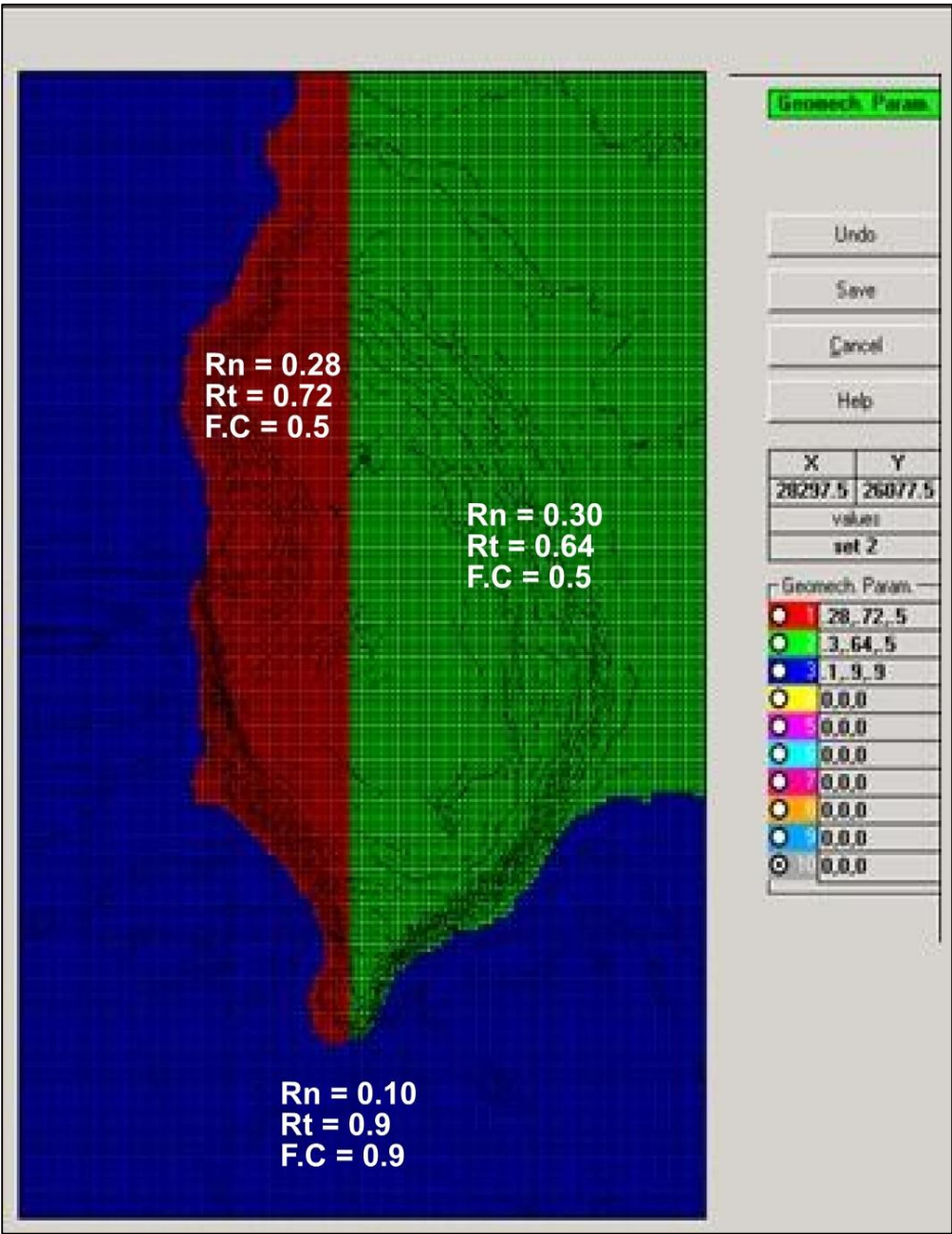
Figure 4.21 Different Rn, Rt and Friction Coefficient values used in the ROTOMAP software.

After selection of geomechanical parameters, the 43 detachment lines data were input. Calculations were carried out by the help of all data inputted the software. The calculation types can be seen in Figure 4.22.
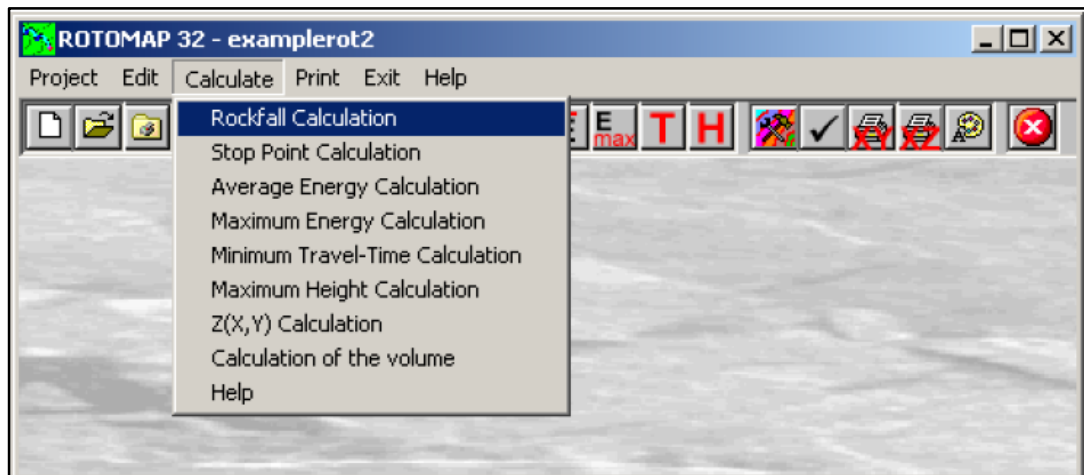
Figure 4.22 The calculation types in the ROTOMAP software.

4.2.2.2 The Calculations Performed in the ROTOMAP Software

Rockfall, stop point, average energy, maximum energy, minimum travel time, maximum height and volume are calculated. The rockfall calculation, rockfall paths, end points and bouncing height outputs are given in the Figures 4.23, 4.24, 4.25 and 4.26, respectively.
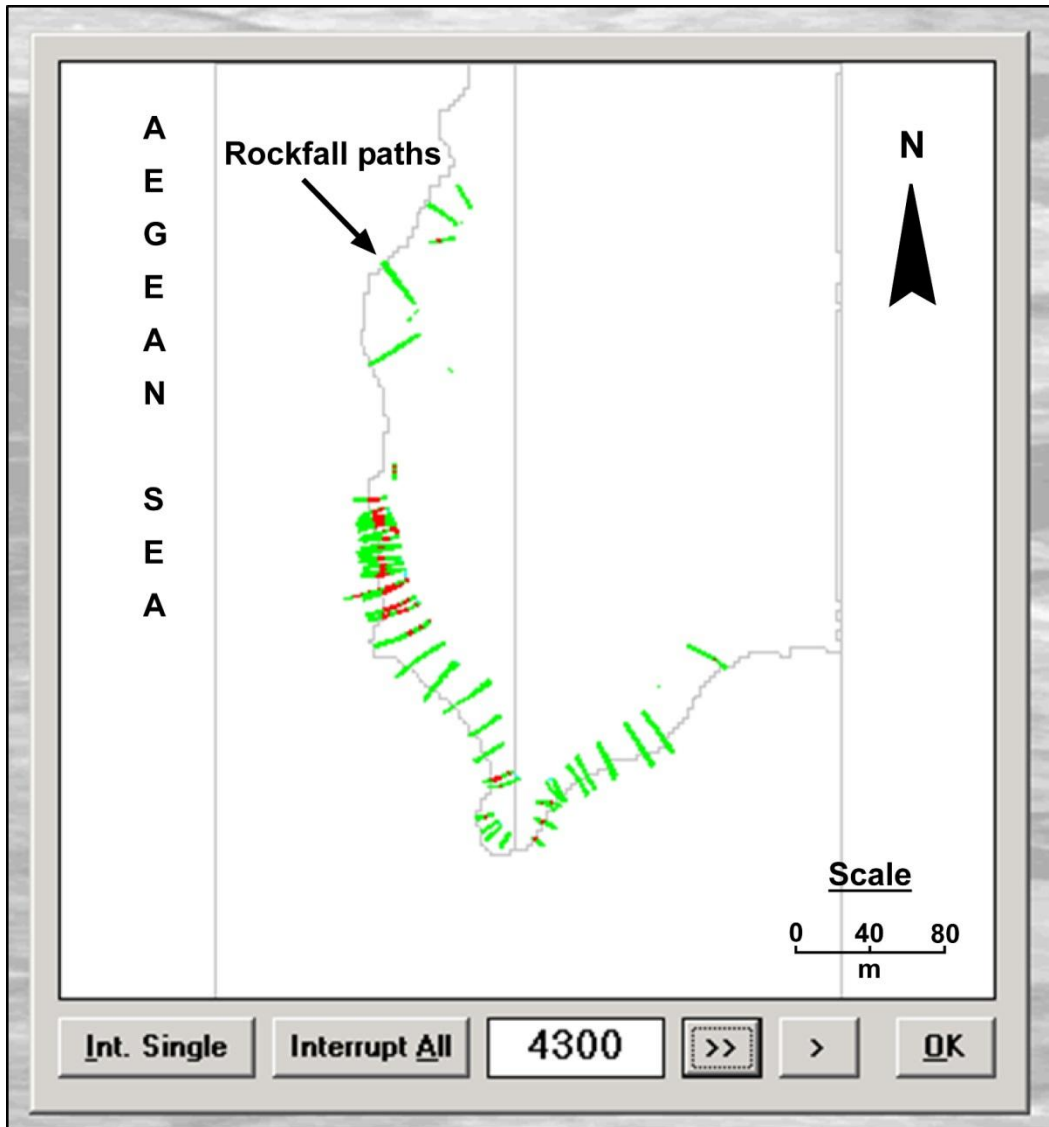
Figure 4.23 Rockfall path calculation output.
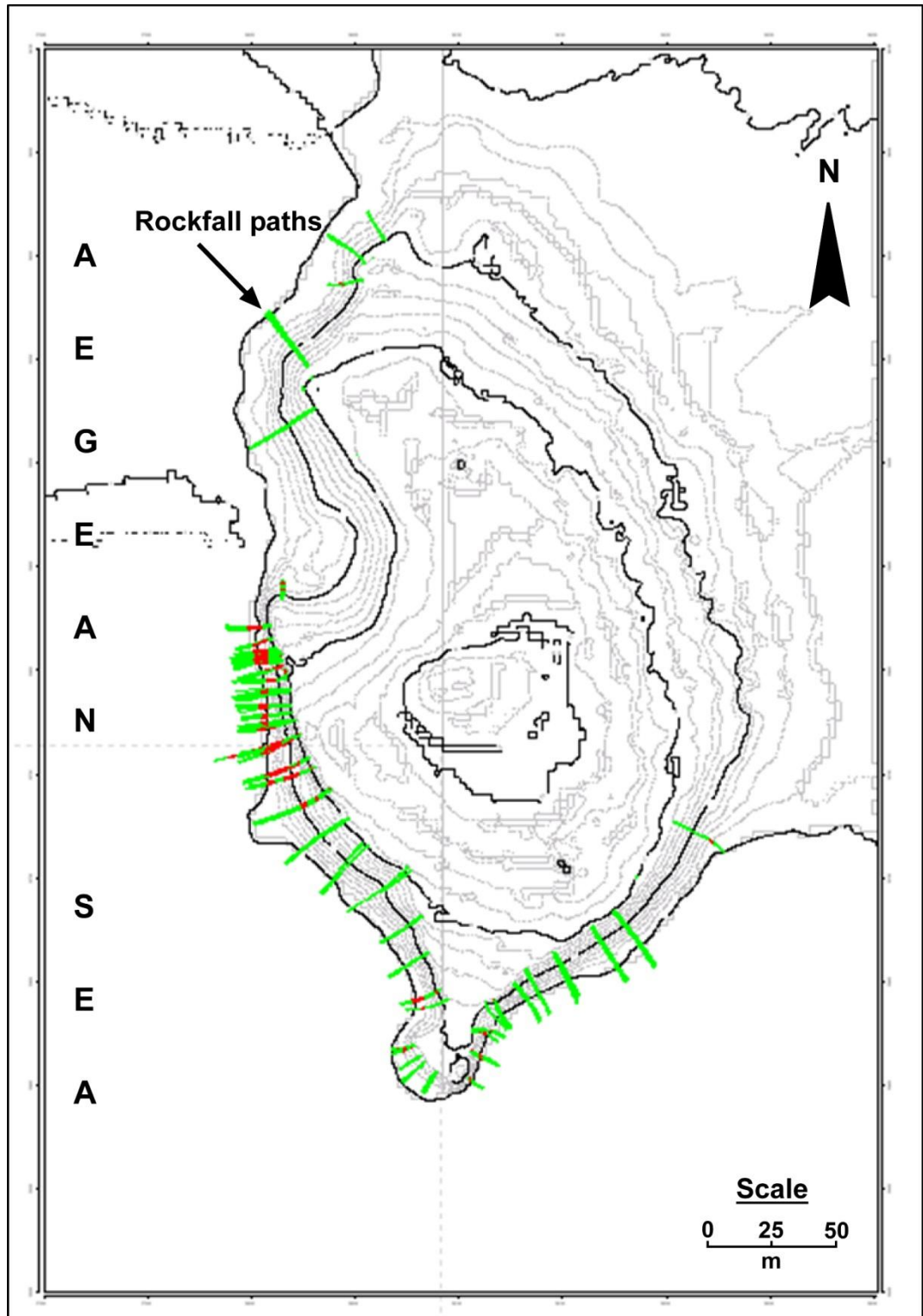
Figure 4.24 Rockfall trajectory map of the study area.
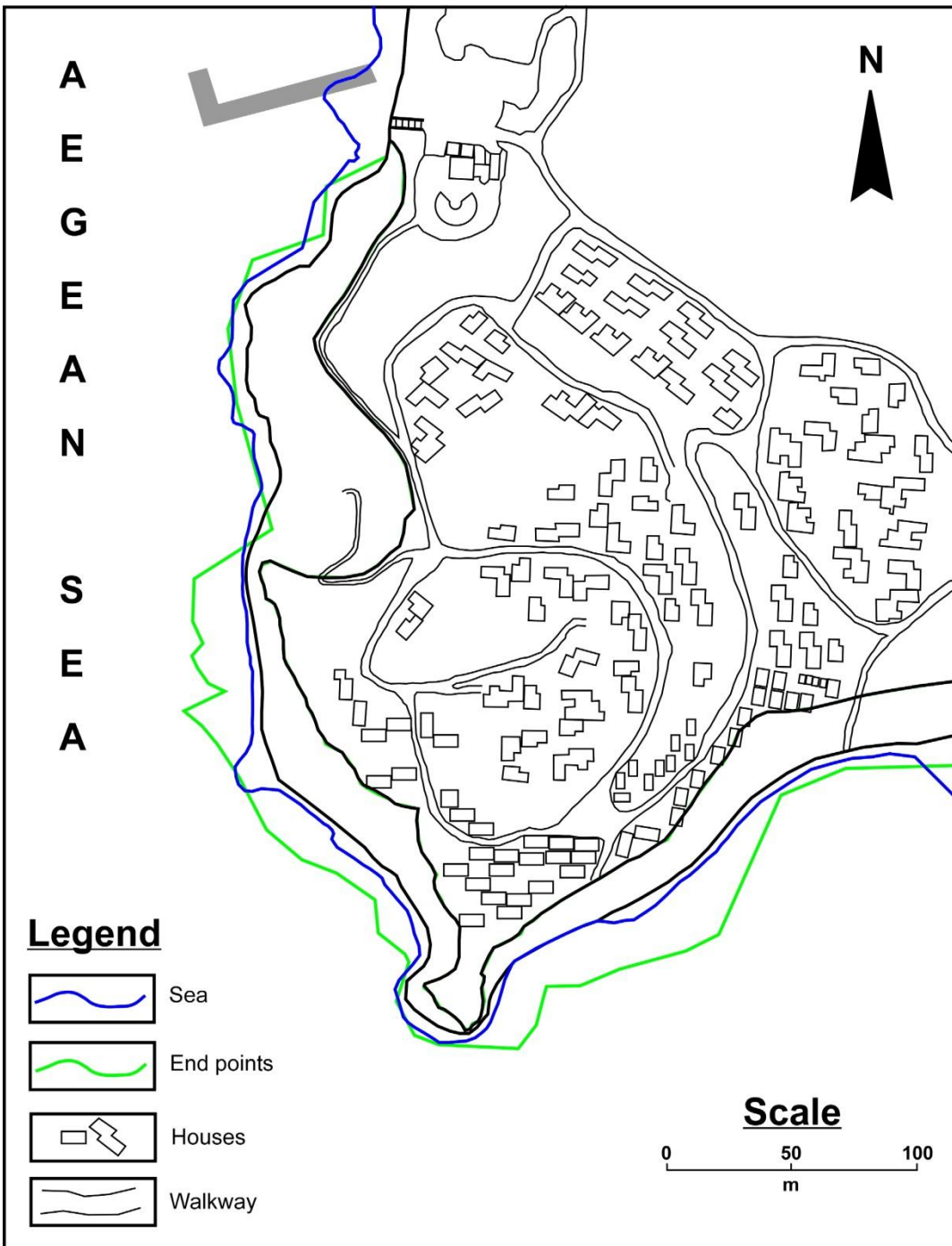
Figure 4.25 Rockfall end points map of the study area obtained from 3-D analysis.
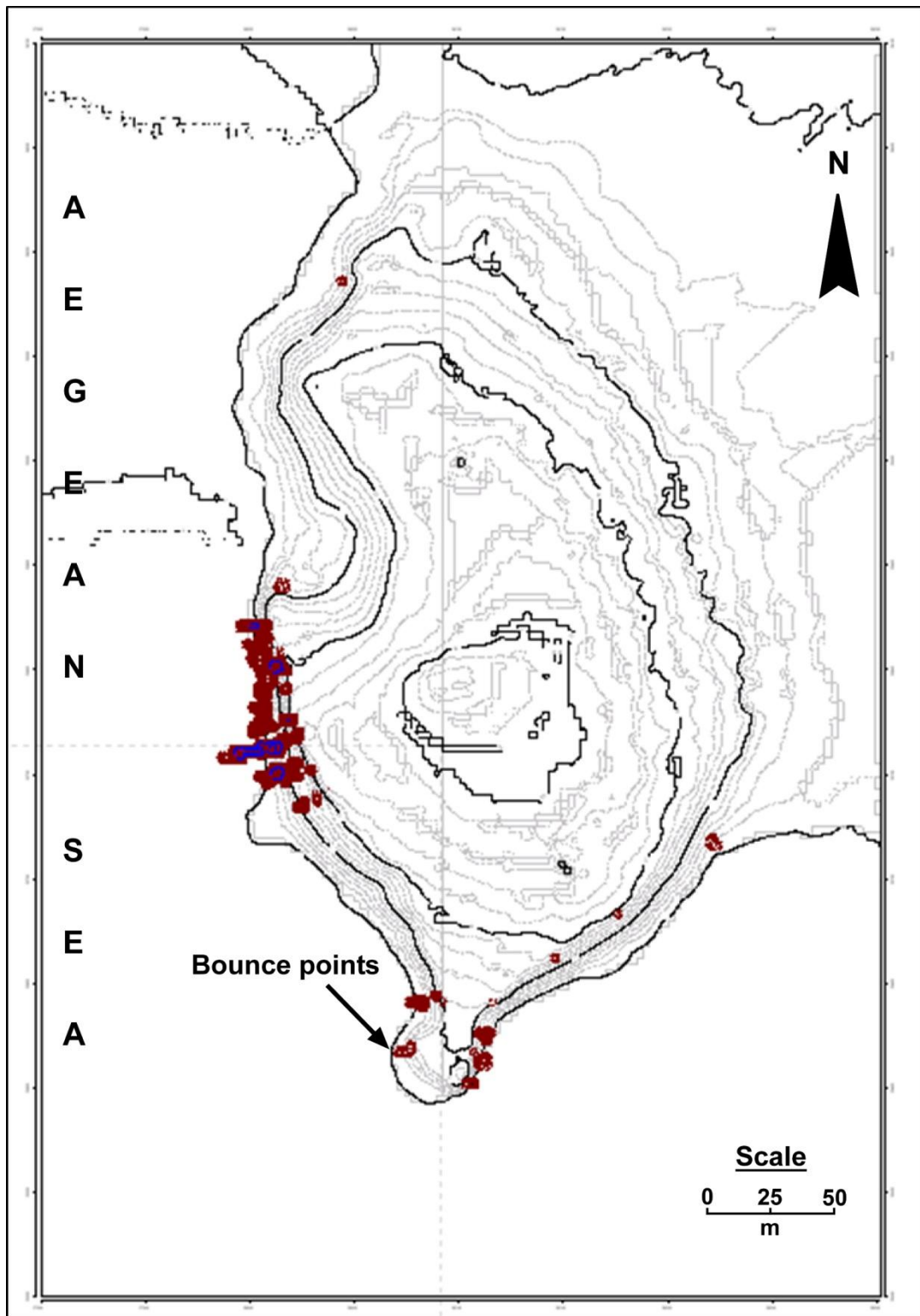
Figure 4.26 Bounce height map of the study area.

CHAPTER 5

GENERAL EVALUATION

In this Chapter, the results obtained from the 2-D and 3-D analyses are evaluated. Field studies, laboratory studies and remediation works constitute main steps in the study. 2-D and 3-D analyses were carried out in the light of the results obtained from the field and laboratory studies then accordingly remedial measures are suggested.

5.1 2-D Analysis& 3-D Analysis

The values obtained from 2-D and 3-D analyses show that there are some differences between the end points (Figure 5.1) and bounce height values (Table 5.1). According to the field observations, the 2-D model seems to be more realistic. In the 3-D model, the stop points of the 43 locations are farther from the coast than 2-D model. This fact could be attributed to the parameters selected in the 3-D analysis. The distance between the coast and end points of the rocks in the 3-D model do not represent the real case observed in the field. Both the field observations and the rockfall analyses performed at the locations 13 and 39 show that 2-D model reveals more realistic results. This can be attributed in terms of three parameters:

5.1.1 Slope Geometry

Slope geometry is important in terms of the direction and movement of the rocks. Variability in slope geometry makes accurate prediction extremely difficult. Small changes in the slope geometry may cause major differences in the results. For the 2-D model, the trajectory and slope are assumed as a straight profile. The inclination of the slope and the surface roughness define the velocity of the rocks and movement type (rolling, bouncing or falling). In 3-D model, the trajectory is not a straight profile. The movement and trajectory of the rocks are defined by the slope geometry. The movement of the rocks is not represented in a single profile. Dimensional changes affect the end points and bounce heights of the rocks.

5.1.2 Algorithm

RocFall (Rocscience, 2004c) which is the software used in 2-D modeling to calculate the rock movement doing particle analysis. The particle analysis can be divided into three main parts: the particle algorithm, the projectile algorithm, and the sliding algorithm. The validation of all simulation parameters and preparation of initial conditions are done by the particle algorithm. In the projectile algorithm, the rock has a velocity to move. To calculate the movement of the rocks, the sliding algorithm is used. Sliding of the rocks can occur any part of the slope. For the purpose of the sliding algorithm, the slope segment or barrier that the

rock slides on, consists of a single straight-profile segment that has properties of slope angle (Θ) and friction angle (Φ) (Stevens, 1998).
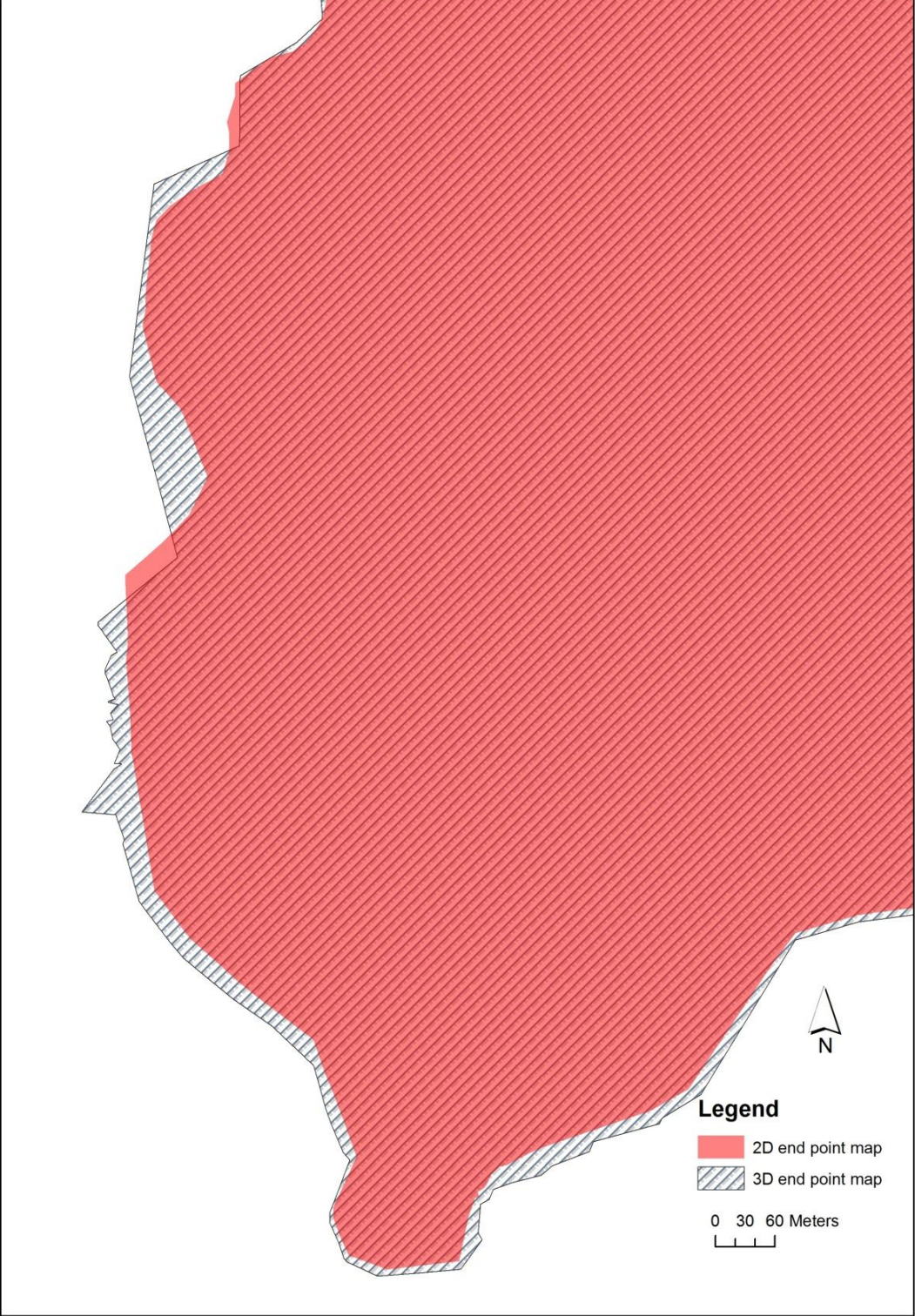
Figure 5.1 The end point boundaries of 2D and 3D analysis.

For the 3-D modeling, the algorithm information could not be obtained and some software bugs occurred while modeling in 3-D. In spite of these problems, the results obtained from the models show that the algorithm of the programs are different. These differences produce different results for the end point and bounce height values.

5.1.3 Input Parameters

Different input parameters cause changes in the results. The variation of these parameters originates from the algorithm and software language used in the program. The end point and bounce height values obtained from 2-D and 3-D analyses can be seen in Table 5.1. The comparison of the input parameters used in the programs is given in Table 5.2.

Table 5.1 End point and bounce height values obtained from 2-D and 3-D analyses.

SECTION	END PT. (2-D) (m)	END PT. (3-D) (m)	MAX. BOUNCE HGT. (2-D) (m)	MAX. BOUNCE HGT. (3-D) (m)
1	20.64	20.44	0.03	0.00
2	26.19	25.32	0.07	0.00
3	19.61	24.95	0.51	0.00
4	20.25	19.22	0.45	0.08
5	32.12	38.59	0.22	0.00
6	34.85	35.95	0.08	0.00
7	29.97	33.15	0.21	0.00
8	28.49	30.50	0.12	0.00
9	33.74	37.23	0.09	0.00
10	32.49	56.02	0.17	0.00
11	18.40	20.09	0.77	1.00
12	16.91	29.51	2.37	1.40
13	19.88	27.74	3.23	0.80
14	15.93	29.05	2.06	1.60
15	18.74	30.19	3.27	1.60
16	17.42	34.37	3.23	0.80
17	21.05	25.14	0.84	0.80
18	20.48	30.80	0.72	0.60
19	22.25	27.62	3.48	0.40
20	19.24	39.53	3.99	0.80
21	26.04	18.82	4.79	2.60
22	26.71	55.04	0.83	2.20
23	29.75	49.32	0.59	1.80
24	35.60	43.63	0.94	0.00
25	28.09	42.18	0.60	0.00
26	34.82	44.34	0.22	0.00
27	27.48	30.82	0.46	0.00
28	18.52	26.96	0.67	0.00
29	17.85	24.61	1.02	0.40

Table 5.1 (continued)

30	15.49	13.75	0.05	0.14
31	16.53	13.82	0.31	0.00
32	15.23	10.06	0.73	0.00
33	15.42	5.29	5.75	0.18
34	14.03	15.37	1.07	0.44
35	22.32	12.18	0.81	0.46
36	16.91	28.78	0.63	0.20
37	20.22	20.11	2.05	0.06
38	22.40	25.54	1.35	0.00
39	30.42	26.66	1.77	0.06
40	26.35	31.35	0.80	0.00
41	23.24	33.41	0.99	0.00
42	24.93	32.97	1.60	0.00
43	26.26	33.32	2.50	0.12

Table 5.2 The input parameters used in the models.

2-D	3-D
Total number of fallen blocks	Flying limit angle (°)
Friction angle (°)	Colliding limit angle (°)
Slope roughness	Bouncing limit angle (°)
Block weight (kg)	Number of starting points
Initial velocity (m/s)	Number of initial velocities
Minimum velocity cut-off (m/s)	Minimum initial velocity (m/s)
Number of throws	Maximum initial velocity (m/s)
Sampling interval	Number of initial directions
Rn	Maximum angular deviation (°)
Rt	Capacity (kJ)
	Boulder mass (t)
	Height of the nets (m)
	Starting angle (°)
	Free fall height (m)
	Rn
	Rt
	Friction coefficient

5.2 Recommendations

5.2.1 Block Removal

As it is seen in the rockfall analyses, the blocks falling from the cliffs can be dangerous, particularly if the end points are considered. Today, the rock blocks with falling potential are removed firstly in all rockfall remedial works in the world. In a similar vein, all rocks having the potential of falling controlled by fracture must be removed. The intact fallen blocks can be used in the wall built. After the opening the area in use, the controls at the study area must be performed periodically at the end of each winter and the blocks having tendency to fall must be removed if necessary.

5.2.2 Drainage

İn the study area, there is a drain line at the crown of the cliffs but some deficiencies were observed in the drain lines in some locations. Additionally, the drain profile turning with the right angle (Figure 5.2) in the north of the study area is not suitable for draining the water in the channel. In this context, the new drain profiles (top width = 50 cm, base width = 30, depth = 40 cm) must be built (Figure 5.3) and the formers must be removed. In this way, the drain profiles which always must be kept clear will prevent the rain water flow into the cliffs and its damage.

Figure 5.2 Improper installation of the old drain line.

Figure 5.3 Proposed drainage profiles.

5.2.3 Greening (Vegetation)

As it is mentioned before, the study area is quite green in comparison to its vicinity. Sliding and rockfall problems do not occur in the areas where scrub kind vegetation is very dense. For this reason, the greening of the poorly vegetated areas not only improve the surrounding

beauty but will reduce geological hazards (sliding, erosion, rockfall etc.). The vegetation must be planned as soon as possible. The suggested areas are given in Figure 5.4.

Figure 5.4 The map showing the areas required greening.

5.2.4 Filling the Caverns

The terrestrial units consisting of alternation of sandstone-claystone-marl have been carved especially at the locations affected by the wave action (Figure 3.14). Small-scale collapsing occurred in the areas with large caverns. Because these caverns are potentially dangerous,

they must be filled fully as earliest as possible with the natural stones. These areas are shown in Figure 5.5.
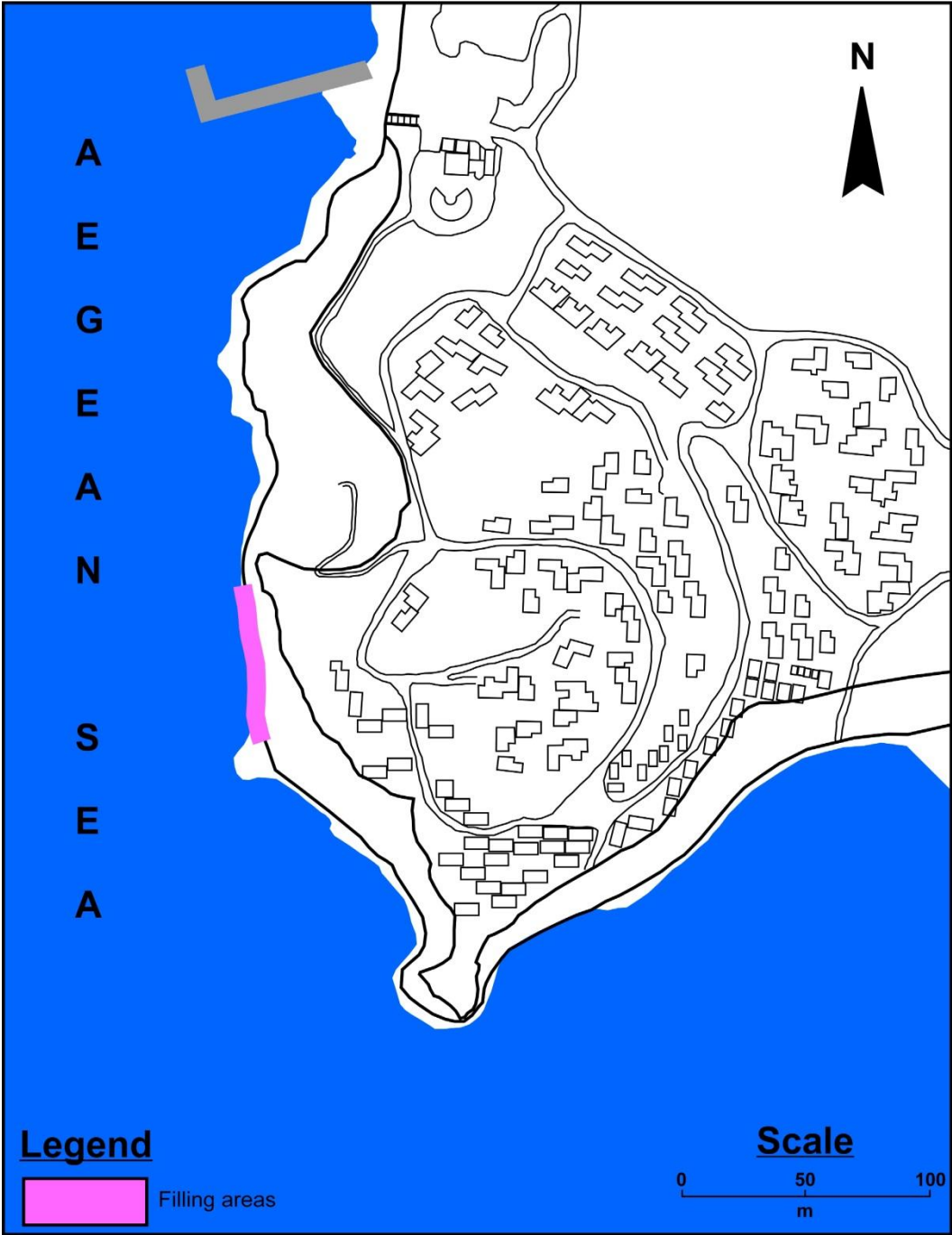
Figure 5.5 The map showing the areas at the coast to be filled.

5.2.5 Wall Building

According to the rockfall analyses in the study area, many blocks reach up to the coast. This situation would be dangerous for the people at the coast. The evaluation was carried out by considering the bounce heights of the rock blocks and the nearest points to the coast were defined where the energy of the block and bounce height are attenuated. The places of optimal wall points were defined by the help of this approach. The places of the walls are given in Figure 5.6.

By considering the environment, the intact rocks around the study area can be used to build the wall. The wall height for the whole area is proposed as 1.5 m. The height of the wall at the north of the study area must be up to 1.5 m. The blocks reaching the coast by crashing to the rocks were observed in the in situ rockfall tests. Graveling should be performed about 30 cm thick at the back side of the wall to attenuate the energy of blocks and decrease the bounce height. When the material collected from back of the wall is removed every year, the wall can function for many years.

This wall will reduce the danger derived from rockfall and minimize the undercutting formed at the coast. The vegetation can be applied on this wall by covering the whole wall.

Figure 5.6 Rockfall barrier map of the study area.

5.2.6 Erosion Prevention

The slope in the north of the study area has the feature of a soft soil rather than a rock (Figure 5.7). Soil erosion occurs occasionally. At the same area, there are densely spaced iron rods to prevent the erosion. This approach prevented the erosion relatively but it could not be effective because of the limited application area. Instead of iron rods, small terracing, wooden roads (wire mesh) and deep-rooted vegetation must be applied. The area suitable for erosion prevention works is given in Figure 5.7.

Figure 5.7 The erosion prevention area.

CHAPTER 6

CONCLUSIONS

This Thesis is aimed to investigate the rockfall problems, to recommend nature-friendly solutions in order to prevent/minimize the hazards, to analyse the rockfall problems in 2-D and 3-D and discuss the results obtained from 2-D and 3-D analyses. Based on the rockfall analyses, field and laboratory studies, the following conclusions are achieved.

1. The study area which will be open to tourism in Kuşadası, Aydın has steep and high cliffs near the coast.
2. The study area is in the western part of the Büyük Menderes Graben. The Menderes Massif Metamorphics comprise the basement of the study area.
3. In the field studies, the terrestrial units in the study area were investigated in terms of geological and geological hazards, the data about the discontinuities were collected by the help of the scan-profile survey carried out along the 10 profiles. From these studies, one bedding plane and two joints observed for every profile except the profile 2.
4. In the laboratory studies, unit weight, effective porosity, water absorption and point load strength tests were performed on the ten samples taken from the field. The laboratory studies show that the terrestrial units have moderate unit weight and porosity and low water absorption and point load strength values.
5. Rockfall analyses were performed 2-D and 3-D respectively. According to these analyses, many blocks reach up to the coast and this situation would be dangerous for the people at the coast. Based on the results obtained from the analyses, there are some differences between the end point and bounce height values. According to the field observations, the 2-D model is more realistic than 3-D model. The differences between the 2-D and 3-D model originate from the slope geometry, the algorithm used in the software and the different input parameters.
6. To protect the people from the geological hazards (sliding, erosion, rockfall etc.) observed in the study area, block removal, drainage, greening, filling the caverns, wall building and erosion prevention are suggested.

REFERENCES

Agliardi, F., Crosta, G.B., 2003. High resolution three-dimensional numerical modelling of rockfalls. Int J Rock Mech Min Sci 40:455–471.

Agliardi, F., Crosta, G.B., Frattini, P., 2009. Integrating rockfall risk assessment and countermeasure design by 3D modelling techniques. Nat Hazards Earth Syst Sci 9:1059–1073.

Alejano, L.R., Ordonez, C., Armesto, J., Rivas, T., 2010. Assessment of the instability hazard of a granite boulder. Nat Hazards 53:77–95.

Anon, 1979. Classification of rocks and soils for engineering geological mapping.
Part 1. Rock and soil materials. Bull. Int. Assoc. Eng. Geol. 19, 364- 371.

Azzoni, A., Barbera, L.G., Zaninetti, A., 1995. Analysis and prediction of rockfalls using a mathematical model. Int J Rock Mech Min Sci Geotech Abstr 32:709–724.

Bozzolo, D., Pamini, R., 1986. Simulation of rock falls down a valley side. Acta Mechanica 63, 113–30.

Bozzolo, D., Pamini, R., Hutter, K., 1988. Rockfall analysis – a mathematical model and its test with field data. Proceedings of the 5th International Symposium on Landslides inLausanne, Rotterdam: Balkema, 555–60.

Broilli, L., 1974. Ein Felssturz in Großversuch. Rock Mechanics Suppl. 3, 69–78.

Budetta, P.,Santo, A., 1994. Morphostructural evolution and related kinematics of rockfalls in Campania (southern Italy): a case study. Engineering Geology 36, 197–210.

Bull, W.B., King, J., Kong, F.C., Moutoux, T., Phillips, W.M., 1994. Lichen dating of coseismic landslide hazards in alpine mountains. Geomorphology 10(1), 253–64.

Chau, K.T., Wong, R.H.C.,Lee, C.F., 1998. Rockfall problems in Hong Kong and some new experimental results for coefficient of restitution. International Journal of RockMechanics and Mining Science 35 (4), 662–63.

Chen, H., Chen, R.H., Huang, T., 1994. An application of an analytical model to a slope subject to rockfalls. Bull As Eng Geol 31:447–458.

Corominas, J., Copons, R., Moya, J, Vilaplana, J.M., Altimir, J., Amig'o, J., 2005. Quantitative assessment of the residual risk in a rockfall protected area. Landslides 2(4):343–357.

Coutard, J.P., Francou, B., 1989. Rock temperature measurements in two alpine environments: implications for frost shattering. Arctic and Alpine Research 21, 399–416.

Çakmakoğlu, A., 2007. Dilek Yarımadası, Söke ve Selçuk çevresinin Neojen öncesi tektonostratigrafisi, MTA Dergisi, 135, 1-17.

Day, R.W., 1997. Case studies of rockfall in soft versus hard rock. Environmental and EngineeringGeoscience 3(1): 133–40.

Descoeudres, F., Stoffel, S.M., Boll, A., Gerber, W., Labiouse, V., 1999. Coping study on Disaster Resilient Infrastructure Cornmissioned by the Secretariat for the International Decade for Natural Disaster Reduction for the IDNDR Programme Forum 1999 ""Partnerships for a safer world in the 21 st century"" CHAPTER 4.

DMİ, 2012. Devlet Meteoroloji İşleri Genel Müdürlüğü, http://www.mgm.gov.tr/veridegerlendirme/il-ve-ilceler-istatistik.aspx?m=AYDIN, last visited on October 2012.

Domaas, U., 1994. Geometrical methods of calculating rockfall range. NGI Report 585910-1. Oslo: Norwegian Geotechnical Institute.

Dorren, L.K.A., 2002. Mountain geoecosytems – GIS modelling of rockfall and protection forest structure. Thesis Universiteit van Amsterdam, The Netherlands Centre for Geo-Ecological Research (ICG) and the Institute for Biodiversity and Ecosystem Dynamics (IBED – Physical Geography), Faculty of Science, University of Amsterdam, The Netherlands, 163 pp (published).

Dorren, L.K.A., 2003. A review of rockfall mechanics and modelling approaches. Prog Phys Geogr 27:69–87.

Ercan, T., Akat, U., Erdoğu, G., Savaşçın, Y., 1986. Söke-Selçuk-Kuşadası Dolaylarının Jeolojisi ve Volkanik Kayaçların Petrokimyasal Özellikleri. Maden Tetkik ve Arama Dergisi, 105-106, 15-38.

Evans, S.G., Hungr, O., 1993. The assessment of rockfall hazard at the base of talus slopes. Canadian Geotechnical Journal 30, 620–36.

Fell, R., Corominas, J., Bonnard, C., Cascini, L., Leroi, E., Savage, W., 2008. Guidelines for landslide susceptibility, hazard and risk zoning for land use planning. Eng Geol 102:85–98.

GDDA, 1996. Earthquake zoning map of Turkey, Earthquake research department, General Directorate of Disaster Affairs, Ministry of Reconstruction and Resettlement of Turkey.

Geobrugg, 2013. http://www.geobrugg.com/contento/en us/Home/Rockfallbarriersandcatchfences/tabid/2050/Default.aspx, last visited on February 2013.

GeoSoft, 2005. ISOMAP&ROTOMAP 3-D Surface Modelling&Rockfall Analysis, Italy, 69 pp.

Giani, G.P., 1992. Rock slope stability analysis. Rotterdam, Balkema, 361 pp.

Goodman, R.E., 1989. Introduction to Rock Mechanics, 2nd edition. Wiley, New York. 562 pp.

Grove, J.M., 1972. The incidence of landslides, avalanches and floods in western Norway during the Little Ice Age. Arctic and AlpineResearch 4, 131–38.

Gürer, Ö.F., Bozcu, M., Yılmaz, K., Yılmaz, Y., 2001. Neogene basin development around Söke-Kuşadası (western Anatolia) and its bearing on tectonic development of the Aegean region. Geodinamica Acta 14, 57–69.

Gürocak, Z., Alemdağ, S., Zaman, M.M., 2008. Rock slope stability and excavatability assessment of rocks at the Kapikaya dam site, Turkey. Engineering Geology 96, 17–27.

Hegg, C., Kienholz, H., 1995. Determining paths of gravity-driven slope processes – the 'Vector Tree Model'. In Carrara, A. and Guzetti, F., editors, Geographic information systems inassessing natural hazards. Dordrecht: Kluwer Academic Publishers, 79–92.

Hoek, E., Bray, J.W., 1981. Rock Slope Engineering, 3rd ed. Institute of Mining and Metallurgy, London. 358 pp.

Hungr, O., Evans, S.G., 1988. Engineering evaluation of fragmental rockfall hazards. Proceedings of the 5th International Symposium onLandslides in Lausanne. Rotterdam: Balkema, 685–90.

ISRM, 1981. Rock characterization, testing and monitoring. International Society for Rock Mechanics Suggested Methods. Pergamon, Oxford. 211 pp.

ISRM, 1985. Suggested method for determining point load strength. International Journal of Rock Mechanics and Mining Sciences &Geomechanics Abstracts 22, 51–60.

Jaboyedoff, M., Dudt, J.P., Labiouse, V., 2005. An attempt to refine rockfall hazard zoning based on the kinetic energy, frequency, and fragmentation degree. Nat Hazards Earth Syst Sci 5:621–632.

Keylock, C., Domaas, U., 1999. Evaluation of topographic models of rockfall travel distance for use in hazard applications. Arctic, Antarctic,and Alpine Research 31 (3), 312–20.

Kirkby, M.J., Statham, I., 1975. Surface stone movement and scree formation. Journal ofGeology 83, 349–62.

Kobayashi, Y., Harp, E.L., Kagawa, T., 1990. Simulation of rockfalls triggered by earthquakes. Rock Mechanics and Rock Engineering 23, 1–20.

Krautblatter, M., Moser, M., 2009. A nonlinear model coupling rockfall and rainfall intensity based on a four year measurement in a high Alpine rock wall (Reintal, German Alps). Nat Hazards Earth Syst Sci 9:1425-1432.

Kuşadası Municipality 2010, http://en.kusadasi.bel.tr/?menuid=kat_detay&katid=11&icid=1, last visited on October 2012.

MaccaferriLtd., http://www.maccaferri.co.uk/media/om_www/uk/Images/Solutions/Rockfall%20Protection/rockfall_embankment_2.jpg, last visited on February 2013.

Marzorati, S., Luzi, L., Amicis, M.D., 2002. Rock falls induced by earthquakes: a statistical approach. Soil Dyn Earthq Eng 22:565–577.
Matsuoka, N. and Sakai, H. 1999. Rockfall activity from an alpine cliff during thawing periods. Geomorphology 28(3), 309–28.

Meissl, G., 1998. Modellierung der Reichweite von Felsstürzen. Fallbeispeile zur GISgestützten Gefahrenbeurteilung aus dem Beierischen und Tiroler Alpenraum. Innsbrucker Geografischen Studien 28. Ph.D. Thesis, Universität Innsbruck, Innsbruck, 249 pp.

Merck, J., 2010. Introduction to Physical Geology. Lecture notes. University of Maryland, Department of Geology, http://www.geol.umd.edu/~jmerck/geol100/images/20/sideling.jpg, last visited on February 2013.

MTA, 2002. 1/500 000 ölçekli Türkiye jeoloji haritaları, Denizli Paftası, MTA Yayınları

MTA, 2012, Yenilenmiş Diri Fay Haritaları, İzmir-Aydın-Urla paftaları, http://www.mta.gov.tr/v2.0/default.php?id=yeni_diri_fay_haritalari-goruntule, last visited on October 2012.

Parejas, E., 1940. La tectonique transversal de la Turquie. Univ İstanbul Geogr Inst Rev 5:133-244.

Pettifer, G.S., Fookes, P.G., 1994. A revision of the graphical method for assessing the excavatability of rock. Quarterly Journal of Engineering Geology 27, 145–164.

Pfeiffer, T.J., Bowen, T.D., 1989. Computer simulation of rockfalls. Bulletin of the Associationof Engineering Geologists XXVI (1), 135–46.

Porter, S.C., Orombelli, G., 1980. Catastrophic rockfall of September 12, 1717 on the Italian flank of the Mont Blanc Massif. Zeitschrift fürGeomorphologie N.F. 24, 200–18.

Porter, S.C., Orombelli, G., 1981. Alpine rockfall hazards. AmericanScientist 69(1), 67–75.

Priest, S.D., 1993. Discontinuity analysis for rock engineering. Chapman & Hall, London.

Raetzo, H., Lateltin, O., Bollinger, D., Tripet, J.P., 2002. Hazard assessment in Switzerland–Code of practice for mass movements. Bull Eng Geol Environ 61:263–268.

Rayudu., D.N.Prasad., 1997. Computer Simulation of Rockfalls - Application to Rockfalls At Fox Glacier, West Coast, New Zealand. A thesis submitted in partial fulfilment of the requirements for the Degree of Master of Engineering (in Rock Engineering), Department of Natural Resources Engineering, Lincoln University, 191 pp (published).

Ring, U., Will, T., glodny, J., Kumerics, C., Gessner, K., Thomson, S., Güngör, T., Monie, P., Okrusch, M., Druppel, K., 2007. Early exhumation of high-pressure rocks in extrusion wedges: Cycladic blueschist unit in the eastern Aegean, Greece, and Turkey. Tectonics, Vol. 26, TC2001, doi:10.1029/2005TC001872.

Ritchie, A.M., 1963.. Evaluation of rockfall and its control. Highw Res Board Rec 17:13–27.

Rocscience, 2004, Scientific Software, Statistical Analysis of Rockfalls, Version 4.0, Rocscience Inc., Canada, 63 pp.

Rocscience, 2004a. Dips 5.1- Data interpretation package using stereographic projection.

Rocscience, 2004b. Slide 5.1-2D limit equilibrium slope stability analysis.

Rocscience, 2004c. RockFall 4.0- , Scientific Software-Statistical Analysis of Rockfalls.

Rocscience, 2012. http://www.rocscience.com/hoek/corner/9_Analysis_of_rockfall_hazards.pdf, last visited on September 2012.

Schumm, S.A., Chorley, R.J., 1964. The fall of endangering rock. American Journal of Science 262, 1041–54.

Scioldo, G., 1991. ISOMAP and ROTOMAP, 3D surface modelling and rockfall analysis. Geo and Soft, Torino.

Spang R.M., 1987. Protection against rockfall – Stepchild in the design of rock slopes, 6th International Congress on Rock Mechanics, International Society for Rock Mechanics, pp 551-557.

Stevens, Warren D., 1998. RocFall: a Tool for Probabilistic Analysis, Design of Remedial Measures and Prediction of Rockfalls. A thesis submitted in conformity with therequirements for the degree of Master of Applied Science, Graduate Department ofCivil Engineering, University of Toronto, 38 pp (published).

Straub, D., Schubert, M., 2008. Modelling and managing uncertainty in rock-fall hazards. Georisk 2(1):1–15.

Sümer, Ö., İnci, U., Sözbilir, H., 2013. Tectonic evolution of the Söke Basin: Extension-dominated transtensional basin formation in western part of the Büyük Menderes Graben, Western Anatolia, Turkey. Journal of Geodynamics,65, 148– 175.

Tianchi, L., 1983. A mathematical model for predicting the extent of a major rockfall. Zeitschrift für Geomorphologie 27 (4), 473–82.

Topal, T., Akın, M., Özden, A. U., 2007, Assessment of rockfall hazard around Afyon castle, Turkey, Environmental Geology , Vol. 53, No.1, 191-200.

Topal, T., Akın, M. K., Akın, M., 2012.Rockfall hazard analysis for an historical Castle in Kastamonu (Turkey). Nat Hazards 62:255-274.

Toppe, R., 1987. Terrain models – a tool for natural hazard mapping. In Salm, B. and Gubler, H., editors, Avalanche formation,movement and effects. IAHS Publication no. 162, 629–38.

Trainweb, 2000. http://www.trainweb.org/railpics/rockshed12.html, last visited on February 2013.

TranBC, 2010. Ministry of Transportation and Infrastructure Online. http://www.flickr.com/photos/tranbc/5212470186/in/set-72157625479893042/, last visited on February 2013.

Ünay, E., Göktaş, F., 1999. Söke çevresi (Aydın) Geç Erken Miyosen ve Kuvaterner yaşlı küçük memelileri: Ön sonuçlar. Türkiye Jeoloji Bülteni 42, 99–113.

Varnes, D. J. 1978. Slope movement types and processes. In: Special Report 176: Landslides: Analysis and Control (Eds: Schuster, R. L. & Krizek, R. J.). Transportation and Road Research Board, National Academy of Science, Washington D. C., 11-33.

Vidrih, R., Ribicv, M., Suhadolc, P., 2001. Seismogeological effects on rocks during the 12 April 1998 upper Socva Territory earthquake (NW Slovenia). Tectonophysics 330(3), 153–75.

Wasowski, J., Gaudio, V.D., 2000. Evaluating seismically induced mass movement hazard in Caramanico Terme (Italy). Eng Geol 58:291–311.

Wick, E., Baumann, V., Jaboyedoff, M., 2010. Report on the impact of the 27 February 2010 earthquake (Chile, Mw 8.8) on rockfalls in the Las Cuevas valley, Argentina. Nat Hazards Earth Syst Sci 10:1989–1993.

Wu, S.-S., 1985. Rockfall evaluation by computer simulation. Transportation Research Record 1031, 1–5.

Yılmazer, S., Şaroğlu, F., Özgür, R., Açıkgöz, S., Ercan, T., Gevrek, İ. A., Yıldırım, N., Aydoğdu, Ö., 1994. Kuşadası – Davutlar (Aydın) Arasının Jeolojisi ve Jeotermal Olanaklarının Değerlendirilmesi. Türkiye 6. Enerji Kongresi, İzmir, Teknik Oturum Tebliğleri c. 1, 156-167.

Zellmer, J.T., 1987. The unexpected rockfall hazard. Bulletin of the Association of EngineeringGeologists 24(2), 281–83.